Enhanced-throughput Platforms to Model Endothelial Biology in Synthetic Hydrogels

By

Eric H. Nguyen

Dissertation Submitted in partial fulfillment of

the requirements for the degree of

Doctor of Philosophy

(Biomedical Engineering)

At the

UNIVERSITY OF WISCONSIN-MADISON

2016

Date of Final Oral Examination: January 19th, 2016

This dissertation is approved by the following members of the Final Oral Committee:

William L. Murphy, Professor, Biomedical Engineering (Thesis Advisor)

David J. Beebe, Professor, Biomedical Engineering

Nader Sheibani, Professor, Ophthalmology and Visual Sciences

Emery H. Bresnick, Professor, Cell and Regenerative Biology

Wan-Ju Li, Assistant Professor, Biomedical Engineering

Abstract

Angiogenesis is a complex series of behaviors carried out by endothelial cells and supporting cell types to develop new blood vessels from existing blood vessel networks. These behaviors, which include proliferation, migration, and tubule formation, are modulated in large part by instructive signals from the extracellular matrix (ECM). Failure to provide proper signaling cues to endothelial cells results in failed tissue vascularization and tissue pathology, and failure to understand the interactions between endothelial cells and the ECM potentially leads to uncertain endothelial cell responses to drug treatments. To address the need to understand how the ECM modulates endothelial cell behavior, we developed enhanced-throughput arrays of defined poly(ethylene glycol) hydrogels to systematically probe how ECM cues, namely cell adhesion, matrix stiffness and growth factor sequestration affect pro-angiogenic behaviors by endothelial cells. Hydrogels were fabricated to have defined functionalization with Arg-Gly-Asp (RGD) peptides to control cell adhesion, defined polymer concentration and crosslinking density to control matrix stiffness, and defined functionalization with growth factor receptor-mimicking peptides to control Vascular Endothelial Growth Factor (VEGF) sequestration. We utilized array-based screening techniques to identify particular hydrogels to consistently induce vascular network formation, and utilized those hydrogels to identify vascular inhibitory compounds in libraries of unknown chemicals. We then investigated how cell adhesion, substrate stiffness and VEGF signaling inhibition act in combination to modulate pro-angiogenic cell behavior, and further, used hydrogel arrays to demonstrate that extracellular environments dictate how endothelial cells respond to Transforming Growth Factor-β signaling. Taken together the hydrogels and arrays utilized in these studies represent adaptable tools to investigate the role of the extracellular matrix in modulating physiological and pathological endothelial cell behaviors.

Acknowledgements

This dissertation is dedicated to the many people who have enriched my life during my graduate career. I am especially grateful to Dr. William Murphy for his mentorship, patience, and support throughout my time in the Bioinspired Materials Laboratory. His leadership through example and his enthusiastic approach to research continue to instill motivation in everyone who works with him. It was a privilege to be a part of his research group. I would also like to thank current and past members of the Bioinspired Materials Laboratory, including Justin Koepsel, William Daly, Michael Schwartz, Ngoc Nhi Le, David Belair, Hamisha Ardalani, Bernard Binder, Andrew Dias, Gianluca Fontana, Matthew Parlato, Jim Molenda and Andrew Khalil for their support during my studies. I am also thankful for the support of Cody Bindl, Matthew Zanotelli and Steve Jeehwan Lee, the three undergraduate students I've had the pleasure of mentoring during my training. I would like to thank my thesis committee for their guidance and collaborations, Dr. Connie Lebakken for assistance with technology transfer and career development, and Timothy Butler for his mentorship during an industrial internship at Genzyme Corporation.

I would especially like to thank my mom, Lana, my dad, Daniel, and my brother, Dennis, for their love, wisdom and unwavering support over the entirety of my life, and I would like to thank a great circle of friends who provided fellowship and lasting moral support as well.

Contents

Abstract ..... **i**

Acknowledgements ..... **ii**

Contents ..... **iii**

List of figures and tables ..... **vii**

Chapter 1: Introduction **1**

1.1 Background and Significance 1
1.2 References 4

Chapter 2: Literature Review **8**

2.1 Preface 8
2.2 Abstract 8
2.3 Introduction 9
2.4 Biomaterials to modulate angiogenesis 11
2.4.1 Material selection 13
2.4.2 Adhesion molecules 15
2.4.3 Growth factor signaling 17
2.4.4 Mechanical properties 20
2.4.5 Hypoxic environments 22
2.4.6 Co-culture systems 23
2.5 Conclusion 24
2.6 References 24

Chapter 3: Differential inhibition of vascular morphogenesis by ToxCast™ chemical library on synthetic substrates and Matrigel™ **33**

3.1 Preface 33
3.2 Abstract 33
3.3 Introduction 34
3.4 Methods 36
3.4.1 Endothelial cell culture and maintenance 36
3.4.2 PEG functionalization with norbornene 37
3.4.3 Conjugating adhesion peptides to PEG 38
3.4.4 Patterned gold slides with hydrophobic and hydrophilic regions 39
3.4.5 Glass slide silanization 40

3.4.6 PEG hydrogel formulations 40
3.4.7 Mechanical properties of PEG hydrogels 41
3.4.8 Thin hydrogel arrays to identify hydrogels that promote vascular network formation....41
3.4.9 Labeling cells with Cell Tracker™ Red 42
3.4.10 Assembling and seeding hydrogel arrays 42
3.4.11 Adapting hydrogels for use in 96-well plates 43
3.4.12 Vascular inhibitor treatment on synthetic hydrogel and Matrigel culture systems 45
3.4.13 Identifying putative vascular inhibitors from Toxcast™ chemical library....47
3.5 Results....47
3.5.1 Identifying synthetic hydrogel formations that promote vascular network assembly 47
3.5.2 Identifying optimal microenvironments to promote vascular network formation....48
3.5.3 Establishing utility of network-inducing and VEGF-binding hydrogels for inhibition assays....52
3.5.4 HUVEC sensitivity to known vascular inhibitors on synthetic hydrogels and Matrigel....55
3.5.5 Exploring the effects of VEGF-independent inhibitors on network formation....56
3.5.6 Differential network formation processes on synthetic hydrogels and Matrigel....58
3.5.7 Identifying inhibitory compounds from ToxCast™ compound library....58
3.6 Discussion....60
3.7 Acknowledgements....62
3.8 Supplemental information....63
3.9 References....68

Chapter 4: Differential effects of cell adhesion, modulus and VEGFR-2 inhibition on capillary network formation in synthetic hydrogel arrays....73

4.1 Preface....73
4.2 Abstract....74
4.3 Introduction....74
4.4 Materials and methods....78
4.4.1 Cell culture....78
4.4.2 PEG functionalization with norbornene....79
4.4.3 Pre-coupling adhesion peptides to PEGNB....80
4.4.4 Forming PEG hydrogels....80
4.4.5 Mechanical properties of PEG hydrogels....83
4.4.6 Hydrogel array stencils....84
4.4.7 Forming PEG hydrogel arrays....84
4.4.8 Peptide incorporation into hydrogel array spots....87

4.4.9 HUVEC viability, tubulogenesis and proliferation in 3D hydrogel arrays.....87
4.4.10 HUVEC proliferation and VEGFR2 inhibition 89
4.4.11 HUVEC tubulogenesis in Matrigel.....89
4.4.12 HUVEC tubulogenesis in confined hydrogels.....90
4.4.13 Statistical analysis.....91
4.5 Results.....91
4.5.1 Hydrogel equilibrium swelling ratio and complex shear modulus.....91
4.5.2 Hydrogel array fabrication and peptide incorporation.....92
4.5.3 Three-dimensional cell viability in PEG hydrogel arrays.....94
4.5.4 Three-dimensional cell proliferation in PEG hydrogel arrays.....95
4.5.5 Three-dimensional tubulogenesis in PEG hydrogel arrays.....97
4.5.6 HUVEC viability, proliferation and tubulogenesis with VEGFR2 inhibition.....100
4.5.7 Tubulogenesis in confined and non-confined hydrogels.....103
4.6 Discussion.....104
4.7 Conclusion.....111
4.8 Acknowledgements.....112
4.9 Supplemental Information.....113
4.10 References.....113

Chapter 5: Endothelial cell responses to TGF-β signaling in 2D and 3D cell culture environments with defined mechanical properties.....120

5.1 Preface.....120
5.2 Abstract.....120
5.3 Introduction.....121
5.4 Experimental Section.....123
5.4.1 Materials.....123
5.4.2 Cell culture.....125
5.4.3 PEG functionalization with norbornene.....125
5.4.4 Pre-coupling adhesion peptides to PEGNB.....127
5.4.5 Mechanical properties of PEG hydrogels.....128
5.4.6 HUVEC culture on Fibronectin-coated TCPS.....129
5.4.7 Hydrogel array stencils.....129
5.4.8 Forming PEG hydrogel arrays for HUVEC monolayer culture.....130
5.4.9 Preparing patterned gold slides with differential wettability.....131
5.4.10 Silanizing glass slides for thin hydrogel arrays.....131
5.4.11 Preparing thin hydrogel arrays for HUVEC encapsulation.....132
5.4.12 Treating HUVECs with TGF-β.....133
5.4.13 HUVEC viability after encapsulation in PEG hydrogels.....133
5.4.14 Antibody staining.....134
5.4.15 Statistical analysis.....135

5.5 Results....135
5.5.1 Hydrogel modulus....135
5.5.2 Marker quantification by nuclear colocalization....137
5.5.3 TGF-β signaling – HUVECs on TCPS....137
5.5.4 Concurrent VEGF and TGF-β treatment on TCPS....140
5.5.5 TGF-β signaling – HUVECs on PEG hydrogels....141
5.5.6 TGF-β treatment – HUVECs encapsulated in PEG hydrogels....143
5.6 Discussion....146
5.7 Conclusion....150
5.8 Acknowledgements....151
5.9 Supplemental information....152
5.10 References....153

Chapter 6: Outlook and Conclusions....158

6.1 Conclusions....158
6.2 Outlook and future directions....159
6.2.1 Endothelial cells from pathological origins....160
6.2.2 Angiogenic rebound....161
6.2.3 Vascular normalization....162
6.2.4 Metastatic switch and mesenchymal transformation....163
6.3 References....164

List of Figures and Equations

Chapter 2: Figure 1. Individual and synergistic effects of ECM properties on endothelial cell behaviors related to angiogenesis. Integrin-mediated cell adhesion modulates endothelial cell viability, proliferation [30-32], migration [30, 32, 33], spatial polarization [34] and lumen formation [35]. ECM modulus influences capillary sprouting rate and directionality [36-38], capillary aspect ratio [36, 38], proliferation, and migration [32]. Growth factor sequestration influences growth factor stability [39-41] and facilitates binding between growth factors and receptors [39, 40, 42]. Synergistically, integrin binding and growth factor sequestration modulate VEGFR2 activity and focal adhesion assembly [43, 44]. Matrix modulus and growth factor sequestration modulate VEGFR2 activity, cytoskeletal stress fiber formation and cell migration rate [45-47]. Finally, integrin binding and matrix modulus modulate cell traction forces exerted and detected by endothelial cells [48].....13

Chapter 3: Figure 1. An endothelial cell culture system identifies environments that enable vascular network formation on synthetic PEG-based hydrogels. (a) Schematic of endothelial cell seeded on synthetic hydrogels and Matrigel. (b) Thin hydrogel arrays and arrays assembled with 3-well ProPlate® Cell Culture Isolators. (c) Left: Vascular network formation on synthetic hydrogels and Matrigel over time. Right: Typical vascular networks formed on synthetic hydrogels and Matrigel 24 hours after seeding. (d) Qualitative scoring system for HUVEC network formation and heat map showing initial screening results for HUVEC and IPSC-EC network formation. Conditions highlighted in violet borders denote environments that enabled HUVEC network formation within 24 hours after seeding and maintained structural integrity over the 48 hour culture period. Red: Cell Tracker Red.....51

Chapter 3: Equation 1. Z' calculation.....52

Chapter 3: Figure 2. Visualization and quantification of vascular networks on synthetic hydrogels and Matrigel. (a) Confocal microscopy images of HUVECs and IPSC-ECs forming networks on synthetic versus Matrigel substrates. Insets: Enhanced magnification of multicellular structures. Scale bar: 0.2 mm (b) HUVECs and IPSC-ECs seeded on synthetic and Matrigel substrates form vascular networks in DMSO-treated conditions. Network formation is disrupted by Sunitinib treatment. (c) HUVEC networks on synthetic and Matrigel substrates are identified by thresholding fluorescence intensity and object size. Network formation is quantified as total object area per substrate. (d) Vascular network formation in synthetic hydrogel and Matrigel systems is quantified and subjected to the Z' test to verify their efficacy of as toxicity screening systems. Red: Cell Tracker Red. 54

Chapter 3: Figure 3. Concentration-dependent inhibition of vascular network formation by known vascular inhibitors. (a) Schematics of synthetic hydrogels functionalized with RGD (synthetic), RGD and VBP (VBP+), and Matrigel™. (b) Sensitivity of HUVECs to inhibitors is compared between the synthetic, VBP+ and Matrigel™ systems. Inhibited samples (+) have a p-

value < 0.05 by One-way ANOVA followed by Dunnet multi-comparisons analysis compared to the DMSO/1X PBS control conditions depending on the vehicle of the inhibitor. 57

Chapter 3: Figure 4. Identification of vascular inhibitors from an unknown library of 53 candidate inhibitory compounds in a synthetic hydrogels screening system, a Matrigel system, and both systems identified inhibiting compounds based on whether total areas of inhibitor-treated vascular networks are two standard deviations above or below the mean of DMSO-treated network areas. 59

Chapter 3: Supplemental Figure 1. Shear modulus of synthetic hydrogels with varying PEG concentration and VBP presence in precursor solutions.....63

Chapter 3: Supplemental Figure 2. A narrow set of conditions comprising 40 mg/mL PEG, 0 – 0.25 mM RGD were tested in the thin-hydrogel screening system to identify HUVEC network-forming conditions on VBP-functionalized synthetic hydrogels. 64

Chapter 3: Supplemental Figure 3. Synthetic PEG hydrogels optimized for use in 96-well angiogenesis plates. Arrowheads indicate parameters used in inhibitor screening studies. (a) Dependence of hydrogel swelling ratio on photoinitiator concentration in the hydrogels. Swelling ratio was taken as ratio of sample diameter compared to the 3.5 mm diameter of the biopsy punch that extracted the samples. Columns in each photoinitiator condition represent swelling ratios measured in the individual rows of the 96 well plate to indicate spatial effects on swelling ratio. (b) Identifying hydrogel volumes that minimize meniscus formation and the appearance of out-of-focus areas in network images. (c) Identifying cell seeding densities that result in interconnected vascular networks. Red: Cell Tracker Red. 64

Chapter 3: Supplemental Figure 4. Fluorescent micrographs comparing HUVEC networks on synthetic hydrogel and Matrigel systems. Endothelial cells were treated with inhibitors to (a) VEGF signaling and (b) Prinomastat HCL as an inhibitor to MMP activity. VEGF inhibitors demonstrate network disruption on synthetic hydrogels but not Matrigel at many inhibitor concentrations. Prinomastat HCL disrupts vascular network formation on synthetic hydrogels at all treatment concentrations but permits network formation on Matrigel at multiple concentrations. Red: Cell Tracker Red. 65

Chapter 3: Supplemental Figure 5. Fluorescent micrographs comparing inhibitor-treated HUVEC networks on synthetic hydrogels and VBP-functionalized hydrogels. The presence of VBP in hydrogels nullify effects of VEGF inhibitors. Red: Cell Tracker Red. 66

Chapter 3: Supplemental Figure 6. Fluorescent micrographs comparing Suramin-treated HUVEC networks on synthetic hydrogels and Matrigel. Suramin dissolves the Matrigel substrate at concentrations of 70 μM and 17.5 μM. Identical concentrations of Suramin on the synthetic hydrogels have little to no effect on vascular network morphology and do not compromise substrate integrity to the same degree as on Matrigel. Red: Cell Tracker Red. 67

Chapter 3: Supplemental Figure 7. Examples of compounds identified as inhibitors by either the synthetic or Matrigel systems but not in both systems. Red: Cell Tracker Red. 68

Chapter 4: Figure 1. Molecules included in PEG-norbornene hydrogels. A) The hydrogels are composed of (i) 8-arm PEG molecules, with each arm functionalized with a norbornene molecule; (ii) Di-thiolated PEG crosslinking molecules bridge multiple 8-arm PEG molecules together into an ordered polymer network. A di-thiolated PEG molecule acts as an inert crosslinking molecule that is not cell-degradable; (iii) In bioactive hydrogels, PEG molecules are decorated with CRGDS adhesion peptide or CRDGS scrambled peptide to modulate cell adhesion to the hydrogel; (iv) Di-thiolated matrix metalloproteinase (MMP) labile crosslinking peptides enable cell-driven hydrogel degradation. B) "Background" hydrogels are void of cell adhesion molecules and are not subject to cell-driven degradation. C) "Hydrogel spots" modulate cell behavior through covalently attached adhesion molecules and are biodegradable via MMP activity.....82

Chapter 4: Equation 1. Mass equilibrium swelling ratio 83

Chapter 4: Figure 2. Schematic representation of hydrogel array fabrication. 1) Separate hydrogel spot solutions containing various ratios of CRGDS adhesion peptide (Red circles) and a scrambled CRDGS non-functional peptide (Blue circles) are pipetted into wells of a PDMS stencil. Total pendant peptide concentration is fixed at 2 mM in all solutions. 2) The hydrogel spots are crosslinked in the stencil using UV light. 3) A crosslinked 1-mm thick "background" hydrogel slab is laid on top of the crosslinked bioactive hydrogel spots. A thin layer of background hydrogel solution is added to the slab to anchor the cured spots to the background. 4) The hydrogel spots are anchored to the background after treatment with UV light. 5) The completed hydrogel array is removed from the stencil. Red boxes highlight the raised spots in the schematic and side view images of the arrays. 86

Chapter 4: Figure 3. Characterizing mechanical properties and pendant peptide incorporation into the hydrogel array. A) Equilibrium swelling ratios of degradable (left) and background (right) and hydrogels used in low, medium and high hydrogel modulus conditions. B) Complex shear modulus of degradable (left) and background (right) hydrogels using in low, medium and high hydrogel modulus conditions. Error bars indicate standard deviation. C) Reduction in norbornene alkene protons due to covalent coupling of CRGDS and CRDGS as measured using NMR. D) N-terminal amines of CRGDS were labeled with Alexa Fluor® 488 (Green). Green fluorescence intensity was quantified from the left to right columns (Black lines: PEG polymer and crosslinker. Red circles: CRGDS).....93

Chapter 4: Figure 4. Viability of HUVECs encapsulated inside the hydrogel array spots. A) Cell viability as determined by counting live cell and dead cell nuclei 48 hours after encapsulation. B) Cell viability measured when VEGFR2 was inhibited by 10 μM SU5416 supplementation. *, p <

0.05. &, $p < 0.05$ compared to all equivalent CRGDS concentration in other modulus conditions C) Viability of SU5416-treated HUVECs normalized to HUVEC viability in growth medium. *, $p < 0.05$; **, $p < 0.01$; ***, $p < 0.001$ compared to growth medium control. 95

Chapter 4: Figure 5. Proliferation of HUVECs encapsulated inside the hydrogel array spots. A) Cell proliferation as determined by Click-it EdU staining 24 hours after encapsulation B) Cell proliferation measured when VEGFR2 was inhibited by 10 μM SU5416 supplementation. *, $p < 0.05$. &, $p < 0.05$ compared to all equivalent CRGDS concentration in other modulus conditions C) Cell proliferation during SU5416 treatment normalized to proliferation in growth medium. *, $p < 0.05$; **, $p < 0.01$; ***, $p < 0.001$ compared to growth medium control. D) Proliferating cells (arrowheads) were localized to multicellular structures. Green: Cell Tracker Green. Blue: Hoescht nuclear stain. Red: Alexa Fluor® 594 labeling nuclei of cells in S-phase. 97

Chapter 4: Figure 6. Tubulogenesis of HUVECs encapsulated inside the hydrogel array spots. A) Total tubule length was determined by manually measuring tubule lengths throughout the spots from epifluorescence Z-stack images. The cells were stained using Cell Tracker Green and Hoescht nuclear stain 24 hours after encapsulation. B) Tubulogenesis when VEGFR2 was inhibited by 10 μM SU5416 supplementation. *, $p < 0.05$. &, $p < 0.05$ compared to all equivalent CRGDS concentration in other modulus conditions C) Tubulogenesis during SU5416 treatment normalized to tubulogenesis in growth medium. *, $p < 0.05$; **, $p < 0.01$; ***, $p < 0.001$ compared to growth medium. D) Confocal microscopy images of low tubulogenesis in low modulus, 2 mM RGDS spots and increased tubulogenesis levels with SU5416 treatment. Bottom: Enlarged examples of capillary-like structures seen in the VEGFR2-inhibited condition. Scale bars: 100 μm. Green: Cell Tracker Green. Blue: Hoescht nuclear stain. 99

Chapter 4: Figure 7. Effects of VEGFR2 inhibition in standard model systems. A) HUVEC proliferation with and without SU5416 supplementation on tissue culture-treated polystyrene (TCPS). *, $p < 0.05$. B) HUVEC tubulogenesis with and without SU5416 supplementation in growth factor-reduced Matrigel. C) HUVEC CLS formation in 0.4 μL Matrigel spots. In each pair of pictures, the tubules in the right hand copy were highlighted. Green: Cell Tracker Green. *, $p < 0.05$ between EGM2 and SU5416-treated conditions. 103

Chapter 4: Supplemental figure 1. Hydrogel homogeneity and heterogeneity in confined vs. non-confined PEGNB hydrogels. A) Hydrogels confined to a 48 well plate at 24 hours after encapsulation. Schematic: Cell-containing hydrogel is anchored by the edges by a background hydrogel (blue rectangles) in order to prevent complete detachment of the hydrogel into medium during swelling. Black circle: buckling area. Arrowheads: CLS formation. B) Freely-swollen hydrogels at 24 hours after encapsulation.....113

Chapter 5: Figure 1. Cell culture systems to investigate phenotypic changes in HUVECs. (**a**) Schematic of hydrogel networks for cell culture. (**b**) Gel-in-gel hydrogel array and

transformation experiments on cell-adhesive PEG hydrogels. (**c**) Thin hydrogel array and transformation experiments in degradable PEG hydrogels. 127

Chapter 5: Figure 2. Hydrogel modulus and corresponding PEG concentration and thiol-ene crosslinking in precursor solutions. (**a**) Non-degradable PEG hydrogels for 2D environments. (**b**) Degradable PEG hydrogels in 3D environments. 136

Chapter 5: Figure 3. Changes in HUVEC marker expression with TGF-β treatment on fibronectin-coated TCPS. (**a**) Phosphorylated SMAD3 immunostaining. Red: pSMAD3. Blue: Hoescht nuclear stain. (**b**) SNAIL expression and immunostaining. Red: SNAIL. Blue: Hoescht nuclear stain. (**c**) CD31 expression and immunostaining. Green: CD31. Blue: Hoescht nuclear stain. (**d**) Von willebrand factor expression and immunostaining. Red: VWF. Blue: Hoescht nuclear stain. (**e**) Smooth muscle actin expression and immunostaining. Green: αSMA. Blue: Hoescht nuclear stain. (**f**) CD34 expression and immunostaining. Green, Arrowhead: CD34+-positive HUVEC. Blue: Hoescht nuclear stain. *, $p < 0.05$ compared to 0.25% FBS control media. 139

Chapter 5: Figure 4. Changes in HUVEC marker expression with concurrent TGF-β and VEGF treatment on fibronectin-coated TCPS. *, $p < 0.05$ compared to 0.5 ng/mL VEGF treatment. #, $p < 0.05$ compared to 0.25% FBS control media. 141

Chapter 5: Figure 5. Changes in HUVEC marker expression with TGF-β treatment on cell adhesive PEG hydrogels of varying modulus. *, $p < 0.05$ compared to 0.25% FBS control media. #, $p < 0.05$ compared to 24, 44 or 69 kPa hydrogels. 143

Chapter 5: Figure 6. Changes in HUVEC marker expression with TGF-β treatment in degradable PEG hydrogels of varying modulus. (**a**) CD31 expression and immunostaining. Green: CD31. Blue: Hoescht nuclear stain. (**b**) Von willebrand factor expression and immunostaining. Red: VWF. Blue: Hoescht nuclear stain. (**c**) Smooth muscle actin expression and immunostaining. Green: αSMA. Blue: Hoescht nuclear stain. (**d**) Collage I expression and immunostaining. Red: Col I. Blue: Hoescht nuclear stain. *, $p < 0.05$ compared to 0.25% FBS control media. #, $p < 0.05$ compared to 14 kPa hydrogel. 145

Chapter 5: Figure 7. Viability of HUVECs cultured in degradable PEG hydrogels. (**a**) Viability in PEG hydrogels of varying modulus 24 hours after encapsulation. (**b**) Viability of HUVECs with TGF-β treatment 72 hours after encapsulation. 146

Chapter 5: Supplemental Figure 1. Comparison of cell marker quantification methods. (**a**) Number of cells positive for α-SMA. (**b**) % nuclear co-localization with α-SMA stain. *, $p < 0.05$ compared to 24 kPa hydrogel. #, $p < 0.05$ compared to 0.25% FBS control media. 152

Chapter 1:

Introduction

1.1 Background and Significance

Angiogenesis, the expansion of blood vessel networks via capillary sprouting [1, 2], is a well-characterized biological process that is controlled by interactions between endothelial cells (ECs) and the extracellular matrix (ECM). In particular, three critical properties of the extracellular matrix modulate numerous cell activities that contribute to angiogenesis: integrin-binding molecules promote cell adhesion, structural proteins and water content provide appropriate matrix stiffness for vascular structure formation, and proteoglycans and glycoproteins promote growth factor sequestering to modulate growth factor signaling dynamics. When these features are defined in cell culture systems, they can be leveraged to generate models of angiogenesis that enable studies of angiogenic mechanisms, screens of chemical compounds that enhance or inhibit angiogenesis, as well as studies of vascular pathology. However, a significant challenge to the achievement of these studies lies in decoding the complexity of how combinations of ECM properties drive changes in endothelial cell behavior. This challenge exists in large part due to the lack of techniques to rapidly study a variety of defined matrices to decouple the effects of individual ECM properties and determine synergies that regulate EC behavior.

Despite what is already known about how individual ECM properties modulate EC behavior, complex synergistic activity between multiple ECM properties is only beginning to be understood. Integrin binding promoted by cell attachment motifs, including Arg-Gly-Asp (RGD) peptide sequences found in fibronectin, vitronectin, fibrin and other ECM proteins [3], promote pro-angiogenic EC behaviors such as survival, migration, and proliferation [4-6]. Additionally

integrin activation is necessary to promote EC polarization and lumen formation [7, 8]. Matrix stiffness affects length, width and directionality of sprouting capillaries [9-11]. Finally, heparin glycosaminoglycans in the ECM enhance activity and stability for numerous pro-angiogenic growth factors including VEGF and FGF2 [12-17]. As an example of synergistic activity between ECM properties, activation of $\alpha_V\beta3$ integrin [18, 19] and the presence of heparin [16-18] enhance EC activation by Vascular Endothelial Growth Factor Receptor-2 (VEGFR2). Conversely, VEGFR2 signaling is required for the formation of the focal adhesion complex mediated by $\alpha_V\beta3$ activation and integrin clustering [20]. Additionally, the activity of RhoA and p190RhoGAP, which modulate signaling and expression of VEGFR2 respectively [21, 22], is mediated by the stiffness of the extracellular matrix and focal adhesion activation. The complexities in these interactions highlight a need to efficiently test EC behaviors in environments where ECM properties can be varied systematically and in various combinations.

While ECM properties modulate angiogenesis individually and synergistically, they are likely to modulate EC pathology as well. Signaling by Transforming Growth Factor β (TGF-β) is known to drive numerous pathological EC behaviors including apoptosis [23, 24] the inhibition of angiogenesis [25], and endothelial-mesenchymal transition (EndMT) [26-31], wherein ECs lose endothelial phenotype to gain a mesenchymal phenotype. EndMT is a known contributor to the onset of fibrosis and fibrodysplasia ossificans progressiva (FOP) [32] during healing of damaged tissues and organs [26-28, 32, 33] as well as to the generation of cancer-associated fibroblasts that support tumor growth and metastasis [34, 35]. The role of the ECM in modulating EndMT and TGF-β signaling is only beginning to be explored, with matrix stiffness being a notable early example of an ECM property that modulates TGF-β-driven EndMT [36]. As examples of additional potential mechanisms by which the ECM modulates TGF-β activity, cell adhesion has

been implicated in facilitating cell responses to TGF-β signaling [37], and heparin binding has been shown to modulate TGF-β activity as well [38]. Synergistic relationships between matrix stiffness, cell-matrix adhesion, and heparin-mediated enhancement of TGF-β-family growth factor signaling are likely to modulate EC pathology, and the application of techniques to efficiently test EC behaviors in a range of ECM-mimicking materials can enable the rapid elucidation of how the ECM modulates TGFβ-driven pathology.

To address these needs, studies in this thesis utilized enhanced-throughput array systems to rapidly screen EC behaviors when seeded on, or encapsulated within poly(ethylene glycol) (PEG) hydrogels that promote varying degrees of cell-matrix adhesion, mechanical stiffness and binding of Vascular Endothelial Growth Factor (VEGF) *via* modular chemistry and chemically-defined peptides or crosslinking groups. The use of a thiol-ene "click" reaction [39] to functionalize and crosslink PEG hydrogels enabled orthogonal control over individual hydrogel properties. In chapter 3 hydrogel arrays identified hydrogels that consistently induce vascular network formation by human ECs on hydrogel surfaces and then identified vascular inhibitors from a library of unknown compounds in a toxicity screening experiment. In chapter 4 hydrogel arrays modeled viability, proliferation, and vascular network formation by ECs encapsulated in a wide variety of hydrogels and demonstrated differential responses to VEGF inhibition in varying hydrogels. Finally, in chapter 5 hydrogel arrays modeled how two-dimensional and three-dimensional culture contexts and hydrogel stiffness affect potentially pathogenic EC responses to TGF-β signaling. These studies demonstrate that multiple material properties may be systematically defined to maximize desired behavioral outputs by ECs in two dimensional and three dimensional cell culture systems. Notably, these studies generated hydrogel-based screening systems to detect chemically-driven vascular disruption with greater sensitivity and

repeatability than Matrigel-based systems. These studies also demonstrate that ECs respond to treatment with growth factors and vascular inhibitors differently depending on matrix properties and culture contexts. In future studies the systems developed in this thesis provide promising tools to optimize materials for therapeutic vascular tissue engineering, identify candidate ECM-driven mechanistic pathways as therapeutic targets for treating vascular disorders, and model short-term and long-term EC responses to drug treatment in environments mimicking physiological and diseased tissue.

1.2 References

[1] De Smet F, Segura I, De Bock K, Hohensinner P, Carmeliet P. Mechanisms of Vessel Branching Filopodia on Endothelial Tip Cells Lead the Way. Arteriosclerosis Thrombosis and Vascular Biology. 2009;29:639-49.

[2] Risau W. Mechanisms of angiogenesis. Nature. 1997;386:671-4.

[3] Ruoslahti E. RGD and other recognition sequences for integrins. Annu Rev Cell Dev Biol. 1996;12:697-715.

[4] Davis G, Senger D. Endothelial extracellular matrix - Biosynthesis, remodeling, and functions during vascular morphogenesis and neovessel stabilization. Circulation Research. 2005;97:1093-107.

[5] Senger DR, Perruzzi CA. Cell migration promoted by a potent GRGDS-containing thrombin-cleavage fragment of osteopontin. Biochim Biophys Acta. 1996;1314:13-24.

[6] Weis SM, Cheresh DA. αV integrins in angiogenesis and cancer. Cold Spring Harb Perspect Med. 2011;1:a006478.

[7] Zovein A, Luque A, Turlo K, Hofmann J, Yee K, Becker M, et al. beta 1 Integrin Establishes Endothelial Cell Polarity and Arteriolar Lumen Formation via a Par3-Dependent Mechanism. Developmental Cell. 2010;18:39-51.

[8] Bayless KJ, Salazar R, Davis GE. RGD-dependent vacuolation and lumen formation observed during endothelial cell morphogenesis in three-dimensional fibrin matrices involves the alpha(v)beta(3) and alpha(5)beta(1) integrins. Am J Pathol. 2000;156:1673-83.

[9] Sun G, Shen YI, Kusuma S, Fox-Talbot K, Steenbergen CJ, Gerecht S. Functional neovascularization of biodegradable dextran hydrogels with multiple angiogenic growth factors. Biomaterials. 2011;32:95-106.

[10] Shamloo A, Heilshorn C. Matrix density mediates polarization and lumen formation of endothelial sprouts in VEGF gradients. Lab on a Chip. 2010;10:3061-8.

[11] Mason B, Starchenko A, Williams R, Bonassar A, Reinhart-King C. Tuning three-dimensional collagen matrix stiffness independently of collagen concentration modulates endothelial cell behavior. Acta Biomaterialia. 2013;9:4635–44.

[12] Hudalla G, Koepsel J, Murphy W. Surfaces That Sequester Serum-Borne Heparin Amplify Growth Factor Activity. Advanced Materials. 2011;23:5415-5418.

[13] Forsten-Williams K, Chua C, Nugent M. The kinetics of FGF-2 binding to heparan sulfate proteoglycans and MAP kinase signaling. Journal of Theoretical Biology. 2005;233:483-99.

[14] Smith JC, Hagemann A, Saka Y, Williams PH. Understanding how morphogens work. Philosophical Transactions of the Royal Society B: Biological Sciences. 2008;363:1387-92.

[15] Wijelath E, Namekata M, Murray J, Furuyashiki M, Zhang S, Coan D, et al. Multiple Mechanisms for Exogenous Heparin Modulation of Vascular Endothelial Growth Factor Activity. Journal of Cellular Biochemistry. 2010;111:461-8.

[16] Steffens G, Yao C, Prevel P, Markowicz M, Schenck P, Noah E, et al. Modulation of angiogenic potential of collagen matrices by covalent incorporation of heparin and loading with vascular endothelial growth factor. Tissue Engineering. 2004;10:1502-9.

[17] Gilmore L, Rimmer S, McArthur S, Mittar S, Sun D, MacNeil S. Arginine functionalization of hydrogels for heparin bindingua supramolecular approach to developing a pro-angiogenic biomaterial. Biotechnology and Bioengineering. 2013;110:296-317.

[18] Cebe-Suarez S, Zehnder-Fjallman A, Ballmer-Hofer K. The role of VEGF receptors in angiogenesis; complex partnerships. Cellular and Molecular Life Sciences. 2006;63:601-15.

[19] Somanath P, Malinin N, Byzova T. Cooperation between integrin alpha(nu)beta(3) and VEGFR2 in angiogenesis. Angiogenesis. 2009;12:177-85.

[20] Matsumoto T, Claesson-Welsh, L. VEGF receptor signal transduction. Science Signaling, the Signal Transduction Knowledge Environment. 2001;2001:re21.

[21] Mammoto A, Connor K, Mammoto T, Yung C, Huh D, Aderman C, et al. A mechanosensitive transcriptional mechanism that controls angiogenesis. Nature. 2009;457:1103-8.

[22] Bryan B, Dennstedt E, Mitchell D, Walshe T, Noma K, Loureiro R, et al. RhoA/ROCK signaling is essential for multiple aspects of VEGF-mediated angiogenesis. Faseb Journal. 2010;24:3186-95.

[23] Leksa V, Godar S, Schiller HB, Fuertbauer E, Muhammad A, Slezakova K, et al. TGF-beta-induced apoptosis in endothelial cells mediated by M6P/IGFII-R and mini-plasminogen. J Cell Sci. 2005;118:4577-86.

[24] Ferrari G, Cook BD, Terushkin V, Pintucci G, Mignatti P. Transforming growth factor-beta 1 (TGF-beta1) induces angiogenesis through vascular endothelial growth factor (VEGF)-mediated apoptosis. J Cell Physiol. 2009;219:449-58.

[25] Pepper MS, Vassalli JD, Orci L, Montesano R. Biphasic effect of transforming growth factor-beta 1 on in vitro angiogenesis. Exp Cell Res. 1993;204:356-63.

[26] Medici D, Shore E, Lounev V, Kaplan F, Kalluri R, Olsen B. Conversion of vascular endothelial cells into multipotent stem-like cells. Nature Medicine. 2010;16:1400-6.

[27] Medici D, Potenta S, Kalluri R. Transforming growth factor-beta 2 promotes Snail-mediated endothelial-mesenchymal transition through convergence of Smad-dependent and Smad-independent signalling. Biochemical Journal. 2011;437:515-20.

[28] Piera-Velazquez S, Li Z, Jimenez S. Role of Endothelial-Mesenchymal Transition (EndoMT) in the Pathogenesis of Fibrotic Disorders. American Journal of Pathology. 2011;179:1074-80.

[29] Arciniegas E, Sutton A, Allen T, Schor A. Transforming growth factor-beta-1 promotes the differentiation of endothelial cells into smooth muscle-like cells-invitro. Journal of Cell Science. 1992;103:521-9.

[30] Nakajima Y, Yamagishi T, Hokari S, Nakamura H. Mechanisms involved in valvuloseptal endocardial cushion formation in early cardiogenesis: Roles of transforming growth factor (TGF)-beta and bone morphogenetic protein (BMP). Anatomical Record. 2000;258:119-27.

[31] ten Dijke P, Arthur H. Extracellular control of TGF beta signalling in vascular development and disease. Nature Reviews Molecular Cell Biology. 2007;8:857-69.

[32] Fukuda T, Kohda M, Kanomata K, Nojima J, Nakamura A, Kamizono J, et al. Constitutively Activated ALK2 and Increased SMAD1/5 Cooperatively Induce Bone Morphogenetic Protein Signaling in Fibrodysplasia Ossificans Progressiva. Journal of Biological Chemistry. 2009;284:7149-56.

[33] Zeisberg E, Tarnavski O, Zeisberg M, Dorfman A, McMullen J, Gustafsson E, et al. Endothelial-to-mesenchymal transition contributes to cardiac fibrosis. Nature Medicine. 2007;13:952-61.

[34] Lin F, Wang N, Zhang TC. The role of endothelial-mesenchymal transition in development and pathological process. IUBMB Life. 2012;64:717-23.

[35] Potenta S, Zeisberg E, Kalluri R. The role of endothelial-to-mesenchymal transition in cancer progression. British Journal of Cancer. 2008;99:1375-9.

[36] Zhang H, Chang H, Wang LM, Ren KF, Martins MC, Barbosa MA, et al. Effect of Polyelectrolyte Film Stiffness on Endothelial Cells During Endothelial-to-Mesenchymal Transition. Biomacromolecules. 2015;16:3584-93.

[37] Tavares A, Mercado-Pimentel M, Runyan R, Kitten G. TGF beta-mediated RhoA expression is necessary for epithelial-mesenchymal transition in the embryonic chick heart. Developmental Dynamics. 2006;235:1589-98.

[38] Lyon M, Rushton G, Gallagher J. The interaction of the transforming growth factor-beta s with heparin heparan sulfate is isoform-specific. Journal of Biological Chemistry. 1997;272:18000-6.

[39] Fairbanks BD, Schwartz MP, Halevi AE, Nuttelman CR, Bowman CN, Anseth KS. A Versatile Synthetic Extracellular Matrix Mimic via Thiol-Norbornene Photopolymerization. Advanced Materials. 2009;21:5005-10.

Chapter 2:

Literature Review

Eric H Nguyen, William L. Murphy. Customizable biomaterials to model complex effects of anti-angiogenic drug treatments in vitro. *In preparation.*

2.1 Preface

The aim of this work was to probe vascular morphogenesis, drug response and pathological behavior by endothelial cells in a wide range of defined environments. To achieve this, we functionalized poly(ethylene glycol) hydrogels with biomolecules and tuned hydrogel stiffness to modulate cell behaviors. This literature review identifies poorly-understood clinical scenarios that benefit from improved vascular models and describes methods to design biomaterials that recapitulate aspects of the extracellular environment that modulate endothelial behavior.

2.2 Abstract

The inhibition of angiogenesis is a critical element of cancer therapy, as tumor vasculature is associated with tumor expansion. While numerous drugs have proven to be effective at disrupting tumor vasculature, patient survival has not significantly improved as a result of anti-angiogenic drug treatment. Emerging evidence suggests that this is due to a combination of unintended side effects resulting from the application of anti-angiogenic compounds, including angiogenic rebound after treatment and the activation of metastasis in the tumor. There is currently a need to better understand the far-reaching effects of anti-angiogenic drug treatments in the context of cancer. Numerous innovations and discoveries in biomaterials design and tissue engineering techniques are providing investigators with tools to develop physiologically relevant

vascular models and gain insights into the holistic impact of drug treatments on tumors. This review examines recent advances in the design of pro-angiogenic biomaterials, specifically in controlling integrin-mediated cell adhesion, growth factor signaling, mechanical properties and oxygen tension, as well as material integration into sophisticated co-culture models of cancer vasculature.

2.3 Introduction

The inhibition of angiogenesis, the growth of new blood vessels from existing vascular networks [1] has been a critical target for cancer therapeutics since Folkman *et al*. demonstrated that tumor growth was dependent on the presence of vasculature [2, 3]. These studies motivated the discovery of numerous drugs that disrupt angiogenesis and consequently deny tumors of oxygen, nutrients and growth factors required for growth. The first drugs that passed clinical trials disrupted Vascular Endothelial Growth Factor (VEGF) signaling pathways that contribute to angiogenesis, either as antibodies to VEGF such as Bevacizumab [4] or as inhibitors to VEGF Receptor Tyrosine Kinases such as Sunitinib [5]. Although several drug candidates such as Bevacizunab, Sunitinib, Sorafenib and others [6] have received FDA approval for the treatment of specific types of cancers, many others failed to improve patient survival [7]. Ultimately the disruption of tumor vasculature is critical to limiting tumor growth and maintaining "progression-free survival" in patients, but it does not fully destroy cancer tumors in many cases [8, 9]. Due to the complexity of the tumor microenvironment, the use of vascular disruption as the sole means of cancer treatment can generate unintended consequences that reverse the progress of treatment or worsen the patient prognoses [10-12].

An example of these consequences is angiogenic rebound, where tumor vasculature that was previously disassembled by anti-angiogenic treatment rapidly regrows after the cessation of treatment [10]. This is the result of multiple contributing mechanisms including the generation of a local hypoxic environment, increased expression of VEGF, PlGF, FGF2, SDF-1 and PDGF within the tumor [10], and putative transformation of tumor cells into endothelial cells [13, 14], all of which can result from initial anti-angiogenic treatment. Another example of an unintended effect is the activation of a metastatic switch in tumors, where cells within the tumor change phenotypes to encourage metastasis [12, 15, 16]. While anti-angiogenic treatment focuses on the deactivation of pro-angiogenic signaling pathways, emerging evidence suggests that those same pathways inhibit the onset of metastasis through inhibition of tumor cell migration and invasion, growth factor production by cancer-associated fibroblasts and the endothelial-mesenchymal transformation [12, 15, 16]. A final example of an unintended consequence is vascular normalization, where prior to complete network disassembly the tumor vasculature restructures itself from tortuous, leaking, non-functional vasculature [17-20] to well-ordered, patent vasculature with short-term anti-angiogenic treatment [20]. Unlike other side effects that hinder cancer treatment, normalization can potentially be exploited to improve the transport of anti-cancer drugs into the interior of a tumor and increase the effectiveness of cancer therapy [21]. Currently, the clinical effectiveness of combined anti-angiogenesis and anti-cancer treatments is debatable [22] due to the timing window of vascular normalization being limited and unknown, and due to the lack of effective biomarkers to detect a normalization event *in situ* [22].

The occurrence of these side effects would be difficult to predict using existing angiogenesis assays *in vitro*. Most functional assays of anti-angiogenic drug activity only demonstrate specific endpoints of vascular network disruption such as decreased cell viability, proliferation, migration

and vascular network formation [23-25]. While these assays can be well-suited for discovering compounds that modulate angiogenesis [26], far-reaching effects beyond initial network inhibition or disruption are less understood and largely became known only after they were first observed *in vivo*.

Advances in the design of biomaterials and cell culture platforms are necessary to enable rapid, detailed characterization of the complex effects of anti-angiogenesis treatments beyond the scope of initial vascular disruption. For example, models of angiogenic rebound will likely require culture environments that support long-term maintenance of vascular networks as well as re-assembly of disrupted vascular networks after the cessation of drug treatment. Models of vascular normalization will require environments that initially promote the formation of diseased vasculature so that signs of normalization may be clearly detected. To achieve these goals biomaterials must recapitulate critical functions of extracellular matrices (ECM) present *in vivo* and promote cell adhesion, modulate growth factor signaling, have physiologically relevant and controlled modulus as well as defined modes of degradation. Cell culture systems must additionally accommodate for heterotypic co-cultures of cells including tumor-associated cell types to more closely mimic tumor environments. This review will examine recently developed biomaterials and cell culture tools that enable unprecedented environmental control in vascular morphogenesis models.

2.4 Biomaterials to modulate angiogenesis

Angiogenesis consists of a complex series of cell actions including detection of soluble growth factor signaling, proliferation, migration, and assembly of multi-cellular tubular structures [1], all

of which are modulated by biomolecules that make up the extracellular matrix (ECM) (Fig. 1). In physiological scenarios microvasculature is in contact with a continuous ECM in the form of a basement membrane composed of Fibronectin, Collagen I, Collagen IV, numerous forms of Laminin, Perlecan and other proteoglycans [27, 28]. In dysfunctional vasculature the continuous ECM contains μm-scale gaps in the membrane [27, 28] and elevated levels of ECM proteins, notably Collagen I, leading to increased mechanical stiffness [29]. Additionally, the typical tumor vasculature exists in hypoxic environments that impact behavior of not only endothelial cells but also tumor cells that can modulate angiogenesis via paracrine signaling [10]. Each of the biomolecules and cells present during angiogenesis plays an important role, and biomaterials are being developed by several groups to recapitulate the most important components of pro-angiogenic environments. The following subsections will review technologies that enable biomaterials to recapitulate instructive environmental cues that are critical to modulating angiogenesis, including presentation of integrin-binding cell adhesion ligands, modulation of mechanical properties, modulation of growth factor signaling, hypoxia and proximity to cancer cell types.

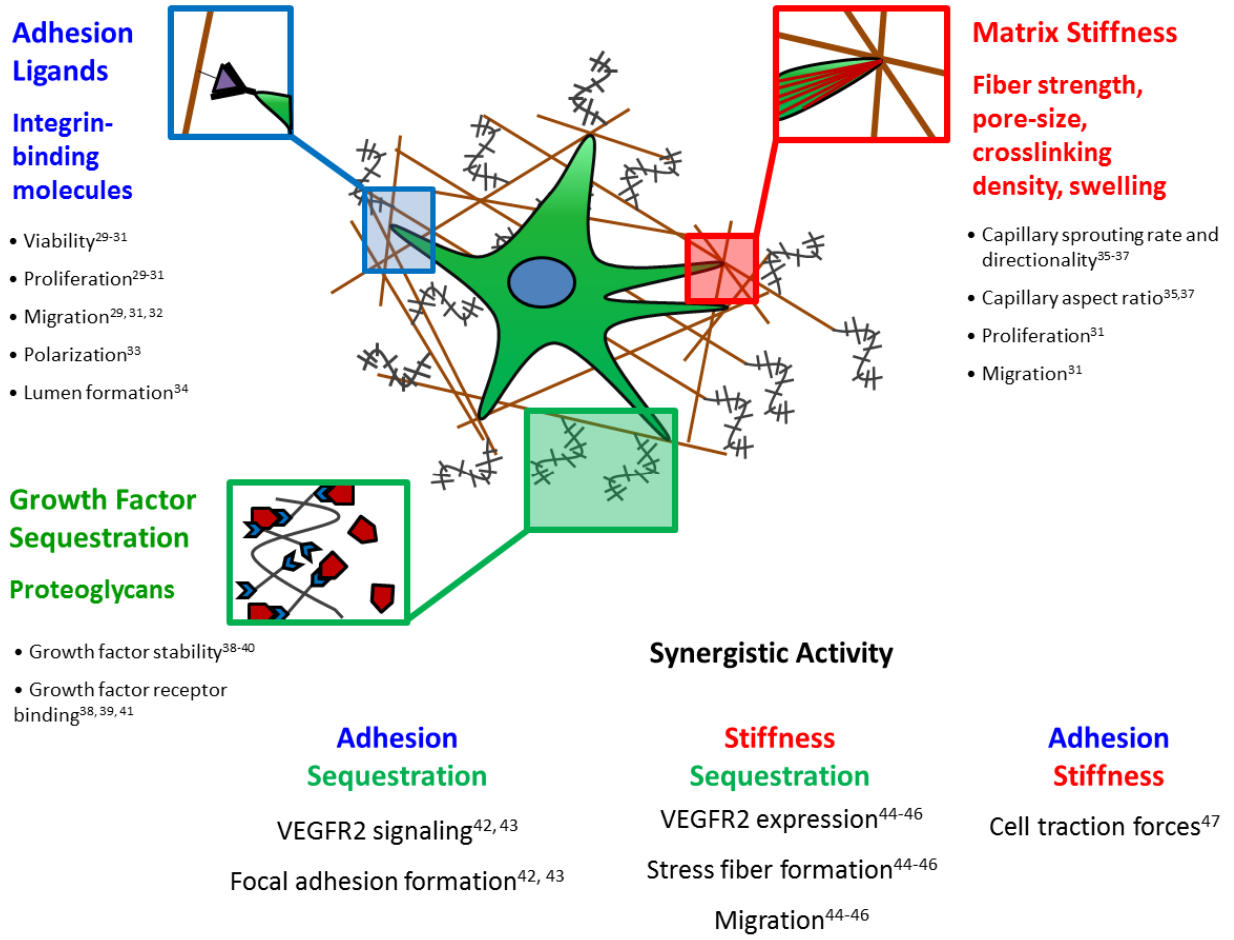

Chapter 2: Figure 1. Individual and synergistic effects of ECM properties on endothelial cell behaviors related to angiogenesis. Integrin-mediated cell adhesion modulates endothelial cell viability, proliferation [30-32], migration [30, 32, 33], spatial polarization [34] and lumen formation [35]. ECM modulus influences capillary sprouting rate and directionality [36-38], capillary aspect ratio [36, 38], proliferation, and migration [32]. Growth factor sequestration influences growth factor stability [39-41] and facilitates binding between growth factors and receptors [39, 40, 42]. Synergistically, integrin binding and growth factor sequestration modulate VEGFR2 activity and focal adhesion assembly [43, 44]. Matrix modulus and growth factor sequestration modulate VEGFR2 activity, cytoskeletal stress fiber formation and cell migration rate [45-47]. Finally, integrin binding and matrix modulus modulate cell traction forces exerted and detected by endothelial cells [48].

2.4.1 Material selection

Biologically-derived extracellular matrix components are commonly adapted as biomaterials to induce angiogenesis and endothelial network formation in endothelial cell culture. Collagen,

Fibrin and Matrigel often present a wealth of signals necessary to drive pro-angiogenic behaviors in endothelial cells with minimal modification. The often cited limitations of naturally-derived materials are poor mechanical integrity, high batch-to-batch variation and complex compositions that mask specific mechanisms driving angiogenesis [49, 50]. However, some of these materials are amenable to customization and enable studies of how biomolecules affect cell fates in highly biomimetic environments. Using customization, investigators may probe the effects of defined ECM signals in environments presenting synergistic and obscure signals that are currently difficult to implement using chemically-defined materials. Although there is difficulty in attributing changes in cell behavior to specific changes in a natural material due to its inherent complexity, studies using natural materials may be coupled to parallel studies on synthetic substrates to gain further insights to mechanisms driving changes in angiogenesis.

Synthetic, chemically defined biomaterials have been adapted as alternatives to naturally-derived ECM components to achieve greater control of cell behavior in angiogenesis models. Synthetic cell culture substrates often consist of bio-inert background materials that present chemically-defined biological cues to drive angiogenic cell behaviors with a high degree of consistency and predictability. A commonly used material is poly(ethylene glycol) (PEG), a hydrophilic polymer that resists non-specific protein adsorption and serves as a “blank slate” material upon which to present biological signals to cells [51]. PEG does not provide molecular signaling cues itself, so any cues that mediate angiogenesis must be purposefully incorporated into PEG-based materials. Other examples of blank background materials include poly(vinyl) alcohol (PVA) [52-54], polyacrylamide (pAm) [54], alginate [55], and dextran [56, 57]. A number of studies have modified these materials with biomolecules that control cell behavior through mechanisms including adhesion, growth factor signaling and matrix degradation, and these cues may be

leveraged to generate synergistic signaling and provide the environments needed to induce desired angiogenic phenotypes from endothelial cells.

2.4.2 Adhesion molecules

Among the most critical biomolecules included into a cell culture material are ligands to promote cell adhesion. The most commonly used mediator of cell-material adhesion is the Arg-Gly-Asp amino acid sequence (RGD) derived from numerous cell-adhesive proteins present in the ECM [58]. Even though its adhesive capabilities are well known and characterized in cell culture systems [59], RGD presentation has been continuously improved in the form of optimized concentrations and spatial patterns to understand and control angiogenesis.

Recently studies have cultured endothelial cells in environments presenting ranges of RGD concentrations to find optimal conditions for promoting pro-angiogenic cell behaviors. Cultures of human umbilical vein endothelial cells (HUVECs) and endothelial cells from aortic ring explants in three dimensional (3D) culture environments have demonstrated that insufficient concentrations of RGD result in decreased cell viability, while excessive RGD concentrations typically result in either arrest of cell migration or excessive matrix degradation through integrin-mediated expression of matrix metalloproteinases (MMPs) [32, 60]. However, exceptions such as a study demonstrating that high concentrations of RGD do not arrest vacuole formation by endothelial colony forming cells (ECFCs) [61] suggest that the effects of adhesion on angiogenic cell behavior may vary between different cell types. To further pursue mechanisms dictating concentration-dependent effects of RGD, the impact of modulating surface RGD molecule spacing on bovine aortic endothelial cell phenotype was investigated. While all investigated

RGD densities supported cell adhesion, the spacing of RGD molecules on a cell culture substrate modulated VEGF signaling and cell migration potential by influencing focal adhesion assembly and focal adhesion kinase (FAK) signaling. Specifically, spacing of approximately 44 nm between RGD molecules enabled maximized FAK signaling [62].

Spatial patterning of RGD via photolithography has been leveraged to modulate endothelial tubule formation. One application of spatial patterning is to define where the formation of microvasculature is permitted in a material, but patterning can also impact morphologies and stability of capillary vessels. In one study the aspect ratios of RGD patterns presented on PEG hydrogels determined whether endothelial cells formed cell sheets or tubule-like structures [63], and that 100-200 μm-wide RGD patterns on PEG hydrogels forced HUVECs to form elongated cell aggregates that resembled tubules [64].

In addition to RGD other studies have explored the ability of the laminin-mimicking peptides YIGSR and IKVAV to modulate numerous angiogenic endothelial cell behaviors. YIGSR or IKVAV presented with RGD in PEG hydrogels have induced greater tubule formation by HUVECs than with RGD alone [65]. Efforts have been taken to optimize the concentrations of multiple adhesion motifs to control angiogenic cell behaviors to a degree that cannot be achieved with RGD alone. An innovative example is a study from Collier and coworkers on the use of cell culture substrates composed entirely of synthetic peptides, and compositionally optimized using a design of experiments approach. The acetylated QQKFQFQFEQQ peptide known as “Q11” has been demonstrated to form β-sheets fibers when used as the basic building block of peptide substrates. These peptides are amenable to modifications, as Q11 can be terminated with cell-adhesive amino acid sequences including RGDS, REDV, IKVAV and YIGSR [66-68]. An advantage to using modified Q11 peptides to modulate cell adhesion is that multiple adhesion

ligands may be added to hydrogel formulations individually and orthogonally. This enabled the optimization of adhesion ligand concentrations in a hydrogel to maximize endothelial cell behaviors such as proliferation, viability and adhesion [68].

While peptides have been shown to be effective for modulating cell-material adhesion and mimicking some of the functions of ECM proteins, studies have begun to explore the incorporation of full-length ECM proteins into synthetic materials. In one study human aortic endothelial cells (HAECs) were cultured in the presence of either full-length Collagen or a Collagen-mimicking peptide SCL2-2 presented on PEG hydrogels. Particularly, SCL2-2 is a Collagen mimicking protein presenting mainly GFPGER as the adhesion domain [69]. The HAECs had greater levels of NOS3 protein expression, gene expression of NOS3, Thrombomodulin and Selectin-E, and proliferation when cultured using full-length Collagen rather than SCL2-2. While the effects of full-length proteins are comprehensive, they may compromise the non-fouling nature of inert background materials and may require greater control of regiospecific chemistries for material incorporations in order to avoid interference with essential biological epitopes.

2.4.3 Growth factor signaling

Growth factor signaling ligands have been integrated into biomaterials as either short growth factor-mimicking peptides or full-length growth factors. For example, a short peptide sequence, termed “QK”, that mimicks the receptor-binding regions of VEGF [70], has been used to enhance angiogenesis. QK was coupled along with RGD to PEG hydrogels and increased the length of endothelial tubule structures to levels above those reached on hydrogels functionalized

with RGD alone [71]. When integrated into Collagen hydrogels via a helical Collagen mimicking domain (CMP) the addition of a modular CMP-QK peptide induced the formation of elongated endothelial cell structures in two-dimensional (2D) cell culture and enhanced capillary sprouting in three dimensional (3D) culture [72, 73]. Analogous techniques have been used to couple the modular QK to PEG hydrogels [64] and to hydroxyapatite scaffolds [74]. Use of the modular peptides enables patterning of QK not just by photopatterning, but also by the use of fluid flow and partial dipping of biomaterials into modular QK solutions.

Full-length VEGF has been coupled to cell culture substrates to enhance angiogenic cell behavior. One study covalently immobilized and spatially patterned VEGF into PEG hydrogels via NHS chemistry and spatially directed endothelial cell network formation [63]. Full-length VEGF has also improved proliferation in endothelial cells when attached via EDC/NHS-coupling to electrospun micro-and nano-fibers of poly(ε-caprolactone) [75]. VEGF was also patterned into Collagen sponges in spatially defined areas to permit formation of microvascular networks. This was achieved by extruding Collagen mixed with an aqueous VEGF solution onto a copper plate, freezing, then inserting the frozen Collagen-VEGF stripes into a larger Collagen sponge [76].

Other growth factors besides VEGF have also been shown to modulate angiogenic cell behaviors when attached to biomaterials. PDGF-BB and bFGF were incorporated into PEG hydrogels via succinimidyl ester coupling to observe effects on HUVEC and 10T1/2 pericyte co-cultures. When attached to a PEG hydrogel bFGF and PDGF-BB worked in concert to increase tubule network length, albeit by different mechanisms. While PDGF-BB increased pericyte proliferation, bFGF increased HUVEC migration speeds in 2D and 3D cultures and thereby induced network disruption. When PDGF-BB was included in hydrogels alone, tubule formation

occurred whether PDGF-BB was soluble or attached to the hydrogel [77]. When HUVECs were cultured in the presence of releasable PDGF-BB and insoluble Ephrin A1, a matrix-bound receptor tyrosine kinase ligand, the PDGF-BB did not affect endothelial tubule widths in a 2D or 3D environment[78].

While the direct attachment of growth factors to scaffolds has been proven to enhance angiogenic response by endothelial cells, one potential limitation of covalently attaching receptor-binding molecules to substrates is that they may prevent receptor internalization or dimerization [79, 80]. In one extreme example, VEGF-mediated endothelial network formation in Matrigel was inhibited by an immobilized QK peptide that could not be released from the surrounding environment, and the putative mechanism involved "receptor pinning" by immobilized QK [81]. Numerous other strategies have been used to modulate soluble growth factor signaling dynamics via strategies that mimic *in-vivo* mechanisms. The *in-vivo* ECM is capable of passive and cell-mediated release of soluble growth factors including VEGF [39], bFGF [40], and other pro-angiogenic growth factors. With the presence of heparin and other proteoglycans the ECM is also capable of modulating growth factor signaling dynamics by enhancing growth factor stabilization and concentration in the matrix [39-42]. Strategies to mimic relevant ECM-growth factor interactions have been extensively reviewed elsewhere, and include temporal control over growth factor release [82], spatial control over growth factor gradients [83], and inclusion of growth-factor binding and sequestering molecules to the matrix [84, 85].

2.4.4 Mechanical properties

The stiffness of the cellular microenvironment is a critical mediator of cell phenotype, and is a distinguishing feature when comparing normal and diseased (e.g. cancerous) tissues [29]. Optimized stiffness ranges have been identified that enable endothelial cell network formation in 2D and 3D environments. For example lower stiffness (140 Pa) polyacrylamide substrates functionalized with 0.1 mM RGD promoted formation of endothelial cell networks while higher stiffness substrates (2500 Pa) promoted formation of confluent endothelial cell sheets [86]. On collagen-coated polyacrylamide substrates stiffness dictated the expression of pro-angiogenic genes as well as osteogenic genes in HUVECs. Specifically, VEGFR2 was upregulated on 3 kPa substrates, while angiogenic and osteogenic genes were upregulated on 30 kPa substrates [87]. In 3D environments a balance between matrix degradability and stability is required to foster HUVEC network formation. One study putatively demonstrated a need for matrices that are degradable to permit remodeling and cell migration, but are stable enough to prevent the collapse of a forming vascular network [32]. Interestingly, HUVECs in 3D environments have variable responses to drug treatment depending on the surrounding stiffness and the presence of tumor-derived growth factors. Specifically, HUVECs in one study were more sensitive to the angiogenesis inhibitor Vandetenib in softer substrates than stiffer substrates, and treatment with tumor-derived growth factors removed stiffness effects on HUVEC network formation and decreased drug sensitivity [88]. Finally, the density of a hydrogel network also affects endothelial cell responses to VEGF gradients. Specifically, enhanced collagen density increased sprout polarization toward increasing concentrations of VEGF and increased sprout stability [36].

Hydrogel stiffness can be tuned by changing polymer concentration [89], crosslinking density [32, 90, 91] or degradation dynamics in most materials. Other strategies have recently been used

to change mechanical properties while also decoupling polymer network density and mechanical stiffness. Collagen modification with tyramine groups and treatment with peroxidases have enabled covalent crosslinking of Collagen substrates while still enabling cell-ECM interactions [92], and the crosslinking density modulated network formation by ECFCs. Additionally the impact of changing stiffness via crosslinking density independently of Collagen density was explored by crosslinking Collagen after non-enzymatic glycation [38]. Increased matrix stiffness increased bovine arterial endothelial cell spreading and capillary sprouting from spheroids. These techniques allowed investigators to explore the effects of changing mechanics without simultaneously affecting the density of structural molecules and insoluble signaling molecules presented to cells.

The degradability of the surrounding matrix can be modulated in synthetic biomaterials. Previous studies have demonstrated that degradability is critical to enabling cellular network formation in 2D [93] and 3D [89] endothelial cell cultures. Many PEG-based hydrogels are crosslinked into a coherent polymer network through the use of cell-degradable crosslinking molecules. Hydrogels are often fully or partially crosslinked using pegylated mimics of a MMP-labile site on Collagen, and the sequence may be modified to enhance or inhibit degradability. For example, the native MMP-labile amino acid sequence of GIAG can be exchanged for GIWG for enhanced degradability or GPAG for inhibited degradability. These changes have been shown to affect the rate of endothelial cell sprouting in an aortic arch assay [94]. Another strategy to modulate degradability is the use of crosslinking peptides with a single MMP-labile site versus peptides with multiple MMP-labile sites, and this strategy has been used to dictate HUVEC migration [95].

To further define the shape of endothelial cell networks and directionality of angiogenic sprouting in biomaterials modulus and degradability can be spatially defined using innovative techniques. For example, perfusion-based frontal polymerization, the uneven photopolymerization of hydrogels as a result of a concentration gradient of Eosin Y photoinitiator, generates hydrogels with graded density that dictates the direction of growth by sprouting endothelial cells [96]. Spatially patterned degradability has been achieved via multiple methods. Degradability in Hyaluronic acid hydrogels was defined by adding MMP-labile crosslinking groups. In addition, a secondary means of regulating degradability was achieved via UV photopolymerization of acrylated hyaluronic acid to make certain areas of the hydrogel impassible, thereby dictating locations of ECFC vessel formation [97].

To further model mechanical stiffness of pathogenic environments, biomaterial mineralization can change both the modulus of a material as well as interactions with cell adhesion ligands and growth factors. One study mineralized Fibrin matrices with 0.2% hydroxyapatite solutions to maximize angiogenic sprout number, length and invasion speed by HUVECs [98]. Scaffold mineralization provides compelling opportunities to culture endothelial cells in matrices where stiffness is tuned without increasing polymer density and crosslinking density, and also enables the generation of sophisticated bone disease models such as bone cancer and ectopic tissue mineralization [99, 100].

2.4.5 Hypoxic environments

Numerous vascular disorders lead to decreased levels of dissolved oxygen present in surrounding tissue. This is known to significantly affect endothelial cell phenotype [101] through signaling by

Hypoxia Inhibitory Factor (HIF). Though tests requiring the establishment of a hypoxic environment can be achieved using specialized incubators and bioreactors with controlled atmospheric conditions, recent work has enabled the use of biomaterials to expose cells to hypoxic conditions for prolonged periods of time and generate spatially varying oxygen gradients in endothelial cell culture.

Oxygen control has been achieved in gelatin-based materials by including a ferulic acid crosslinking molecule and initiating a crosslinking reaction with Laccase. The crosslinking reaction then consumes oxygen and maintains low oxygen conditions for up to 1 hour after polymerization. This has caused increased expression of HIF1α and HIF2α in ECFCs, both of which are necessary to achieve vascular network formation [102]. The Laccase-based crosslinking mechanism was carried over to Dextran-based hydrogels in which oxygen consumption was achieved during crosslinking of tyramine-functionalized dextran. Here, hypoxic conditions in the hydrogels were maintained for up to 12 hours in the hydrogels, and the duration of hypoxia is tunable through polymer concentration and stiffness [103]. Materials that regulate dissolved oxygen levels in endothelial cell culture represent an adaptable approach to regulating the cellular microenvironment without the need for bioreactors or similar instrumentation.

2.4.6 Co-culture systems

In tumors endothelial cells are not exclusively affected by environmental features discussed so far. Cancer cells in the tumor also respond to environmental cues and subsequently affect the vascular network through physical contact and paracrine signaling. Studies utilizing biomaterials

to define populations of endothelial-cancer cell co-cultures and affect phenotypes of heterotypic cell populations are only beginning to be applied toward modeling tumor vasculature.

Discrete spatial patterning of heterotypic cell populations has been achieved though micro-contact printing. The segregation of breast cancer cells in Hyaluronic acid hydrogels from ECFCs in Fibrin hydrogels was performed using sequential micro-contact printing [104]. Discrete patterning of HUVECs and HeLa cancer cell populations has been recently achieved on 2D cell culture systems by combining micro-contact printing, activation of un-patterned PVA with dopamine, and sequential cell seeding [105]. Taken together, these technologies enable the construction of models where ECM cues reviewed here modulate behavior of both endothelial cells and surrounding tumor cells to holistically recapitulate features of an *in-vivo* tumor environment.

2.5 Conclusion

Recently developed technologies in biomaterials development are leading to unprecedented control over *in-vitro* endothelial cell culture environments as well as the ability to model phenomena surrounding normal and pathological angiogenesis. With the systematic utilization of the techniques reviewed here, models of tumor vasculature will cultivate a greater understanding of far-reaching side effects of anti-angiogenic that will translate into dramatic improvements in cancer therapy.

2.6 References

[1] De Smet F, Segura I, De Bock K, Hohensinner P, Carmeliet P. Mechanisms of Vessel Branching Filopodia on Endothelial Tip Cells Lead the Way. Arteriosclerosis Thrombosis and Vascular Biology. 2009;29:639-49.

[2] Ribatti D. Judah Folkman, a pioneer in the study of angiogenesis. Angiogenesis. 2008;11:3-10.

[3] Folkman J, Long DM, Becker FF. Growth and metastasis of tumor in organ culture. Cancer. 1963;16:453-67.

[4] Wang Y, Fei D, Vanderlaan M, Song A. Biological activity of bevacizumab, a humanized anti-VEGF antibody in vitro. Angiogenesis. 2004;7:335-45.

[5] Mendel DB, Laird AD, Xin X, Louie SG, Christensen JG, Li G, et al. In vivo antitumor activity of SU11248, a novel tyrosine kinase inhibitor targeting vascular endothelial growth factor and platelet-derived growth factor receptors: determination of a pharmacokinetic/pharmacodynamic relationship. Clin Cancer Res. 2003;9:327-37.

[6] De Falco S. Antiangiogenesis therapy: an update after the first decade. Korean J Intern Med. 2014;29:1-11.

[7] Cao Y, Langer R. Optimizing the delivery of cancer drugs that block angiogenesis. Sci Transl Med. 2010;2:15ps3.

[8] Batchelor TT, Mulholland P, Neyns B, Nabors LB, Campone M, Wick A, et al. Phase III randomized trial comparing the efficacy of cediranib as monotherapy, and in combination with lomustine, versus lomustine alone in patients with recurrent glioblastoma. J Clin Oncol. 2013;31:3212-8.

[9] Gilbert MR, Dignam JJ, Armstrong TS, Wefel JS, Blumenthal DT, Vogelbaum MA, et al. A randomized trial of bevacizumab for newly diagnosed glioblastoma. N Engl J Med. 2014;370:699-708.

[10] Loges S, Schmidt T, Carmeliet P. Mechanisms of resistance to anti-angiogenic therapy and development of third-generation anti-angiogenic drug candidates. Genes Cancer. 2010;1:12-25.

[11] Welti J, Loges S, Dimmeler S, Carmeliet P. Recent molecular discoveries in angiogenesis and antiangiogenic therapies in cancer. J Clin Invest. 2013;123:3190-200.

[12] Lu KV, Chang JP, Parachoniak CA, Pandika MM, Aghi MK, Meyronet D, et al. VEGF inhibits tumor cell invasion and mesenchymal transition through a MET/VEGFR2 complex. Cancer Cell. 2012;22:21-35.

[13] Seftor RE, Hess AR, Seftor EA, Kirschmann DA, Hardy KM, Margaryan NV, et al. Tumor cell vasculogenic mimicry: from controversy to therapeutic promise. Am J Pathol. 2012;181:1115-25.

[14] Maniotis AJ, Folberg R, Hess A, Seftor EA, Gardner LM, Pe'er J, et al. Vascular channel formation by human melanoma cells in vivo and in vitro: vasculogenic mimicry. Am J Pathol. 1999;155:739-52.

[15] Zeisberg E, Potenta S, Xie L, Zeisberg M, Kalluri R. Discovery of endothelial to mesenchymal transition as a source for carcinoma-associated fibroblasts. Cancer Research. 2007;67:10123-8.

[16] Potenta S, Zeisberg E, Kalluri R. The role of endothelial-to-mesenchymal transition in cancer progression. British Journal of Cancer. 2008;99:1375-9.

[17] Ma J, Waxman DJ. Combination of antiangiogenesis with chemotherapy for more effective cancer treatment. Mol Cancer Ther. 2008;7:3670-84.

[18] Nagy JA, Chang SH, Dvorak AM, Dvorak HF. Why are tumour blood vessels abnormal and why is it important to know? Br J Cancer. 2009;100:865-9.

[19] McDonald DM, Baluk P. Significance of blood vessel leakiness in cancer. Cancer Res. 2002;62:5381-5.

[20] Goel S, Duda DG, Xu L, Munn LL, Boucher Y, Fukumura D, et al. Normalization of the vasculature for treatment of cancer and other diseases. Physiol Rev. 2011;91:1071-121.

[21] Huang Y, Yuan J, Righi E, Kamoun WS, Ancukiewicz M, Nezivar J, et al. Vascular normalizing doses of antiangiogenic treatment reprogram the immunosuppressive tumor microenvironment and enhance immunotherapy. Proc Natl Acad Sci U S A. 2012;109:17561-6.

[22] Cesca M, Bizzaro F, Zucchetti M, Giavazzi R. Tumor delivery of chemotherapy combined with inhibitors of angiogenesis and vascular targeting agents. Front Oncol. 2013;3:259.

[23] Sarkanen JR, Mannerström M, Vuorenpää H, Uotila J, Ylikomi T, Heinonen T. Intra-Laboratory Pre-Validation of a Human Cell Based in vitro Angiogenesis Assay for Testing Angiogenesis Modulators. Front Pharmacol. 2010;1:147.

[24] Faulkner A, Purcell R, Hibbert A, Latham S, Thomson S, Hall WL, et al. A thin layer angiogenesis assay: a modified basement matrix assay for assessment of endothelial cell differentiation. BMC Cell Biol. 2014;15:41.

[25] Evensen L, Micklem DR, Link W, Lorens JB. A novel imaging-based high-throughput screening approach to anti-angiogenic drug discovery. Cytometry A. 2010;77:41-51.

[26] Staton CA, Reed MW, Brown NJ. A critical analysis of current in vitro and in vivo angiogenesis assays. Int J Exp Pathol. 2009;90:195-221.

[27] Jakobsson L, Claesson-Welsh L. Vascular basement membrane components in angiogenesis-an act of balance. ScientificWorldJournal. 2008;8:1246-9.

[28] Baluk P, Morikawa S, Haskell A, Mancuso M, McDonald DM. Abnormalities of basement membrane on blood vessels and endothelial sprouts in tumors. Am J Pathol. 2003;163:1801-15.

[29] Fang M, Yuan J, Peng C, Li Y. Collagen as a double-edged sword in tumor progression. Tumour Biol. 2014;35:2871-82.

[30] Davis G, Senger D. Endothelial extracellular matrix - Biosynthesis, remodeling, and functions during vascular morphogenesis and neovessel stabilization. Circulation Research. 2005;97:1093-107.

[31] Weis SM, Cheresh DA. αV integrins in angiogenesis and cancer. Cold Spring Harb Perspect Med. 2011;1:a006478.

[32] Nguyen EH, Zanotelli MR, Schwartz MP, Murphy WL. Differential effects of cell adhesion, modulus and VEGFR-2 inhibition on capillary network formation in synthetic hydrogel arrays. Biomaterials. 2014;35:2149-61.

[33] Senger DR, Perruzzi CA. Cell migration promoted by a potent GRGDS-containing thrombin-cleavage fragment of osteopontin. Biochim Biophys Acta. 1996;1314:13-24.

[34] Zovein A, Luque A, Turlo K, Hofmann J, Yee K, Becker M, et al. beta 1 Integrin Establishes Endothelial Cell Polarity and Arteriolar Lumen Formation via a Par3-Dependent Mechanism. Developmental Cell. 2010;18:39-51.

[35] Bayless KJ, Salazar R, Davis GE. RGD-dependent vacuolation and lumen formation observed during endothelial cell morphogenesis in three-dimensional fibrin matrices involves the alpha(v)beta(3) and alpha(5)beta(1) integrins. Am J Pathol. 2000;156:1673-83.

[36] Shamloo A, Heilshorn C. Matrix density mediates polarization and lumen formation of endothelial sprouts in VEGF gradients. Lab on a Chip. 2010;10:3061-8.

[37] Sun G, Shen YI, Kusuma S, Fox-Talbot K, Steenbergen CJ, Gerecht S. Functional neovascularization of biodegradable dextran hydrogels with multiple angiogenic growth factors. Biomaterials. 2011;32:95-106.

[38] Mason B, Starchenko A, Williams R, Bonassar A, Reinhart-King C. Tuning three-dimensional collagen matrix stiffness independently of collagen concentration modulates endothelial cell behavior. Acta Biomaterialia. 2013;9:4635–44.

[39] Wijelath E, Namekata M, Murray J, Furuyashiki M, Zhang S, Coan D, et al. Multiple Mechanisms for Exogenous Heparin Modulation of Vascular Endothelial Growth Factor Activity. Journal of Cellular Biochemistry. 2010;111:461-8.

[40] Forsten-Williams K, Chua C, Nugent M. The kinetics of FGF-2 binding to heparan sulfate proteoglycans and MAP kinase signaling. Journal of Theoretical Biology. 2005;233:483-99.

[41] Smith JC, Hagemann A, Saka Y, Williams PH. Understanding how morphogens work. Philosophical Transactions of the Royal Society B: Biological Sciences. 2008;363:1387-92.

[42] Hudalla G, Koepsel J, Murphy W. Surfaces That Sequester Serum-Borne Heparin Amplify Growth Factor Activity. Advanced Materials. 2011;23:5415-8.

[43] Cebe-Suarez S, Zehnder-Fjallman A, Ballmer-Hofer K. The role of VEGF receptors in angiogenesis; complex partnerships. Cellular and Molecular Life Sciences. 2006;63:601-15.

[44] Somanath P, Malinin N, Byzova T. Cooperation between integrin alpha(nu)beta(3) and VEGFR2 in angiogenesis. Angiogenesis. 2009;12:177-85.

[45] Mammoto A, Connor K, Mammoto T, Yung C, Huh D, Aderman C, et al. A mechanosensitive transcriptional mechanism that controls angiogenesis. Nature. 2009;457:1103-U57.

[46] Bryan B, Dennstedt E, Mitchell D, Walshe T, Noma K, Loureiro R, et al. RhoA/ROCK signaling is essential for multiple aspects of VEGF-mediated angiogenesis. Faseb Journal. 2010;24:3186-95.

[47] van Nieuw Amerongen GP, Koolwijk P, Versteilen A, van Hinsbergh VW. Involvement of RhoA/Rho kinase signaling in VEGF-induced endothelial cell migration and angiogenesis in vitro. Arterioscler Thromb Vasc Biol. 2003;23:211-7.

[48] Ingber DE. Mechanical signaling and the cellular response to extracellular matrix in angiogenesis and cardiovascular physiology. Circ Res. 2002;91:877-87.

[49] Smithmyer ME, Sawicki LA, Kloxin AM. Hydrogel scaffolds as in vitro models to study fibroblast activation in wound healing and disease. Biomater Sci. 2014;2:634-50.

[50] Cushing MC, Anseth KS. Materials science. Hydrogel cell cultures. Science. 2007;316:1133-4.

[51] Lutolf MP, Hubbell JA. Synthetic biomaterials as instructive extracellular microenvironments for morphogenesis in tissue engineering. Nature Biotechnology. 2005;23:47-55.

[52] Nuttelman CR, Henry SM, Anseth KS. Synthesis and characterization of photocrosslinkable, degradable poly(vinyl alcohol)-based tissue engineering scaffolds. Biomaterials. 2002;23:3617-26.

[53] Schmedlen KH, Masters KS, West JL. Photocrosslinkable polyvinyl alcohol hydrogels that can be modified with cell adhesion peptides for use in tissue engineering. Biomaterials. 2002;23:4325-32.

[54] Zustiak SP, Wei Y, Leach JB. Protein-hydrogel interactions in tissue engineering: mechanisms and applications. Tissue Eng Part B Rev. 2013;19:160-71.

[55] Sun J, Tan H. Alginate-Based Biomaterials for Regenerative Medicine Applications. Materials. 2013;6:1285-309.

[56] Lévesque SG, Shoichet MS. Synthesis of cell-adhesive dextran hydrogels and macroporous scaffolds. Biomaterials. 2006;27:5277-85.

[57] Lévesque SG, Lim RM, Shoichet MS. Macroporous interconnected dextran scaffolds of controlled porosity for tissue-engineering applications. Biomaterials. 2005;26:7436-46.

[58] Ruoslahti E. RGD and other recognition sequences for integrins. Annu Rev Cell Dev Biol. 1996;12:697-715.

[59] Bellis SL. Advantages of RGD peptides for directing cell association with biomaterials. Biomaterials. 2011;32:4205-10.

[60] Shen C, Raghavan S, Xu Z, Baranski J, Yu X, Wozniak M, et al. Decreased cell adhesion promotes angiogenesis in a Pyk2-dependent manner. Experimental Cell Research. 2011;317:1860-71.

[61] Hanjaya-Putra D, Bose V, Shen Y, Yee J, Khetan S, Fox-Talbot K, et al. Controlled activation of morphogenesis to generate a functional human microvasculature in a synthetic matrix. Blood. 2011;118:804-15.

[62] Le Saux G, Magenau A, Gunaratnam K, Kilian K, Bocking T, Gooding J, et al. Spacing of Integrin Ligands Influences Signal Transduction in Endothelial Cells. Biophysical Journal. 2011;101:764-73.

[63] Leslie-Barbick JE, Shen C, Chen C, West JL. Micron-scale spatially patterned, covalently immobilized vascular endothelial growth factor on hydrogels accelerates endothelial tubulogenesis and increases cellular angiogenic responses. Tissue Eng Part A. 2011;17:221-9.

[64] Stahl P, Chan T, Shen Y-I, Sun G, Gerecht S, Yu M. Capillary Network-Like Organization of Endothelial Cells in PEGDA Scaffolds Encoded with Angiogenic Signals via Triple Helical Hybridization. Advanced Functional Materials. 2014;24:3213–25.

[65] Ali S, Saik JE, Gould DJ, Dickinson ME, West JL. Immobilization of Cell-Adhesive Laminin Peptides in Degradable PEGDA Hydrogels Influences Endothelial Cell Tubulogenesis. Biores Open Access. 2013;2:241-9.

[66] Jung JP, Jones JL, Cronier SA, Collier JH. Modulating the mechanical properties of self-assembled peptide hydrogels via native chemical ligation. Biomaterials. 2008;29:2143-51.

[67] Jung JP, Nagaraj AK, Fox EK, Rudra JS, Devgun JM, Collier JH. Co-assembling peptides as defined matrices for endothelial cells. Biomaterials. 2009;30:2400-10.

[68] Jung JP, Moyano JV, Collier JH. Multifactorial optimization of endothelial cell growth using modular synthetic extracellular matrices. Integr Biol (Camb). 2011;3:185-96.

[69] Munoz-Pinto DJ, Guiza-Arguello VR, Becerra-Bayona SM, Erndt-Marino J, Samavedi S, Malmut S, et al. Collagen-mimetic hydrogels promote human endothelial cell adhesion, migration and phenotypic maturation Journal of Materials Chemistry B. 2015;3:7912-9.

[70] D'Andrea LD, Iaccarino G, Fattorusso R, Sorriento D, Carannante C, Capasso D, et al. Targeting angiogenesis: structural characterization and biological properties of a de novo engineered VEGF mimicking peptide. Proc Natl Acad Sci U S A. 2005;102:14215-20.

[71] Leslie-Barbick J, Saik J, Gould D, Dickinson M, West J. The promotion of microvasculature formation in poly(ethylene glycol) diacrylate hydrogels by an immobilized VEGF-mimetic peptide. Biomaterials. 2011;32:5782-9.

[72] Chan T, Stahl P, Yu S. Matrix-Bound VEGF Mimetic Peptides: Design and Endothelial-Cell Activation in Collagen Scaffolds. Advanced Functional Materials. 2011;21:4252-62.

[73] Chan T, Stahl P, Li Y, Yu M. Collagen–gelatin mixtures as wound model, and substrates for VEGF-mimetic peptide binding and endothelial cell activation. Acta Biomaterialia. 2015;15:164-72.

[74] Lee JS, Wagoner Johnson AJ, Murphy WL. A modular, hydroxyapatite-binding version of vascular endothelial growth factor. Adv Mater. 2010;22:5494-8.

[75] Guex AG, Hegemann D, Giraud MN, Tevaearai HT, Popa AM, Rossi RM, et al. Covalent immobilisation of VEGF on plasma-coated electrospun scaffolds for tissue engineering applications. Colloids Surf B Biointerfaces. 2014;123:724-33.

[76] Oh HH, Lu H, Kawazoe N, Chen G. Spatially guided angiogenesis by three-dimensional collagen scaffolds micropatterned with vascular endothelial growth factor. J Biomater Sci Polym Ed. 2012;23:2185-95.

[77] Saik J, Gould D, Watkins E, Dickinson M, West J. Covalently immobilized platelet-derived growth factor-BB promotes antiogenesis in biomirnetic poly(ethylene glycol) hydrogels. Acta Biomaterialia. 2011;7:133-43.

[78] Saik JE, Gould DJ, Keswani AH, Dickinson ME, West JL. Biomimetic hydrogels with immobilized ephrinA1 for therapeutic angiogenesis. Biomacromolecules. 2011;12:2715-22.

[79] Santos SC, Miguel C, Domingues I, Calado A, Zhu Z, Wu Y, et al. VEGF and VEGFR-2 (KDR) internalization is required for endothelial recovery during wound healing. Exp Cell Res. 2007;313:1561-74.

[80] Simons M. An inside view: VEGF receptor trafficking and signaling. Physiology (Bethesda). 2012;27:213-22.

[81] Koepsel J, Nguyen E, Murphy W. Differential effects of a soluble or immobilized VEGFR-binding peptide. Integrative Biology. 2012;4:914-24.

[82] Lee K, Silva EA, Mooney DJ. Growth factor delivery-based tissue engineering: general approaches and a review of recent developments. J R Soc Interface. 2011;8:153-70.

[83] Nguyen E, Schwartz M, Murphy W. Biomimetic Approaches to Control Soluble Concentration Gradients in Biomaterials. Macromolecular Bioscience. 2011;11:483-92.

[84] Belair DG, Le NN, Murphy WL. Design of growth factor sequestering biomaterials. Chem Commun (Camb). 2014;50:15651-68.

[85] Hudalla GA, Murphy WL. Biomaterials that regulate growth factor activity via bioinspired interactions. Adv Funct Mater. 2011;21:1754-68.

[86] Saunders R, Hammer D. Assembly of Human Umbilical Vein Endothelial Cells on Compliant Hydrogels. Cellular and Molecular Bioengineering. 2010;3:60-7.

[87] Santos L, Fuhrmann G, Juenet M, Amdursky N, Horejs CM, Campagnolo P, et al. Extracellular Stiffness Modulates the Expression of Functional Proteins and Growth Factors in Endothelial Cells. Adv Healthc Mater. 2015.

[88] Wu Y, Guo B, Ghosh G. Differential Effects of Tumor Secreted Factors on Mechanosensitivity, Capillary Branching, and Drug Responsiveness in PEG Hydrogels. Ann Biomed Eng. 2015;43:2279-90.

[89] Moon JJ, Saik JE, Poche RA, Leslie-Barbick JE, Lee SH, Smith AA, et al. Biomimetic hydrogels with pro-angiogenic properties. Biomaterials. 2010;31:3840-7.

[90] Kloxin AM, Kloxin CJ, Bowman CN, Anseth KS. Mechanical Properties of Cellularly Responsive Hydrogels and Their Experimental Determination. Advanced Materials. 2010;22:3484-94.

[91] Hansen TD, Koepsel JT, Le NN, Nguyen EH, Zorn S, Parlato M, et al. Biomaterial arrays with defined adhesion ligand densities and matrix stiffness identify distinct phenotypes for tumorigenic and nontumorigenic human mesenchymal cell types. Biomater Sci. 2014;2:745-56.

[92] Kuo KC, Lin RZ, Tien HW, Wu PY, Li YC, Melero-Martin JM, et al. Bioengineering vascularized tissue constructs using an injectable cell-laden enzymatically crosslinked collagen hydrogel derived from dermal extracellular matrix. Acta Biomater. 2015;27:151-66.

[93] Zhu J, He P, Lin L, Jones DR, Marchant RE. Biomimetic poly(ethylene glycol)-based hydrogels as scaffolds for inducing endothelial adhesion and capillary-like network formation. Biomacromolecules. 2012;13:706-13.

[94] Miller J, Shen C, Legant W, Baranski J, Blakely B, Chen C. Bioactive hydrogels made from step-growth derived PEG-peptide macromers. Biomaterials. 2010;31:3736-43.

[95] Sokic S, Christenson M, Larson J, Appel A, EM B, Papavasiliou G. Evaluation of MMP substrate concentration and specificity for neovascularization of hydrogel scaffolds. Biomaterials Science. 2014;2:1343-54.

[96] Turturro MV, Christenson MC, Larson JC, Young DA, Brey EM, Papavasiliou G. MMP-sensitive PEG diacrylate hydrogels with spatial variations in matrix properties stimulate directional vascular sprout formation. PLoS One. 2013;8:e58897.

[97] Hanjaya-Putra D, Wong KT, Hirotsu K, Khetan S, Burdick JA, Gerecht S. Spatial control of cell-mediated degradation to regulate vasculogenesis and angiogenesis in hyaluronan hydrogels. Biomaterials. 2012;33:6123-31.

[98] Jusoh N, Oh S, Kim S, Kim J, Jeon NL. Microfluidic vascularized bone tissue model with hydroxyapatite-incorporated extracellular matrix. Lab Chip. 2015;15:3984-8.

[99] Medici D, Shore E, Lounev V, Kaplan F, Kalluri R, Olsen B. Conversion of vascular endothelial cells into multipotent stem-like cells. Nature Medicine. 2010;16:1400-U80.

[100] Cenni E, Perut F, Baldini N. In vitro models for the evaluation of angiogenic potential in bone engineering. Acta Pharmacol Sin. 2011;32:21-30.

[101] Kusuma S, Zhao S, Gerecht S. The extracellular matrix is a novel attribute of endothelial progenitors and of hypoxic mature endothelial cells. FASEB J. 2012;26:4925-36.

[102] Park KM, Gerecht S. Hypoxia-inducible hydrogels. Nat Commun. 2014;5:4075.

[103] Park KM, Blatchley MR, Gerecht S. The design of dextran-based hypoxia-inducible hydrogels via in situ oxygen-consuming reaction. Macromol Rapid Commun. 2014;35:1968-75.

[104] Dickinson LE, Lütgebaucks C, Lewis DM, Gerecht S. Patterning microscale extracellular matrices to study endothelial and cancer cell interactions in vitro. Lab Chip. 2012;12:4244-8.

[105] Beckwith KM, Sikorski P. Patterned cell arrays and patterned co-cultures on polydopamine-modified poly(vinyl alcohol) hydrogels. Biofabrication. 2013;5:045009.

Chapter 3:

Differential inhibition of vascular morphogenesis by ToxCast™ chemical library on synthetic substrates and Matrigel™

Eric H. Nguyen, William T. Daly, Michael P. Schwartz, Ngoc Nhi Le, Thomas B. Knudsen, Nader Sheibani, William L. Murphy. Differential inhibition of vascular morphogenesis by ToxCast™ chemical library on synthetic substrates and Matrigel™. *In preparation*.

3.1 Preface

The purpose of these studies was to identify hydrogel substrates that mediate vascular network formation by endothelial cells and use them to identify potential vascular inhibitors from libraries of known and unknown chemical compounds. Here, cell adhesivity, elastic modulus and the ability to bind and sequester vascular endothelial growth factor were orthogonally controlled in poly(ethylene glycol) hydrogels. This study established methods to systematically vary multiple cell-instructive cues in defined hydrogels and identify desired hydrogels from large libraries of candidate formulations. In addition, this study established superiority of poly(ethylene glycol) hydrogels over Matrigel for screening chemical compounds.

3.2 Abstract

We describe the identification of synthetic hydrogels that promote in-vitro vascular network formation by endothelial cells as well as their utilization in screening systems to detect putative vascular disruptive compounds. Cell culture conditions that promoted vascular network formation were identified using a thin hydrogel array format for human umbilical vein endothelial cells as well as endothelial cells derived from induced pluripotent stem cells. A

screening system composed of synthetic hydrogels was compared directly to a Matrigel screening system and found to have superior sensitivity and repeatability as well as the ability to detect inhibition by mechanisms that are not detectable on Matrigel. The synthetic hydrogels were also customized to have a defined ability to bind and sequester vascular endothelial growth factor from the surrounding environment and this was demonstrated as a possible mechanism behind the reduced sensitivity of the Matrigel screening system.

3.3 Introduction

The ability to detect compounds which affect the human vasculature is of high importance due to the increasing number of diseases which are associated with vascular disorders within the human body. These disorders include various forms of cancer, atherosclerosis, stroke, diabetic retinopathy and developmental complications which can often result from exposure to compounds present within in our environment [1, 2]. In order to identify new drugs for treatment of these diseases and to protect against exposure to vascular disrupting compounds present within our environment, the ability to screen large chemical libraries for their ability to affect the vasculature is essential. Early investigations resulted in the development of an in-vitro vascular network formation assay in 1980 by Folkman and Haudenschild [3, 4]. Here cloned bovine and human capillary endothelial cells formed interconnected vascular networks in culture that were comparable to those seen in vivo in approximately 10 days. A more rapid assay (<24h) was later described in 1988 by Kubuto and colleagues and has become the gold standard method for the identification of inhibitors and stimulators of angiogenesis in drug discovery [5] and toxicological screens [6-8]. However, results of these screens are often uncertain, as evidenced

by significant numbers of pro- or anti-angiogenic drugs that fail in clinical trials [2, 9-11]. This highlights a need to redefine methodologies of such vascular screens.

The assay developed by Kabuto and colleagues has a number of inherent limitations due to the use of a natural extracellular matrix derived from Englebreth-Holm-Swarm (EHS) tumors produced in mice, now referred to as Matrigel™, EHS matrix™, Geltrex™ etc (hitherto referred to as Matrigel) [12-14], as a cell culture substrate. Matrigel consists of a laminin-rich matrix with an inherent compositional complexity and lack of lot-to-lot reproducibility. Proteomics analysis of consolidated normal and growth factor reduced Matrigel yielded a total of 1851 unique proteins that make up Matrigel and individual tests from two manufacturers showed only 53% batch-to-batch similarity in proteins identified [15]. Highly variable mechanical properties ranging from of 120 to 840 Pa [16, 17] elastic modulus at 37˚C results in poor handling characteristics and the need for precise temperature control during handling, resulting in user-to-user variability in addition to lot-to-lot variability. Numerous confounding factors such as locally sequestered and matrix-bound growth factors [18] as well as physiologically irrelevant mechanisms of inhibition such as bulk matrix dissolution by Suramin treatment [19, 20], have previously resulted in the identification of false positives and negatives in chemical compound screens. While Matrigel is a readily-available material capable of supporting long-term endothelial network assembly in the absence of support cell types, the limitations associated with the material motivate a need for alternative materials that enable the development of more advanced vascular screening assays.

Here we used an array-based material screening method to identify chemically defined, synthetic materials that provide an alternative to Matrigel for use in vascular screening systems. In this study poly (ethylene glycol) (PEG) hydrogels were developed to have defined characteristics

including cell adhesion, modulus, degradation and local sequestration of soluble growth factors from the environment [21]. In particular, a peptide mimicking vascular endothelial growth factor receptor 2 (VEGFR2), which has been demonstrated to non-coavlently bind and sequester soluble vascular endothelial growth factor (VEGF) [22, 23] was leveraged to overcome the inhibitory effects of certain vascular disrupting compounds within our assay system as a possible mechanism for modulating cell sensitivity to chemicals. The hydrogels also demonstrated customization for use with endothelial cells derived from multiple sources (human umbilical vein endothelial cells (HUVECs) and endothelial cells derived from induced pluripotent stem cells (IPSCs)), batch-to-batch reproducibility, and increased sensitivity over Matrigel for identifying inhibited and non-inhibited vascular development scenarios. To validate the new screening system, the synthetic hydrogel-based assay was compared directly to a Matrigel-based assay in its ability to identify compounds from the EPA's ToxCast™ chemical library.

3.4 Methods

3.4.1 Endothelial cell culture and maintenance

Human umbilical vein endothelial cells (HUVECs) were purchased from Lonza (Walkersville, MD) and cultured in growth medium consisting of medium 199 (M199) (Mediatech Inc, Manassas, VA) supplemented with EGM-2 Bulletkit (Lonza). The medium supplement contained 2% fetal bovine serum as well as hydrocortisone, hFGF-B, VEGF, R3-IGF-1, Ascorbic Acid, Heparin, FBS, hEGF, and GA-1000. Growth medium was changed every other day and cells were passaged every 5–7 days. Cell passages were performed using 0.05% trypsin solution (Thermo Fisher Scientific, Inc., Carlsbad, CA) and detached cells were recovered in

M199 supplemented with 10% cosmic calf serum (Thermo Fisher Scientific, Inc., Carlsbad, CA). All media was supplemented with 100 U/mL Penicillin/100 µg/mL Streptomycin (Thermo Fisher Scientific, Inc., Carlsbad, CA). The cells were maintained in a humidified 37 ˚C incubator with 5% CO_2 and used between 5 and 16 population doublings in all experiments.

Induced pluripotent stem cell derived endothelial cells (IPSC-ECs) were purchased from Cellular Dynamics International (Madison, WI) and cultured in full vasculife growth medium (Lifeline, Plateville, WI). Culture flasks were coated with 30 µg/ml human plasma fibronectin (Corning) for 30 minutes prior to use. Growth media was changed every other day and passaged every 3-4 days. Cells were detached using 0.05 % trypsin and recovered in basal media supplemented with 10 % cosmic calf serum. The cells were maintained in a humidified 37 ˚C incubator with 5% CO_2 and used between 5 and 16 population doublings in all experiments.

3.4.2 PEG functionalization with norbornene

Modification of PEG molecules with terminal norbornene groups was performed using methods similar to previous studies [24, 25]. Briefly, PEG-OH (20 kDa molecular weight, 8-arm, tripentaerythritol core, Jenkem USA, Allen TX), dimethylaminopyridine and pyridine (Sigma Aldrich, St. Louis, MO) were dissolved in anhydrous dichloromethane (Fisher Scientific, Waltham, MA). In a separate reaction vessel, N,N'-dicyclohexylcarbodiimide (Thermo Scientific, Waltham, MA) and norbornene carboxylic acid (Sigma Aldrich) were dissolved in anhydrous dichloromethane and reacted for 30 minutes to activate the norbornene. Norbornene carboxylic acid was covalently coupled to the PEG-OH through the carboxyl group by combining the PEG solution and norbornene solutions and stirring the reaction mixture overnight under anhydrous

conditions. Urea byproduct was removed from the reaction mixture using a glass fritted funnel and the filtrate was precipitated in cold diethyl ether (Thermo Fisher Scientific, Inc., Carlsbad, CA) to extract the norbornene-functionalized PEG (PEGNB). The precipitated PEGNB was collected and dried overnight in a ceramic fritted filter. To remove impurities, the PEGNB was dissolved in chloroform (Sigma Aldrich), precipitated in diethyl ether and dried a second time in a buchner funnel. To remove excess norbornene carboxylic acid, PEGNB was dissolved in de-ionized H_2O, dialyzed in de-ionized H_2O for 1 week and filtered through a Millex® 0.45 μm pore-size PVDF syringe filter (Millipore). The aqueous PEGNB solution was frozen using liquid nitrogen and lyophilized. Functionalization of PEG was quantified using proton nuclear magnetic resonance spectroscopy (NMR) to detect protons of the norbornene-associated alkene groups located at 6.8–7.2 PPM. Functionalization efficiency for norbornene coupling to PEG-OH arms was above 90% for all PEGNB used in these experiments.

3.4.3 Conjugating adhesion peptides to PEG

Lyophilized PEGNB was dissolved in DI- H_2O at a 0.5 mM concentration and combined with 0.05% w/v Irgacure 2959 photoinitiator (I2959) (Ciba Specialty Chemicals, Tarrytown, NY) as well as a 2x molar excess of either head-to-tail cyclized Arg-Gly-Asp-[d-Phe]-Cys (cyclic RGD, Genscript, Piscataway, NJ) adhesion peptide; 2x molar excess of linear Cys-Arg-Gly-Asp-Ser (CRGDS, Genscript, Piscataway, NJ); 2x molar excess of non-functional amidated Cys-Arg-Asp-Gly-Ser scrambled adhesion peptide (CRDGS, Genscript, Piscataway, NJ); 3x molar excess of amidated Cys-Glu-[d-Phe]-[d-Ala]-[d-Tyr]-[d-Leu]-Iso-Asp-Phe-Asn-Trp-Glu-Tyr-Pro-Ala-Ser-Lys (VBP), or 3x molar excess of the non-functional scrambled VBP peptide Cys-Asp-[d-Ala]-Pro-Tyr-Asn-[d-Phe]-Glu-Phe-Ala-Trp-Lys-[d-Tyr]-Iso-Ser-[d-Leu]-Glu. The mixtures

were reacted under 365 nm ultraviolet (UV) light for 5 min at a dose rate of 4.5 mW/cm^2 to covalently attach the peptides to norbornene groups via the thiol-ene reaction [26]. To remove buffer salts and unreacted peptides from the decorated PEGNB, the reaction mixtures were dialyzed in de-ionized H_2O for 2 days. The dialyzed solutions were frozen in liquid nitrogen and lyophilized. The coupling efficiency of peptides to the PEGNB was quantified using proton NMR to detect disappearances of alkene protons at 6.8–7.2 PPM caused by covalent bonding of the peptides to the norbornene group.

3.4.4 Patterned gold slides with hydrophobic and hydrophilic regions

Gold coated glass slides (EMF, Ithaca, NY) were sonicated in 100 % ethanol for 5 minutes and immersed in a 0.1 mM FlouroSAM solution (HS-C_{11}-O-C_2-$(CF_2)_5$-CF_3, Pro Chimia, Sopot, Poland) prepared in 100 % ethanol for 2 h protected from light at room temperature. This created a hydrophobic region on the surface of the glass. A PDMS mask with the pattern of choice was aligned with the gold slide and adhered to the surface. The exposed hydrophobic regions of the mask were etched by surface plasma treatment using a Diener Plasma Treatment Chamber (Diener Electronic, Ebhausen, Germany) at 40 sccm and 50 W for approximately one minute. After etching, the PDMS mask was removed and slides were rinsed in 100 % ethanol. The etched gold slide was placed into a 0.25 mM solution of [HS–C_{11}–$(O–CH_2–CH_2)_3$–OH] (EG_3-OH) in 100% ethanol for 2 h at room temperature to create hydrophilic regions on the surface of the gold slide.

3.4.5 Glass slide silanization

Glass slides were sonicated for 45 minutes in 100 % acetone to remove any surface impurities. Slides were rinsed three times in 100 % ethanol to remove excess acetone from the surface. Cleaned glass slides were surface plasma treated using the Diener Plasma Treatment Chamber on both sides of slides for 5 minutes at 40 sccm and 50 W. The activated slides were transferred to 2.5 % 3-mercatopropyl trimethoxylsilane (3-MPTS) (Sigma Aldrich) in toluene overnight. After retrieval, samples were cleaned by subsequent rinses of toluene, 1:1 toluene: ethanol and three rinses of 100 % ethanol respectively. Slides were cured in a nitrogen-purged pressure chamber at 100 °C for 1h. After curing, silanized glass slides were placed in an airtight container and protected from light until use.

3.4.6 PEG hydrogel formulations

Hydrogels consisted of PEGNB molecules, PEG molecules preconjugated to RGD adhesion peptides and VBP, MMP-degradable KCGGPQGIWGQGCK crosslinking peptide (Genscript) and I2959 photoinitiator dissolved in 10 mM phosphate buffered saline (1x PBS). PEGNB, adhesion peptide and VBP concentrations were adjusted to varying levels to achieve different levels of stiffness, cell adhesion and VEGF-binding capabilities in the hydrogels. To vary cell adhesion to the hydrogels, precoupled-PEGNB-CRGDS and PEGNB-RGDFC molecules were added to the solutions to achieve desired adhesion peptide concentrations between 0-4 mM. PEGNB-CRDGS molecules were added along with the functional adhesion molecules to provide a total of 4 mM pendant adhesion peptide included in every solution. To vary VEGF binding to the hydrogels, precoupled-PEGNB-VBP molecules were added to the solutions to achieve

desired peptide concentrations of 0.3 mM VBP. To vary the modulus of the hydrogels PEGNB was added at 40, 50 or 70 mg/mL concentrations and crosslinking molecules were added to the solution to achieve crosslinking of 50% total norbornene functional groups present in solution.

3.4.7 Mechanical properties of PEG hydrogels

Shear modulus was measured in bulk samples of hydrogel spot formulations. To measure shear modulus, 72 μL of pro-tubulogenic precursor solutions were pipetted into 8.0 mm diameter, 1.2 mm depth Teflon wells and cured for 8 seconds using 365 nm UV light at a 90 mW/cm^2 dose rate. The resulting hydrogels were swollen in 1x PBS for 24 h and cut, if necessary, to a final diameter of 8 mm using a hole punch. The samples were tested using an Ares-LS2 rheometer (TA Instruments, New Castle, DE). A 20 g force was applied to the samples via parallel plate crossheads and a strain sweep test at 1Hz fixed frequency was performed from 0.1 to 20% strain. If the sample was not robust enough to withstand a 20 g force the gap between the parallel plates of the rheometer was set to 1.0 mm distance instead. Complex shear modulus of each sample was as the average of measurements taken at 10 Hz, 2 to10% strain.

3.4.8 Thin hydrogel arrays to identify hydrogels that promote vascular network formation

To prepare the silanized glass slides for formation of the thin hydrogel arrays, samples were treated in 10 mM dithiothreitol (Sigma) in 1x PBS at 37°C for 1 hour to increase the number of free thiols on the surface of the slide. After incubation, slides were sequentially rinsed in 1x PBS, 100 % ethanol and dried with Nitrogen gas. Patterned gold slides were rinsed with ethanol and

dried using N_2 gas. A PDMS spacer was applied to the surface of the gold slide to control the height of the hydrogels. 0.8 µL of the prepared PEG solutions were pipetted onto the hydrophilic spots of the glass slide in a humidity chamber. A silanized glass slide was slowly placed onto the surface of the gold slide and transferred under a UV lamp. The hydrogel spots were exposed to 365 nm ultraviolet light at 4.5 mW/cm^2 for eight minutes. Following polymerization, the glass slide was removed from the underlying gold slide. This resulted in a patterned hydrogel array on the surface of the glass slide. Samples were stored in 1x PBS overnight at 4°C prior to sterilization and seeding.

3.4.9 Labeling cells with Cell Tracker™ Red

One day prior to seeding the HUVECs/IPSC-ECs onto the hydrogel spots, the cells were stained with cell tracker red to aid in automated tubulogenesis quantification. Briefly, the HUVECs were rinsed in basal M199 for 5 minutes and stained with 1.3 µM Cell Tracker Red (Invitrogen) in M199 for 45 minutes. Afterward, the cells were rinsed again in basal M199 for 5 minutes before incubating in growth medium overnight to allow the cells to sufficiently recover.

3.4.10 Assembling and seeding hydrogel arrays

On the day of culture, the arrays were assembled within a three chamber Proplate Isolator assemblies (Grace Bio-labs, Bend, OR). Arrays were allowed to warm to room temperature and removed from the 1x PBS rinse. Arrays were subsequently sterilized by immersion in 70% ethanol for 30 minutes, followed by two rinses in 1x PBS. Residual PBS was carefully aspirated from the regions surrounding the hydrogel spots to guarantee adherence to the grace bio isolators.

Using sterile technique, the hydrogel arrays were subsequently assembled within the Grace Bio Isolator system and the individual wells were bathed into basal M199 until use. Cell Tracker Red stained cells were removed from the incubator and subsequently rinsed with 1x PBS. Cells were passaged by incubating the cells in 0.05% trypsin (Hyclone) for 5 minutes, quenching the enzyme through addition of basal M199 with 10 % cosmic calf serum, subsequently counted and resuspended to give a cell count of approximately 85,000 cells/cm^2. Residual media was removed from the assembled arrays and replaced with the resuspended cell solution. When seeding HUVECs the cells were resuspended in M199 containing either 0, 5 or 10 ng/ml VEGF and EGM2 (without VEGF) (Figure 1D). When seeding IPSC-ECs the cells were resuspended in full Vasculife growth medium supplemented with 0, 5 or 10 ng/mL additional VEGF. After seeding, the assembled constructs were transferred to a 37º C incubator for 72 hours. During this period, hydrogel spots were imaged using a Nikon Ti inverted florescent microscope and individual spots were subsequently qualitatively scored on their ability to promote tubule formation (Figure 1D). Briefly, spots were qualitatively assigned a score from 0 – 3 where: 0 = no adhesion; 1 = low cell adhesion; 2 – monolayer formation; and 3 = network formation.

3.4.11 Adapting hydrogels for use in 96-well plates

To ensure substrate stability and repeatable network area measurements in 96-well Angiogenesis plates (Ibidi, USA, Madison WI) photoinitiator concentration, solution volume and cell seeding density were optimized.

For all hydrogel formation and cell seeding operations screening arrays were constructed as follows: the 96-well angiogenesis plates were coated using 150 - 300 kDa poly(L-lysine) (PLL,

Sigma Aldrich). A 1 mM solution of PLL in de-ionized H_2O was pipetted into the wells at 8 µL volume to evenly coat the bottoms of the wells. After 5 minutes incubation at room temperature, the solution was aspirated from all wells. Each well was then washed with de-ionized H_2O three times before drying. Hydrogel solutions identified as enabling vascular network formation were pipetted into the wells, cured for 8 minutes under 365 nm, 4.5 mW/cm^2 UV light and swollen in 70 µL 1x PBS overnight. Afterward the PBS was aspirated and replaced with 35 µL media (network-forming media was identified in the thin-hydrogel screening experiments) by itself, or containing vehicle or inhibitors at desired concentrations. Cell suspensions were added as 35 µL volumes on top of the other 35 µL media. Cells were left undisturbed for 24 hours when vascular networks were photographed by epifluorescence and phase-contrast microscopy using a Nikon Eclipse microscope.

To enhance substrate stability in the 96 well plates photoinitiator concentration was increased from the original 0.05% wt/volume concentration used in the thin hydrogel arrays to 0.1, 0.2 and 0.4% wt/volume. Hydrogel stability was measured as swollen diameters of hydrogels retrieved from the 96 well plates. Test hydrogels were cured as 8 µL volumes per well using the aforementioned array assembly procedure. A 3.5 mm diameter hole punch was used to retrieve hydrogel samples from the wells before the diameter of the samples was measured using a micrometer. Unstable hydrogels were evaluated as having the largest diameters after removal from the wells, indicating high swelling at equilibrium.

To reduce the impact of meniscus formation on image of vascular networks 7, 8 9 and 10 µL volumes of hydrogel were cured in the well plates using the aforementioned array assembly procedure. The hydrogels contained 0.2% w/v photoinitiator as was found to be the optimal concentration in the swelling experiments. HUVECs were stained with cell tracker red and

seeded at a density of 1.2 x 10^5 cells/cm^2 onto the hydrogels. Meniscus formation was evaluated by observing in-focus and out-of-focus areas in a typical image of HUVEC network formation 24 hours after seeding.

To ensure the consistent formation of vascular networks in the arrays HUVEC seeding density was explored at 1.2 x 10^5 cells/cm^2, 1.8 x 10^5 cells/cm^2, and 2.4 x 10^5 cells/cm^2. IPSC-EC seeding density was also explored at 1.8 x 10^5 cells/cm^2, and 2.4 x 10^5 cells/cm^2. Here hydrogels were pipetted into the wells as 9 µL volumes as was determined to be optimal for meniscus reduction. Network formation was evaluated 24 hours after seeding.

3.4.12 Vascular inhibitor treatment on synthetic hydrogel and Matrigel culture systems

Synthetic hydrogel and Matrigel conditions were included in the screening arrays as follows: synthetic hydrogels were added to the 96 well plates in 9 µL volumes with HUVECs seeded at a density of 2.4 x 10^5 cells/cm^2 and IPSC-ECs seeded at a density of 1.8 x 10^5 cells/cm^2. Matrigel was added to the 96 well plates in 10 µL volumes and incubated in a humidified 37˚C incubator for 30 minutes. Afterward either HUVECs or IPSC-ECs were seeded at a density of 1.2 x 10^5 cells/cm^2 using the aforementioned seeding procedure in 96 well plates. Network formation was evaluated 24 hours after seeding in the 96 well plates. To conduct timelapse microscopy of HUVEC network formation on synthetic hydrogels or Matrigel HUVECs were seeded onto substrates as dictated for the initial inhibitor screens, treated with 0.2% DMSO in media, incubated on an environmentally controlled stage on the Nikon TI Eclipse microscope to match

atmospheric conditions of a humidified 37˚C incubator and photographed every 15 minutes using phase contrast microscopy.

In the Z-prime test for assessing accuracy the of the synthetic hydrogel and Matrigel screening systems PEG and Matrigel substrates were formed in separate 96 well plates. Each plate was divided into four 24 well corners with 0.1% DMSO controls occupying two opposite corners and 20 μM Sunitinib controls occupying the other two opposite corners. From each data set a Grubbs Test was performed on the DMSO and Sunitinib groups for outlier removal prior to the application of the Z' equation to each data set.

The optimized PEG formulations with or without a VEGF binding component were compared directly to growth factor reduced Matrigel using an initial panel of five inhibitors i.e. 1) Vatalanib – a clinically tested inhibitor to vascular endothelial growth factor receptor activity [27] 2) SU5416 – a clinically approved inhibitor of vascular endothelial growth factor receptor activity [28]; 3) soluble fms-like tyrosine kinase 1 (sFlt-1) – an antagonist of VEGF and placental growth factor [29-31]; 4) Anti-VEGF – a human monoclonal antibody to bind soluble VEGF [32]; 5) Sunitinib, a clinically approved inhibitor of vascular endothelial growth factor receptor activity [33, 34]. Endothelial cells were additionally treated on PEG and Matrigel substrates with inhibitors acting independently of VEGF signaling, including 1) Prinomastat HCL – an antagonist to the activity of MMPs 2, 3, 9, 13, and 14; and 2) Suramin HCL, an inhibitor to EGF, PDGF and TGFβ signaling [19].

3.4.13 Identifying putative vascular inhibitors from Toxcast™ chemical library

To demonstrate the capability of the screening system to identify vascular inhibitors from a library of unknown chemical compounds samples from the Toxcast® library of chemicals were applied to HUVECs similarly to the known vascular inhibitors screened on the 96 well plate. Of the 4000 compounds provided from the library 53 were selected by the EPA as a number of control conditions, though the identities of the chemicals were not made known until after the experiments concluded. The stock solutions from the library were diluted using tubulogenic media at a 1:1000 dilution prior to their additions into the screening system. Each compound was tested in the network formation assay in triplicate experiments. Total network area was quantified in each well of the compound plates. Inhibitors were identified as compounds that resulted in network areas 2 standard deviations away from the mean area of the 0.2% DMSO-treated control wells of each plate. Compounds identified as inhibitors in a majority of the triplicate plates were counted as inhibitors in the synthetic hydrogel and Matrigel systems.

3.5 Results

3.5.1 Identifying synthetic hydrogel formations that promote vascular network assembly

Synthetic poly(ethylene glycol) (PEG) hydrogels were designed to mimic properties of the native extracellular matrix (ECM) that are critical to modulating vascular network formation by endothelial cells. These properties included presentation of integrin-binding adhesion ligands, varying substrate modulus and the ability to non-covalently sequester soluble growth factors

(Figure 1A). The inclusion of CRGDS and cyclized RGDFC (cyclic RGD) adhesion peptides modulated cell adhesivity to the hydrogels through a RGD amino acid motif commonly present in integrin-binding ECM proteins such as laminin, vitronectin, and fibronectin [35-37]. The mechanical properties of the hydrogels were modulated by tuning concentrations of norbornene-functionalized 20 kDa, 8-arm PEG (PEG-NB) and crosslinking molecules within the hydrogel. All hydrogel solutions were polymerized using a crosslinking peptide KCGGPQGIWGQGCK that is degradable by cell-secreted matrix metalloproteinases (MMPs) [38], thereby enabling cell-mediated degradation and remodeling of the hydrogel substrates. All peptides included in the hydrogels are covalently attached to PEG via the thiol-ene reaction [26], a photopolymerization reaction that couples thiols present in cysteine residues to norbornene groups on the PEG molecules. Taken together these hydrogels present a set of cell-signaling cues that is simple compared to the complex microenvironment presented by Matrigel.

3.5.2 Identifying optimal microenvironments to promote vascular network formation

Cell culture environments were systematically varied to elucidate appropriate conditions for promoting vascular network assembly by HUVECs. Defined properties of the culture environments included hydrogel substrate stiffness within a range of 400 (soft), 1100 (medium) and 2400 (stiff) Pa (Figure 1E, Supp. Fig. 1), adhesion ligand presentation and identity in the substrate as well as VEGF concentration in media. A thin hydrogel array (Figure 1B) was employed to enable rapid testing of a large number of culture conditions with minimal use of material spent per condition (0.8 μL precursor solution per hydrogel spot) [39, 40]. Successful conditions supported vascular network formation in less than 24 hours after seeding (Figure 1C)

and maintained network stability over 48 hours (Figure 1E). Overall, 300 potential culture conditions (1,200 individual hydrogel spots) were screened in this study (Figure 1E). Across the range of conditions tested, one condition was identified as a successful network-forming condition in HUVECs (Figure 1E). The identified hydrogel substrate contained 40 mg/mL PEG, 0.125 mM cyclic RGD, and 4 mM crosslinking peptide. The 400 Pa shear modulus of the substrate fell approximately in the average modulus range of the Matrigel substrates [16, 17]. Soluble VEGF as included in media at a 5 ng/mL concentration to induce vascular network formation on the substrate. The condition defined here reproducibly formed vascular networks in approximately 6 to 8 hours (Figure 1C) and remained stable for 48 hours.

To enable investigations of the role of growth factor sequestration on inhibitor sensitivity additional conditions were identified as promoting vascular network formation in the presence of a VEGFR2-mimicking peptide (aka VEGF binding peptide (VBP)) to the hydrogels. HUVECs were seeded onto thin hydrogel arrays, as above, where the concentration of cyclic RGD was varied within a range of 0 to 0.25 mM concentrations and VBP was included in the hydrogel at a concentration of 0.3 mM. Here, one condition with a substrate containing 40 mg/mL PEG, 0.25 mM cyclic RGD, 4 mM crosslinking peptide, and 0.3 mM VBP as well as 5 ng/mL rhVEGF included in media promoted stable vascular network formation which lasted 48 hours in culture (Supp. Fig. 2).

To demonstrate the capability of the synthetic culture system to investigate vascular network formation for multiple endothelial cell types, endothelial cells derived from human induced pluripotent stem cells (IPSC-ECs, Cellular Dynamics International, Madison, WI) were seeded onto a thin hydrogel array identical to those initially used to induce network formation by HUVECs. These conditions did not contain VBP. In contrast to HUVECs, IPSC-ECs formed

networks on multiple hydrogel substrates rather than one specific condition. These hydrogels spanned multiple substrate moduli, adhesion molecule species and concentrations as well as soluble VEGF concentrations in media. This indicates that differing micro-environmental conditions induce network formation by differing cell types (Figure 1E). For future experiments IPSC-EC network formation was induced in a culture condition with a substrate containing 40 mg/mL PEG, 1.0 mM CRGDS and 4 mM crosslinking peptide as well as 10 ng/mL rhVEGF included in media.

HUVECs and IPSC-ECs were labelled using CD31 antibody (Millipore), Cell Tracker Red and DAPI nuclear stain and photographed under epifluorescence and confocal microscopy to confirm the interconnectivity of vascular networks formed in the synthetic hydrogel and Matrigel culture systems. Images showed the organization of cells into clearly branching, interconnected networks for both cell types and on both synthetic hydrogels and Matrigel (Figure 1D, Figure 2A). Though lumen did not form over the course of the experiments described here, all endothelial cells displayed a clear ability to migrate and develop cell-cell contacts that contribute partly to the process of angiogenesis in vivo (Figure 1C).

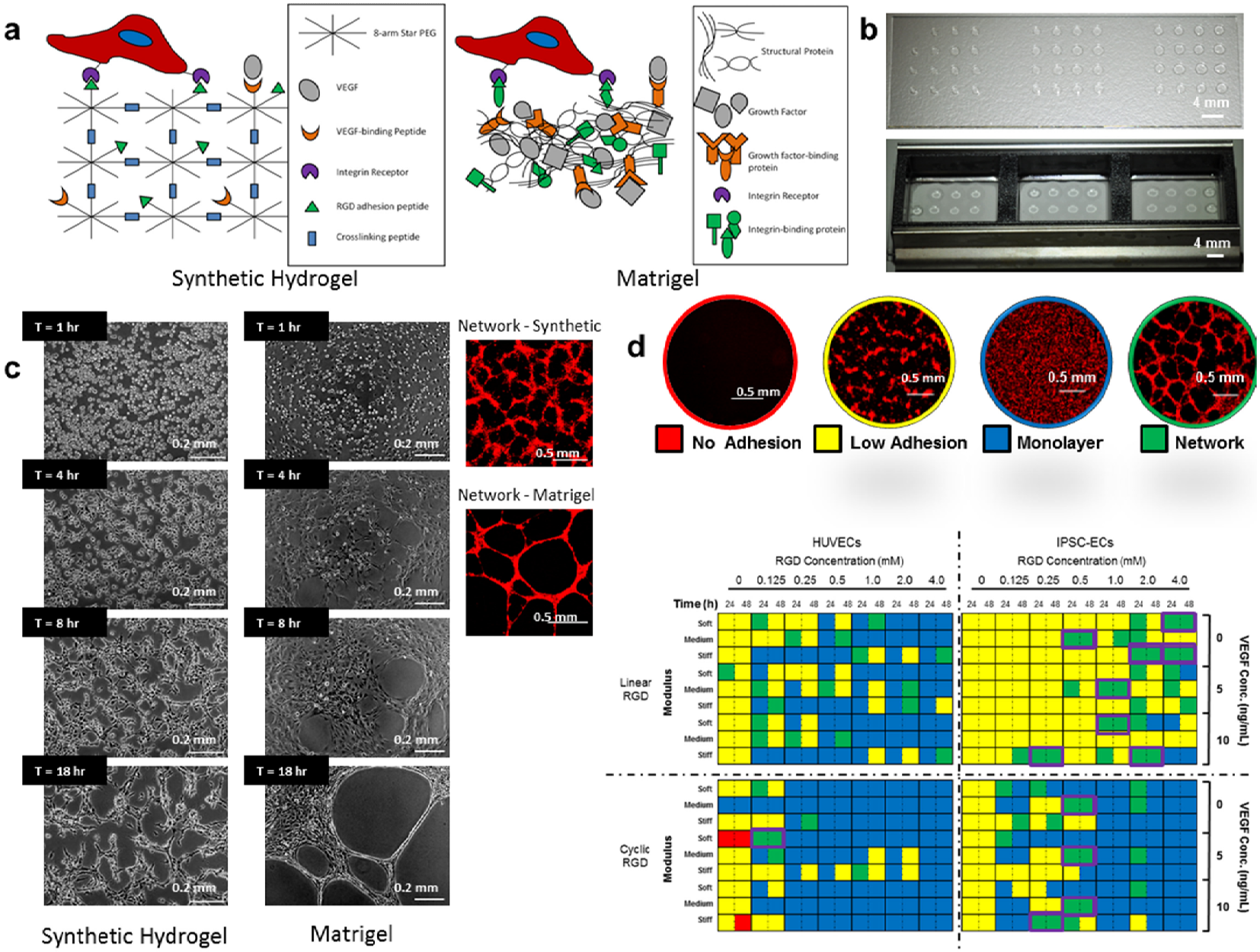
a
8-arm Star PEG
VEGF
VEGF-binding Peptide
Integrin Receptor
RGD adhesion peptide
Crosslinking peptide
Structural Protein
Growth Factor
Growth factor-binding protein
Integrin Receptor
Integrin-binding protein
Synthetic Hydrogel
Matrigel
b
4 mm
4 mm
c
T = 1 hr
T = 4 hr
T = 8 hr
T = 18 hr
0.2 mm
Network - Synthetic
Network - Matrigel
0.5 mm
Synthetic Hydrogel
Matrigel
d
0.5 mm
No Adhesion
Low Adhesion
Monolayer
Network
HUVECs
IPSC-ECs
RGD Concentration (mM)
0 0.125 0.25 0.5 1.0 2.0 4.0
Time (h)
24 48
Linear RGD
Cyclic RGD
Modulus
Soft
Medium
Stiff
VEGF Conc. (ng/mL)
0
5
10

Chapter 3: Figure 1. An endothelial cell culture system identifies environments that enable vascular network formation on synthetic PEG-based hydrogels. **(a)** Schematic of endothelial cell seeded on synthetic hydrogels and Matrigel. **(b)** Thin hydrogel arrays and arrays assembled with 3-well ProPlate® Cell Culture Isolators. **(c)** Left: Vascular network formation on synthetic hydrogels and Matrigel over time. Right: Typical vascular networks formed on synthetic hydrogels and Matrigel 24 hours after seeding. **(d)** Qualitative scoring system for HUVEC network formation and heat map showing initial screening results for HUVEC and IPSC-EC network formation. Conditions highlighted in violet borders denote environments that enabled HUVEC network formation within 24 hours after seeding and maintained structural integrity over the 48 hour culture period. Red: Cell Tracker Red.

3.5.3 Establishing utility of network-inducing and VEGF-binding hydrogels for inhibition assays

When compared directly to Matrigel, vascular screening systems utilizing synthetic hydrogels were found to be superior in accurately distinguishing between normal vascular networks and networks disrupted using a known vascular inhibitor Sunitinib, as quantified using the Z' score (Equation 1).

$$Z' = 1 - \frac{3(SD\ of\ sample + SD\ of\ control)}{|mean\ of\ sample - mean\ of\ control|}$$

Chapter 3: Equation 1. Z' calculation

Hydrogel formulations identified as enabling vascular network formation were adapted for use in 96-well Angiogenesis Plates (Ibidi, Martinsreid, Germany). Photoinitiator concentration, hydrogel solution volume and cell seeding density were adjusted and all future chemical screening experiments were performed using this screening format (Supp. Figure 3). To perform the Z' test HUVECs cultured in the synthetic hydrogel and Matrigel screening systems were treated using 0.2% v/v DMSO in media as vehicle in non-inhibited control wells while cells in the inhibited wells were treated using 20 μM Sunitinib in media (Figure 2B). Network formation

in the inhibited and non-inhibited conditions was quantified as total network area after structure identification and thresholding in NIS Elements (Figure 2C). On synthetic hydrogels differences in the means as well as the standard deviations of the treatment conditions resulted in a Z' score of 0.66 which is considered to indicate an excellent assay (Z' score> 0.5) [41]. The test was performed on Matrigel and resulted in a Z' score of -0.74, indicating that inconsistencies in the assay interfere with the identification of inhibiting and non-inhibiting culture conditions in a high-throughput setting (Figure 2D).

After the Z' test confirmed inhibitor detection in HUVEC networks, the Z' test was repeated to evaluate the detection of IPSC-EC network inhibition. IPSC-ECs seeded on the synthetic hydrogel and Matrigel substrates were prone to increased spreading compared to HUVECs (Figure 2A, B) and resulted in lower Z-prime scores on both synthetic hydrogels and Matrigel: 0.20 and -1.06 respectively (Figure 2D). Due to superior Z' scores HUVEC networks were used in future experiments to evaluate the effects of known and unknown angiogenesis inhibitors on vascular network formation.

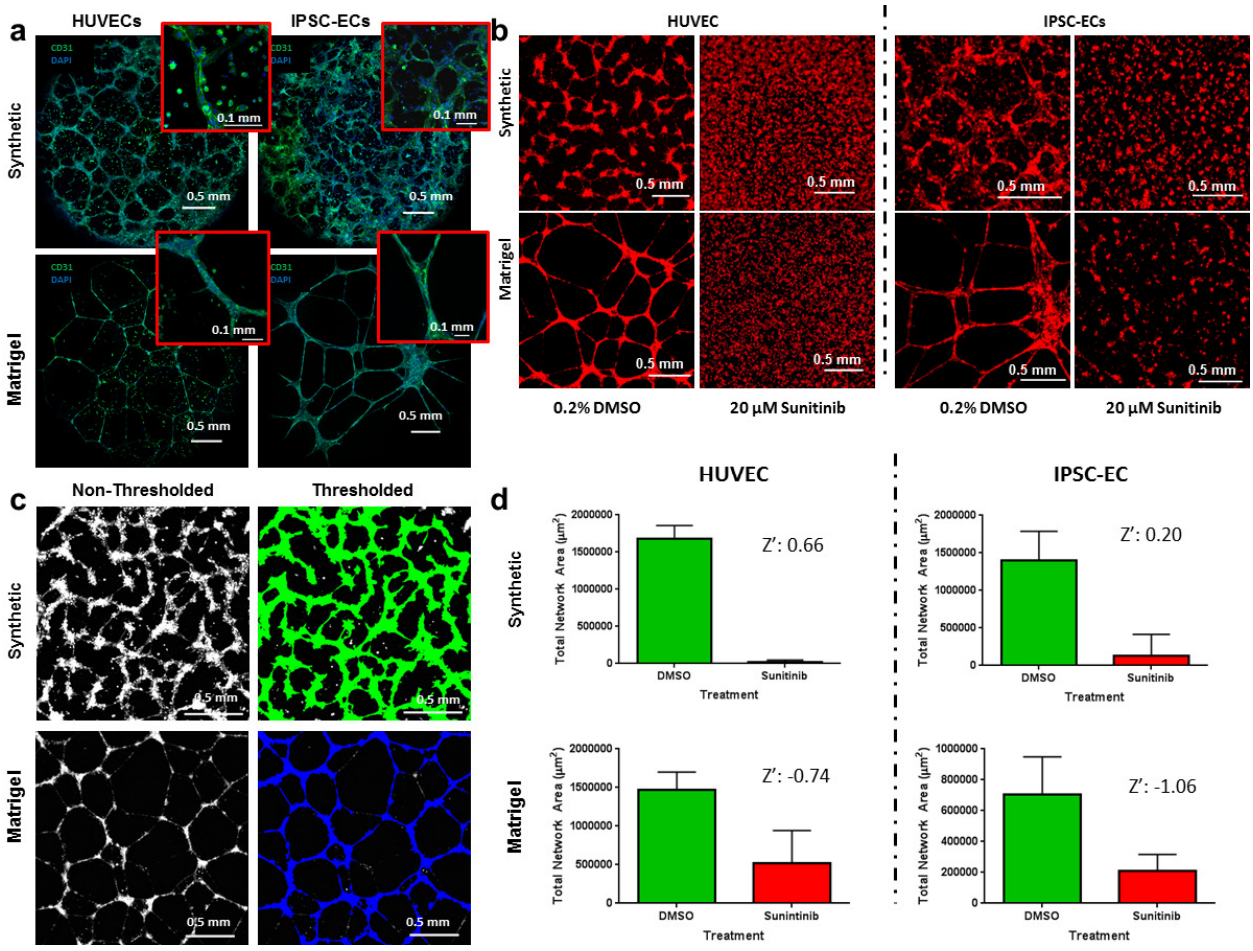

Chapter 3: Figure 2. Visualization and quantification of vascular networks on synthetic hydrogels and Matrigel. **(a)** Confocal microscopy images of HUVECs and IPSC-ECs forming networks on synthetic versus Matrigel substrates. Insets: Enhanced magnification of multicellular structures. Scale bar: 0.2 mm **(b)** HUVECs and IPSC-ECs seeded on synthetic and Matrigel substrates form vascular networks in DMSO-treated conditions. Network formation is disrupted by Sunitinib treatment. **(c)** HUVEC networks on synthetic and Matrigel substrates are identified by thresholding fluorescence intensity and object size. Network formation is quantified as total object area per substrate. **(d)** Vascular network formation in synthetic hydrogel and Matrigel systems is quantified and subjected to the Z' test to verify their efficacy of as toxicity screening systems. Red: Cell Tracker Red.

3.5.4 HUVEC sensitivity to known vascular inhibitors on synthetic hydrogels and Matrigel

HUVECs seeded onto synthetic hydrogels demonstrated increased sensitivity to a number of known inhibitors in comparison to cells seeded on Matrigel. Known inhibitors to VEGF signaling were applied to HUVEC networks in synthetic hydrogel and Matrigel screening systems to evaluate their ability to detect network disruption across a broad range of inhibitor concentrations. Inhibitors included Vatalanib®, Semaxanib®, Sunitinib®, a soluble flt-1 (sFlt-1) receptor antibody, and a recombinant antibody to VEGFA (anti-VEGF). With the exception of Vatalanib HUVECs were responsive to the vascular inhibitors in a wider range of conditions on synthetic hydrogels than on Matrigel (Figure 3B, Supp. Fig. 4A). Notably, in all concentrations tested anti-VEGF, and Sunitinib inhibited vascular network formation in the synthetic screening system.

Due to the decreased detection of inhibitory activity by the Matrigel screening systems we hypothesized that the capability of naturally-derived matrices to non-covalently bind and sequester growth factors helped to overcome the ability of the VEGF inhibitors to affect VEGF signaling in HUVECs. To investigate this possibility, synthetic hydrogels were functionalized with VBP to enable non-covalent binding and sequestration of soluble VEGF from surrounding media (Figure 3A). HUVECs seeded on the VBP-modified synthetic hydrogels showed little response to the added panel of known VEGF inhibitors used previously as network areas deviated little from non-inhibited control networks (Figure 3B, Supp. Fig. 4A).

3.5.5 Exploring the effects of VEGF-independent inhibitors on network formation

A common source of error in drug discovery is the failure of screening platforms to model the multiple mechanisms that drive angiogenesis [42, 43]. Limiting drug targets to those that disrupt VEGF and its receptors has been implicated in the limited long term efficacy of anti-angiogenic therapies. Here, we demonstrated the ability to explore multiple mechanisms of inhibition within the synthetic hydrogel system. Known inhibitors independent of VEGF signaling were applied to HUVECs: Prinomastat HCL, a broad-base inhibitor to matrix metalloproteinases 2, 3, 9, 13, and 14, and Suramin HCL, an inhibitor to EGF, PDGF and TGFβ signaling [19] that has demonstrated an ability to solubilize Matrigel substrates [20]. On synthetic hydrogels HUVECs responded to Prinomastat HCL treatment by assembling into confluent cell sheets rather than well-defined vascular networks. HUVECs plated on Matrigel did not show appreciable morphological changes from vehicle controls at most doses of Prinomastat HCL (Supp. Fig. 4B). Additionally the presence of VBP in synthetic hydrogels did not interfere with the inhibitory effects of Prinomastat HCL, suggesting that Prinomastat acts independently of VEGF signaling on the synthetic hydrogels (Figure 3B). Taken together these results suggest that substrate degradation is necessary for network formation on hydrogels, and that systems with defined matrix metalloproteinase-mediated degradation modes can model the inhibitory activity of protease inhibitors. In contrast Matrigel cannot model this activity due to its poorly defined degradation modes.

In vascular inhibition studies it was noted that, as per Progozhina et al., there were a potential number of compounds which disrupt vascular networks via to Matrigel dissolution including Suramin Hydrochloride [20], resulting in the identification of a number of false inhibitory

compounds. Here treatment with Suramin Hydrochloride resulted in dose-dependent disruption of HUVEC networks on Matrigel as well as dissolution of the Matrigel. In contrast, Suramin Hydrochloride treatment on synthetic hydrogels resulted in little morphological impact on vascular networks, suggesting the inhibitory effect was almost exclusively attributed to substrate dissolution (Supp. Fig. 6).

a

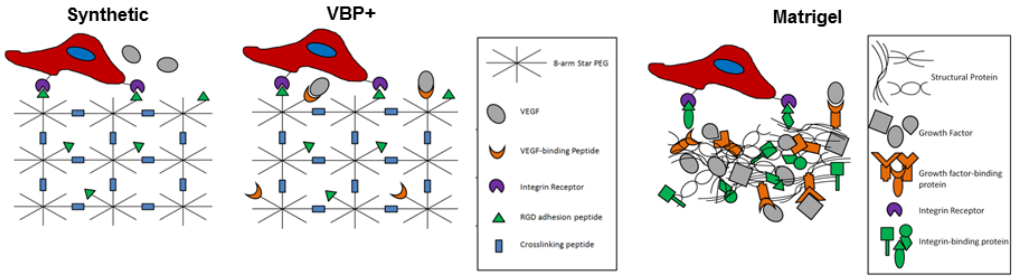

b

ANTI-VEGF

Conc. (ug/ml)	Synthetic	VBP+	Matrigel
	Inhibition (+/-)		
1	+	-	-
0.5	+	-	-
0.25	+	-	-
0.125	+	-	-
0.062	+	-	-
0.031	+	-	-
0.015	+	-	-
0.008	+	-	-

Semaxinib (SU5416)

Conc. (uM)	Synthetic	VBP+	Matrigel
	Inhibition (+/-)		
40	+	-	+
20	-	-	-
10	-	-	-
5	-	-	+
2.5	+	-	-
1.25	+	-	-
0.625	+	-	-
0.3125	+	-	-

sFLT-1

Conc. (ug/ml)	Synthetic	VBP+	Matrigel
	Inhibition (+/-)		
1	+	-	-
0.5	-	-	-
0.25	-	-	-
0.125	+	-	-
0.062	+	-	-
0.031	+	-	-
0.015	+	-	-
0.008	-	-	-

Vatalaninb (PTK787)

Conc. (uM)	Synthetic	VBP+	Matrigel
	Inhibition (+/-)		
20	+	-	-
10	-	-	+
5	-	-	+
2.5	-	-	-
1.25	+	-	-
0.625	-	-	-
0.3125	-	-	+
0.1562	+	-	+

Sutent (Sunitinib)

Conc. (uM)	Synthetic	VBP+	Matrigel
	Inhibition (+/-)		
40	+	+	+
20	+	+	-
10	+	+	-
5	+	-	+
2.5	+	-	-
1.25	+	-	-
0.625	+	-	-
0.3125	+	-	-

Prinomastat HCL

Conc. (uM)	Synthetic	VBP+	Matrigel
	Inhibition (+/-)		
20	+	+	-
10	+	+	+
5	+	+	+
2.5	+	+	-
1.25	+	+	-
0.625	+	+	-
0.3125	+	+	+
0.1562	+	+	+

Chapter 3: Figure 3. Concentration-dependent inhibition of vascular network formation by known vascular inhibitors. **(a)** Schematics of synthetic hydrogels functionalized with RGD (synthetic), RGD and VBP (VBP+), and Matrigel^{TM}. **(b)** Sensitivity of HUVECs to inhibitors is compared between the synthetic, VBP+ and Matrigel^{TM} systems. Inhibited samples (+) have a p-

value < 0.05 by One-way ANOVA followed by Dunnet multi-comparisons analysis compared to the DMSO/1X PBS control conditions depending on the vehicle of the inhibitor.

3.5.6 Differential network formation processes on synthetic hydrogels and Matrigel

The synthetic hydrogel demonstrated a different vascular assembly process to that of the vascular networks formed on Matrigel. Timelapse microscopy was utilized to evaluate network formation over the course of 24 hours after HUVEC seeding. On synthetic hydrogels HUVECs did not immediately spread on the gel surfaces, but instead migrated to the closest possible neighbors to immediately define the vascular branching networks. As a result, networks formed within 6-8 hours after seeding. In contrast cells on Matrigel spread upon substrate attachment to form continuous cell sheets. Afterward, the sheets would contract into elongated structures over the course of 18 hours after seeding. The differing mechanisms of network formation between synthetic hydrogels and Matrigel may contribute to the differential responses to vascular network inhibition in the culture systems. Specifically, the networks of contracted cell sheets that exist on Matrigel may resist inhibitor-induced structural disintegration more than the cell networks on synthetic hydrogels, resulting in more dramatic inhibitory effects quantified in synthetic systems and more sensitive inhibitor detection (Figure 1C).

3.5.7 Identifying inhibitory compounds from ToxCast^{TM} compound library

The synthetic hydrogel-based screening system demonstrated the ability to detect an increased number of putative vascular disrupting compounds from a library of 53 unknown chemical

compounds when compared to the Matrigel system. In these assays vascular network inhibition was evaluated by quantifying total areas vascular networks treated with unknown compounds and comparing them to mean areas of control networks treated with 0.2% DMSO in media. Specifically networks with areas greater than 2 standard deviations away from the mean of control areas were counted as being inhibited by the candidate compound. All tests were performed in triplicate and compounds that resulted in inhibition for a majority of replicates were counted as inhibitors. After 24 hours culture the synthetic hydrogel system detected 18 compounds as inhibitors whereas the Matrigel platform detected 9 compounds as inhibitors. Of the detected compounds 8 were detected as inhibitors by both the synthetic hydrogel and Matrigel systems (Figure 4). To determine why some inhibitors were detected on one screening platform but not both, fluorescence micrographs of inhibitor conditions were compared between synthetic hydrogels and Matrigel. Inhibitors 8, 9, 16 and 40 resulted in the formation of broad sheets on synthetic hydrogels but did not impede network formation on Matrigel. Inhibitor 10 resulted in network disruption on Matrigel while structures on synthetic hydrogels were insufficiently affected to be identified as inhibited networks. Inhibitors 11 and 19 disrupted network coherency on synthetic hydrogels but did not impede network formation on Matrigel. Inhibitors 18, 21, 38 and 48 resulted in network disruption on both synthetic hydrogels and Matrigel, but the cells on Matrigel remained clustered together and were therefore falsely detected as intact vascular structures (Supp. Fig. 7).

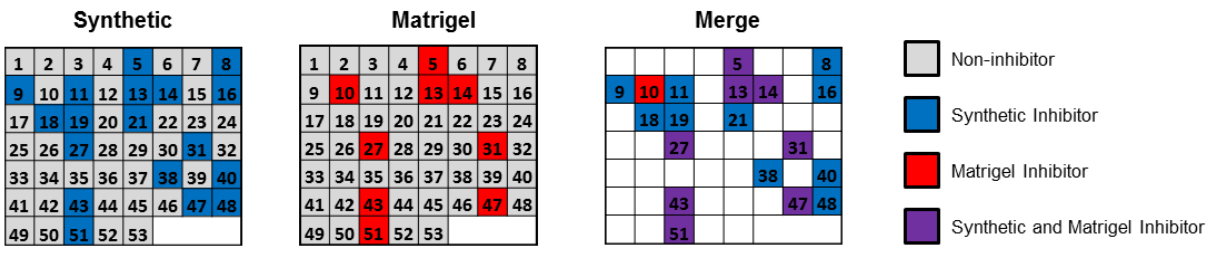

Chapter 3: Figure 4. Identification of vascular inhibitors from an unknown library of 53 candidate inhibitory compounds in a synthetic hydrogels screening system, a Matrigel system, and both systems identified inhibiting compounds based on whether total areas of inhibitor-treated vascular networks are two standard deviations above or below the mean of DMSO-treated network areas.

3.6 Discussion

Generation of novel methods for drug discovery, disease modeling and toxin screening is essential to accurately predict human biological responses to chemical exposure. Current models of chemical exposure are failing to accurately predict these responses and global efforts are targeted towards creating improved human tissue models with a reduction in the current overreliance of animal models. In particular, regulatory bodies such as REACH in the EU, the NIH NCATS program, the FDA, EPA Star Program in the U.S., and other global organizations are encouraging reduction and replacement of animal testing [44, 45]. Here an enhanced throughput array-based screening method identified multiple vascular network-forming synthetic hydrogels which demonstrated superior properties to the Matrigel network formation assay. The synthetic systems provided a defined microenvironment with increased sensitivity to vascular disrupted compounds compared to the Matrigel substrate. Presence of locally bound sequestered growth factors, undefined material components and the need for precise temperature control are circumvented through the use of the synthetic, photopolymerized hydrogel. Collagen and fibrin gel systems are often used to replace Matrigel but suffer from similar pitfalls e.g. lot-to-lot variation, defined temperature control and derivation from non-human origins [46, 47]. With the synthetic hydrogel system it is possible to define substrate modulus, degradability, adhesion ligand presentation and the presence of growth factor sequestering moieties to a degree that is difficult to achieve using a Matrigel-based system. Additionally, control of the stiffness of the

underlying matrix allowed IPSC-ECs to form vascular networks in increasingly stiff microenvironments. This would allow endothelial cells to be studied in models of healthy, developing and diseased microenvironments [48]. Used in combination with the vascular screening developed here IPSC's derived from different patient subpopulations would provide a diverse model for future screening approaches.

Building upon this initial assay, using a bottom-up approach it is possible to generate increasingly complex microenvironments to culture numerous cell types, model distinct aspects of their environment and understand the contribution of each factor to tissue assembly. This has been demonstrated in a number of assays of increasingly complex biological assemblies such as neurite outgrowth models, cellular migration assays and neural organoid models. Synthetic materials would allow the roles of individual signaling cues from the extracellular matrix to be elucidated during drug discovery and toxicity profiling and would lend themselves to in-silico models for predictive biological responses [44, 49]. Relevance to in-vivo mechanisms toward vascular network formation is a particular concern in mechanistic studies of angiogenesis and drug screening. The physiological relevance of Matrigel as a culture substrate is often called into question as the formation of vascular networks is not specific to endothelial cells. Multiple non-endothelial cell types including melanoma, gliablastoma and breast cancer cell lines, retinal epithelial and lens cells, murine Leydeg cells and human fibroblasts [14, 50-52] have formed cellular networks resembling vasculature, and it has been suggested that these networks form via cell traction and malleability of the matrix [52] rather than relevant mechanisms of vascular morphogenesis (Figure 1C). Though this non-endothelial effect in cancer cells has been attributed to its similarity to an in vivo process dubbed vasculogenic mimicry [53, 54], processes such as these can generate misleading insights on vascular network formation as well as

inhibitory activities vascular disrupting compounds. Our findings from observing vascular network formation on synthetic and Matrigel substrates corroborate these doubts about the physiological relevance of Matrigel, as we observed drastically distinct mechanisms of de novo vascular network formation on the synthetic and Matrigel systems over time. Cell migration and multicellular vessel assembly demonstrated by HUVECs on synthetic hydrogels may resemble angiogenic processes more closely than monolayer contraction on Matrigel and therefore provide a more physiologically-relevant scenario to investigate vascularization mechanisms and drug activities [55].

In future studies candidate compounds can be passed through an initial sensitive screening system such as the one described here and then sequentially passed through a series of more complex models for increasingly rigorous evaluations of inhibitory compounds. In particular the activity of VBP in modulating endothelial cell sensitivity to VEGF inhibitors can be mechanistically investigated in a controlled synthetic hydrogel system. Taken together we predict that the use of synthetic hydrogel-based culture systems will ultimately lead to a significant reduction in false positives and false negatives in drug and toxicity screening, a reduction in compounds taken to preliminary animal testing and therefore an overall reduction of cost in the screening process.

3.7 Acknowledgements

The authors would like to acknowledge funding from the National Institutes of Health (NIH R01 HL093282-01A1, NIH R21 EB016381-01, NIH 1UH2 TR000506-01, the UW-Madison Biotechnology Training Program NIGMS 5T32GM08349, and the UW-Madison Cardiovascular

Research Center T32-HL 07936) as well as the UW Madison Graduate Engineering Research Scholars program. We would also like to acknowledge funding from the Environmental Protection Agency (US EPA STAR Program 835737). We would like to thank Justin Williams and David Beebe for their assistance with soft lithography techniques. This study made use of the National Magnetic Resonance Facility at Madison, which is supported by NIH grants P41RR02301 (BRTP/ NCRR) and P41GM10399 (NIGMS). Additional equipment was purchased with funds from the University of Wisconsin, the NIH (RR02781, RR08438), the NSF (DMB-8415048, OIA-9977486, BIR-9214394), the DOE, and the USDA. Small angle X-ray scattering (SAXS) equipment was purchased with funds from NIH grant S100RR027000 (NCRR). Mechanical testing data was obtained using the Ares LS2 rheometer at the UW Madison Soft Materials Laboratory. Robotic liquid handling was provided with assistance from the UW Madison Small Molecule Screening Facility.

3.8 Supplemental information

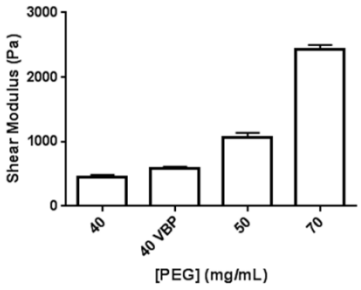

Chapter 3: Supplemental Figure 1. Shear modulus of synthetic hydrogels with varying PEG concentration and VBP presence in precursor solutions.

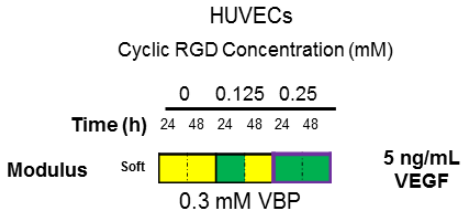

Chapter 3: Supplemental Figure 2. A narrow set of conditions comprising 40 mg/mL PEG, 0 – 0.25 mM RGD were tested in the thin-hydrogel screening system to identify HUVEC network-forming conditions on VBP-functionalized synthetic hydrogels.

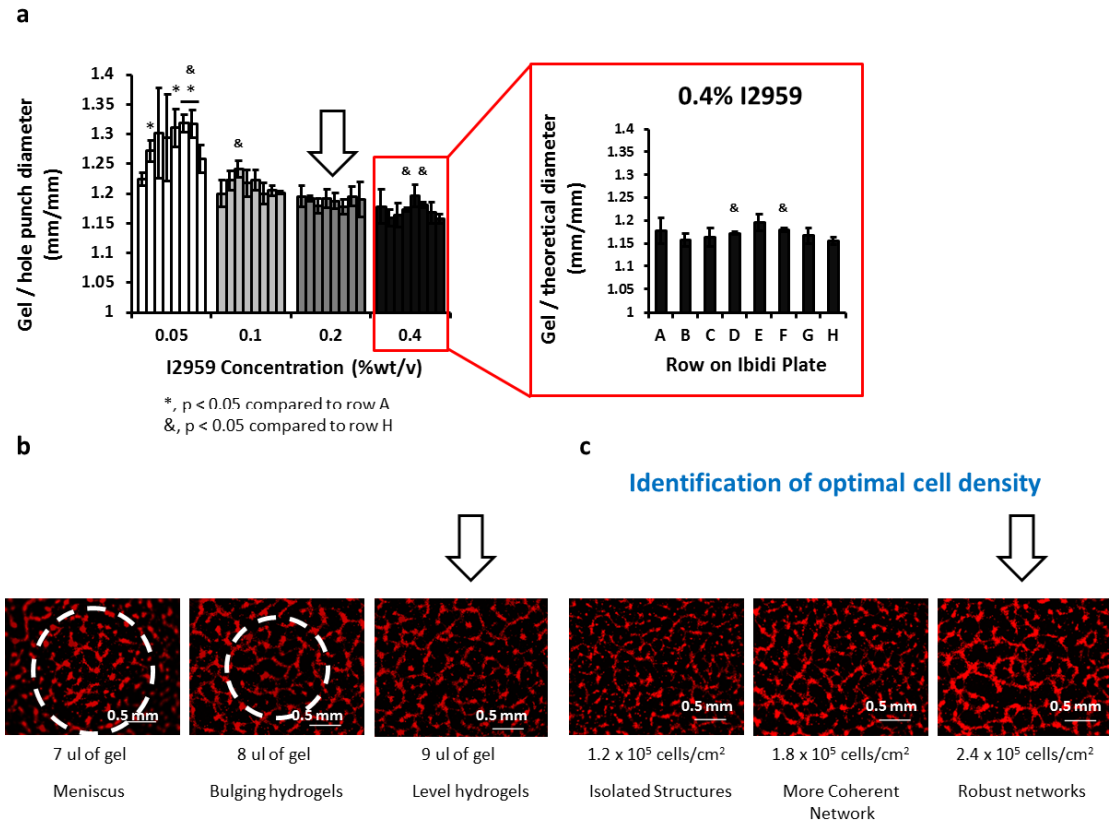

Chapter 3: Supplemental Figure 3. Synthetic PEG hydrogels optimized for use in 96-well angiogenesis plates. Arrowheads indicate parameters used in inhibitor screening studies. (**a**) Dependence of hydrogel swelling ratio on photoinitiator concentration in the hydrogels. Swelling ratio was taken as ratio of sample diameter compared to the 3.5 mm diameter of the biopsy punch that extracted the samples. Columns in each photoinitiator condition represent swelling ratios measured in the individual rows of the 96 well plate to indicate spatial effects on swelling ratio. (**b**) Identifying hydrogel volumes that minimize meniscus formation and the appearance of out-of-focus areas in network images. (**c**) Identifying cell seeding densities that result in interconnected vascular networks. Red: Cell Tracker Red.

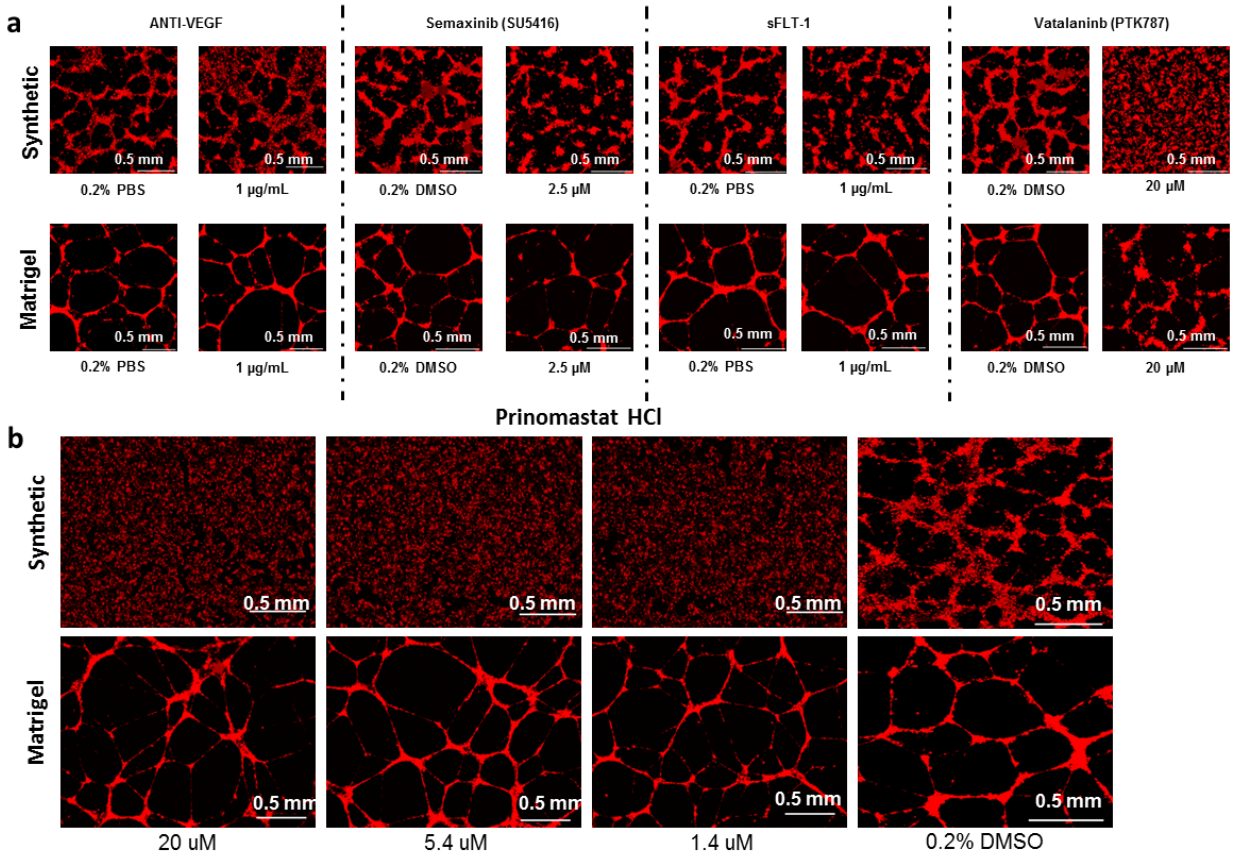

Chapter 3: Supplemental Figure 4. Fluorescent micrographs comparing HUVEC networks on synthetic hydrogel and Matrigel systems. Endothelial cells were treated with inhibitors to **(a)** VEGF signaling and **(b)** Prinomastat HCL as an inhibitor to MMP activity. VEGF inhibitors demonstrate network disruption on synthetic hydrogels but not Matrigel at many inhibitor concentrations. Prinomastat HCL disrupts vascular network formation on synthetic hydrogels at all treatment concentrations but permits network formation on Matrigel at multiple concentrations. Red: Cell Tracker Red.

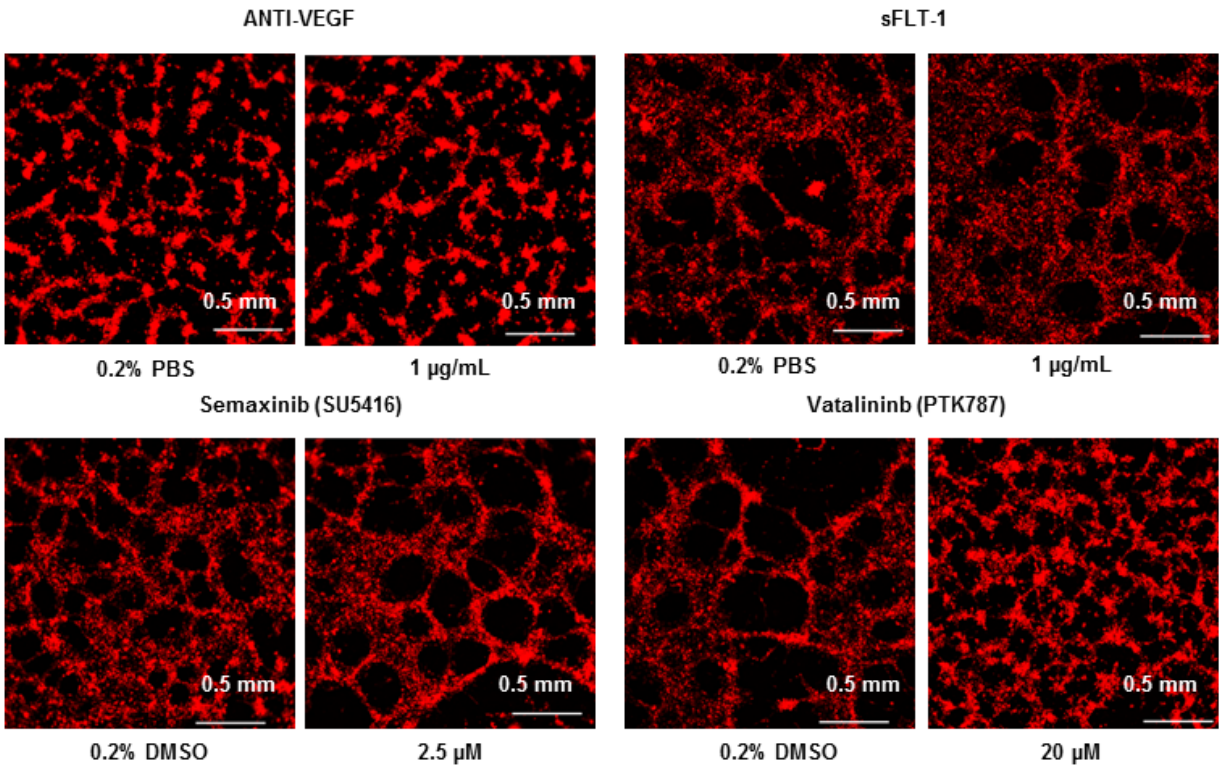

Chapter 3: Supplemental Figure 5. Fluorescent micrographs comparing inhibitor-treated HUVEC networks on synthetic hydrogels and VBP-functionalized hydrogels. The presence of VBP in hydrogels nullify effects of VEGF inhibitors. Red: Cell Tracker Red.

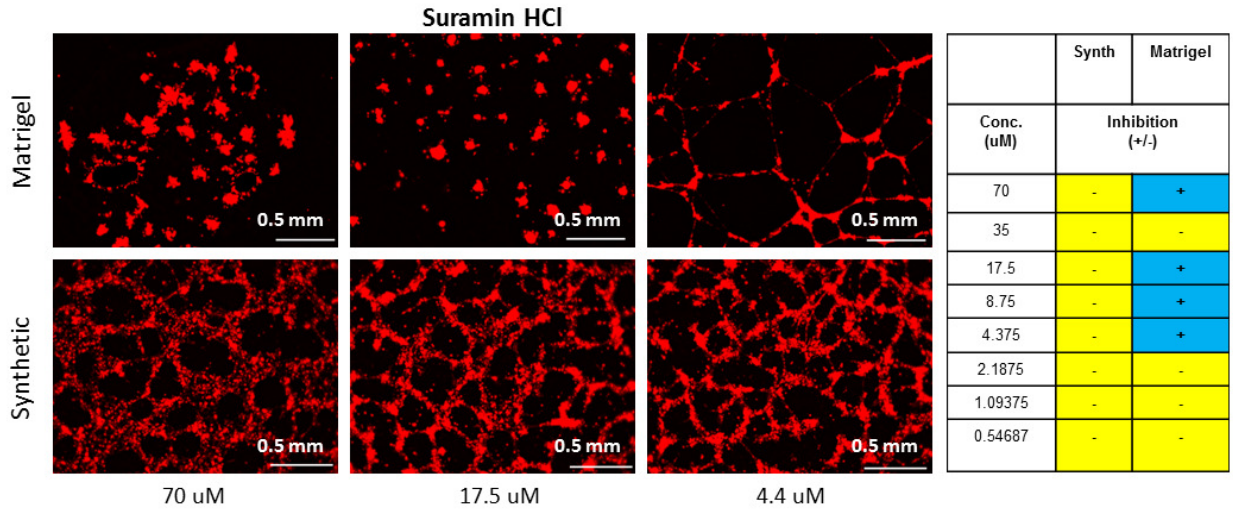

Chapter 3: Supplemental Figure 6. Fluorescent micrographs comparing Suramin-treated HUVEC networks on synthetic hydrogels and Matrigel. Suramin dissolves the Matrigel substrate at concentrations of 70 µM and 17.5 µM. Identical concentrations of Suramin on the synthetic hydrogels have little to no effect on vascular network morphology and do not compromise substrate integrity to the same degree as on Matrigel. Red: Cell Tracker Red.

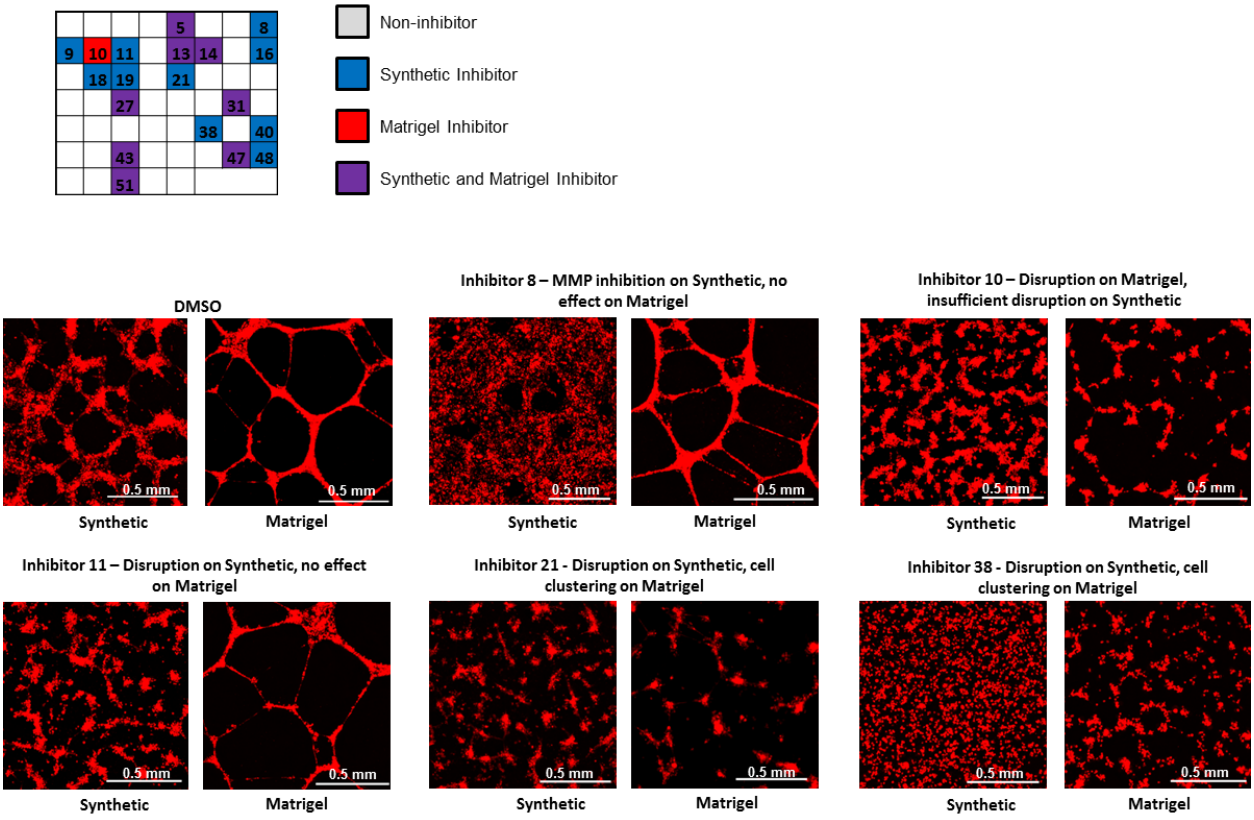

Chapter 3: Supplemental Figure 7. Examples of compounds identified as inhibitors by either the synthetic or Matrigel systems but not in both systems. Red: Cell Tracker Red.

3.9 References

[1] Knudsen TB, Kleinstreuer NC. Disruption of embryonic vascular development in predictive toxicology. Birth Defects Res C Embryo Today. 2011;93:312-23.

[2] De Falco S. Antiangiogenesis therapy: an update after the first decade. Korean J Intern Med. 2014;29:1-11.

[3] Folkman J, Haudenschild C. Angiogenesis by capillary endothelial cells in culture. Trans Ophthalmol Soc U K. 1980;100:346-53.

[4] Folkman J, Haudenschild C. Angiogenesis in vitro. Nature. 1980;288:551-6.

[5] Kubota Y, Kleinman HK, Martin GR, Lawley TJ. Role of laminin and basement membrane in the morphological differentiation of human endothelial cells into capillary-like structures. The Journal of cell biology. 1988;107:1589-98.

[6] Faulkner A, Purcell R, Hibbert A, Latham S, Thomson S, Hall WL, et al. A thin layer angiogenesis assay: a modified basement matrix assay for assessment of endothelial cell differentiation. BMC Cell Biol. 2014;15:41.

[7] Arnaoutova I, Kleinman HK. In vitro angiogenesis: endothelial cell tube formation on gelled basement membrane extract. Nat Protoc. 2010;5:628-35.

[8] Koepsel JT, Nguyen EH, Murphy WL. Differential effects of a soluble or immobilized VEGFR-binding peptide. Integr Biol (Camb). 2012;4:914-24.

[9] Crawford Y, Ferrara N. VEGF inhibition: insights from preclinical and clinical studies. Cell and Tissue Research. 2009;335:261-9.

[10] Kerbel R, Folkman J. Clinical translation of angiogenesis inhibitors. Nature Reviews Cancer. 2002;2:727-39.

[11] Sennino B, McDonald DM. Controlling escape from angiogenesis inhibitors. Nature Reviews Cancer. 2012;12:699-709.

[12] Kleinman HK, Martin GR. Matrigel: basement membrane matrix with biological activity. Matrigel: basement membrane matrix with biological activity. 2005;15:378-86.

[13] Gilbert P, Havenstrite K, Magnusson K, Sacco A, Leonardi N, Kraft P, et al. Substrate Elasticity Regulates Skeletal Muscle Stem Cell Self-Renewal in Culture. Science. 2010;329:1078-81.

[14] Donovan D, Brown NJ, Bishop ET, Lewis CE. Comparison of three in vitro human 'angiogenesis' assays with capillaries formed in vivo. Angiogenesis. 2001;4:113-21.

[15] Hughes C, Postovit L, Lajoie G. Matrigel: A complex protein mixture required for optimal growth of cell culture. Proteomics. 2010;10:1886-90.

[16] Wood JA, Liliensiek SJ, Russell P, Nealey PF, Murphy CJ. Biophysical Cueing and Vascular Endothelial Cell Behavior. Materials. 2010;3:1620-39.

[17] Soofi SS, Last JA, Liliensiek SJ, Nealey PF, Murphy CJ. The elastic modulus of Matrigel (TM) as determined by atomic force microscopy. J Struct Biol. 2009;167:216-9.

[18] Vukicevic S, Kleinman HK, Luyten FP, Roberts AB, Roche NS, Reddi AH. Identification of multiple active growth factors in basement membrane Matrigel suggests caution in interpretation of cellular activity related to extracellular matrix components. Exp Cell Res. 1992;202:1-8.

[19] Stein CA, Larocca RV, Thomas R, Mcatee N, Myers CE. Suramin - an Anticancer Drug with a Unique Mechanism of Action. Journal of Clinical Oncology. 1989;7:499-508.

[20] Prigozhina NL, Heisel AJ, Seldeen JR, Cosford ND, Price JH. Amphiphilic suramin dissolves Matrigel, causing an 'inhibition' artefact within in vitro angiogenesis assays. Int J Exp Pathol. 2013;94:412-7.

[21] Murphy WL, McDevitt TC, Engler AJ. Materials as stem cell regulators. Nat Mater. 2014;13:547-57.

[22] Belair DG, Murphy WL. Specific VEGF sequestering to biomaterials: Influence of serum stability. Acta Biomaterialia. 2013.

[23] Impellitteri N, Toepke M, Levengood S, Murphy W. Specific VEGF sequestering and release using peptide-functionalized hydrogel microspheres. Biomaterials. 2012;33:3475-84.

[24] Nguyen EH, Zanotelli MR, Schwartz MP, Murphy WL. Differential effects of cell adhesion, modulus and VEGFR-2 inhibition on capillary network formation in synthetic hydrogel arrays. Biomaterials. 2014;35:2149-61.

[25] Hansen TD, Koepsel JT, Le NN, Nguyen EH, Zorn S, Parlato M, et al. Biomaterial arrays with defined adhesion ligand densities and matrix stiffness identify distinct phenotypes for tumorigenic and nontumorigenic human mesenchymal cell types. Biomater Sci. 2014;2:745-56.

[26] Fairbanks BD, Schwartz MP, Halevi AE, Nuttelman CR, Bowman CN, Anseth KS. A Versatile Synthetic Extracellular Matrix Mimic via Thiol-Norbornene Photopolymerization. Advanced Materials. 2009;21:5005-10.

[27] Hojjat-Farsangi M. Small-molecule inhibitors of the receptor tyrosine kinases: promising tools for targeted cancer therapies. Int J Mol Sci. 2014;15:13768-801.

[28] Fong TAT, Shawver LK, Sun L, Tang C, App H, Powell TJ, et al. SU5416 is a potent and selective inhibitor of the vascular endothelial growth factor receptor (Flk-1/KDR) that inhibits tyrosine kinase catalysis, tumor vascularization, and growth of multiple tumor types. Cancer Research. 1999;59:99-106.

[29] Maynard SE, Min JY, Merchan J, Lim KH, Li JY, Mondal S, et al. Excess placental soluble fms-like tyrosine kinase 1 (sFlt1) may contribute to endothelial dysfimction, hypertension, and proteinuria in preeclampsia. Journal of Clinical Investigation. 2003;111:649-58.

[30] Clark DE, Smith SK, He YL, Day KA, Licence DR, Corps AN, et al. A vascular endothelial growth factor antagonist is produced by the human placenta and released into the maternal circulation. Biology of Reproduction. 1998;59:1540-8.

[31] Belgore FM, Blann AD, Lip GYH. sFlt-1, a potential antagonist for exogenous VEGF. Circulation. 2000;102:E108-E.

[32] Hashizume H, Falcón BL, Kuroda T, Baluk P, Coxon A, Yu D, et al. Complementary actions of inhibitors of angiopoietin-2 and VEGF on tumor angiogenesis and growth. Cancer Res. 2010;70:2213-23.

[33] Rosenberg SA. Interleukin 2 for patients with renal cancer. Nat Clin Pract Oncol. 2007;4:497.

[34] Cao Y, Langer R. Optimizing the delivery of cancer drugs that block angiogenesis. Sci Transl Med. 2010;2:15ps3.

[35] Ruoslahti E, Pierschbacher MD. New perspectives in cell adhesion: RGD and integrins. Science. 1987;238:491-7.

[36] Ruoslahti E. RGD and other recognition sequences for integrins. Annu Rev Cell Dev Biol. 1996;12:697-715.

[37] Koepsel J, Loveland S, Schwartz M, Zorn S, Belair D, Le N, et al. A chemically-defined screening platform reveals behavioral similarities between primary human mesenchymal stem cells and endothelial cells. Integrative Biology. 2012;4:1508-21.

[38] Nagase H, Fields GB. Human matrix metalloproteinase specificity studies using collagen sequence-based synthetic peptides. Biopolymers. 1996;40:399-416.

[39] Hansen TD, Koepsel JT, Le NN, Nguyen EH, Zorn S, Parlato M, et al. Biomaterial arrays with defined adhesion ligand densities and matrix stiffness identify distinct phenotypes for tumorigenic and non-tumorigenic human mesenchymal cell types. Biomaterials Science. 2014;2:745-56.

[40] Le NNT, Zorn S, Schmitt SK, Gopalan P, Murphy WL. Hydrogel arrays formed via differential wettability patterning enable combinatorial screening of stem cell behavior. Acta Biomaterialia. 2015;Accepted.

[41] Zhang JH, Chung TD, Oldenburg KR. A Simple Statistical Parameter for Use in Evaluation and Validation of High Throughput Screening Assays. J Biomol Screen. 1999;4:67-73.

[42] Loges S, Schmidt T, Carmeliet P. Mechanisms of resistance to anti-angiogenic therapy and development of third-generation anti-angiogenic drug candidates. Genes Cancer. 2010;1:12-25.

[43] Welti J, Loges S, Dimmeler S, Carmeliet P. Recent molecular discoveries in angiogenesis and antiangiogenic therapies in cancer. J Clin Invest. 2013;123:3190-200.

[44] Knudsen TB, Keller DA, Sander M, Carney EW, Doerrer NG, Eaton DL, et al. FutureTox II: In vitro Data and In Silico Models for Predictive Toxicology. Toxicological Sciences. 2015;143:256-67.

[45] Benam KH, Dauth S, Hassell B, Herland A, Jain A, Jang KJ, et al. Engineered In Vitro Disease Models. Annual Review of Pathology: Mechanisms of Disease, Vol 10. 2015;10:195-262.

[46] Cushing MC, Anseth KS. Materials science. Hydrogel cell cultures. Science. 2007;316:1133-4.

[47] Smithmyer ME, Sawicki LA, Kloxin AM. Hydrogel scaffolds as in vitro models to study fibroblast activation in wound healing and disease. Biomater Sci. 2014;2:634-50.

[48] Aird WC. Endothelial cell heterogeneity. Cold Spring Harb Perspect Med. 2012;2:a006429.

[49] Pellett S, Schwartz MP, Tepp WH, Josephson R, Scherf JM, Pier CL, et al. Human Induced Pluripotent Stem Cell Derived Neuronal Cells Cultured on Chemically-Defined Hydrogels for Sensitive In Vitro Detection of Botulinum Neurotoxin. Scientific Reports. 2015;5.

[50] Francescone RA, 3rd, Faibish M, Shao R. A Matrigel-based tube formation assay to assess the vasculogenic activity of tumor cells. J Vis Exp. 2011.

[51] Song J, Rolfe BE, Hayward IP, Campbell GR, Campbell JH. Reorganization of structural proteins in vascular smooth muscle cells grown in collagen gel and basement membrane matrices (Matrigel): a comparison with their in situ counterparts. J Struct Biol. 2001;133:43-54.

[52] Vernon RB, Angello JC, Iruela-Arispe ML, Lane TF, Sage EH. Reorganization of basement membrane matrices by cellular traction promotes the formation of cellular networks in vitro. Lab Invest. 1992;66:536-47.

[53] Seftor RE, Hess AR, Seftor EA, Kirschmann DA, Hardy KM, Margaryan NV, et al. Tumor cell vasculogenic mimicry: from controversy to therapeutic promise. Am J Pathol. 2012;181:1115-25.

[54] Maniotis AJ, Folberg R, Hess A, Seftor EA, Gardner LM, Pe'er J, et al. Vascular channel formation by human melanoma cells in vivo and in vitro: vasculogenic mimicry. Am J Pathol. 1999;155:739-52.

[55] De Smet F, Segura I, De Bock K, Hohensinner P, Carmeliet P. Mechanisms of Vessel Branching Filopodia on Endothelial Tip Cells Lead the Way. Arteriosclerosis Thrombosis and Vascular Biology. 2009;29:639-49.

Chapter 4:

Differential effects of cell adhesion, modulus and VEGFR-2 inhibition on capillary network formation in synthetic hydrogel arrays

Eric H. Nguyen, Matthew R. Zanotelli, Michael P. Schwartz, William L. Murphy. Differential effects of cell adhesion, modulus and VEGFR-2 inhibition on capillary network formation in synthetic hydrogel arrays. *Biomaterials*, 2014. **35**(7): p. 2149-2161.

4.1 Preface

In chapter 3 we described an approach to simultaneously tune cell adhesivity and modulus of poly(ethylene glycol) hydrogels to modulate vascular network formation on hydrogel surfaces. In this chapter, the purpose of these studies was to develop a screening array platform that enabled three dimensional culture of dispersed human umbilical vein endothelial cells in similarly customizable hydrogels and study how combinatorial changes in the cell microenvironment impacted pro-angiogenic endothelial cell behavior. Changes in cell viability, proliferation and tubule network formation were explored with combinatorial changes to cell adhesion, hydrogel modulus and inhibition of VEGF signaling. While individual cell behaviors were differentially affected by the various microenvironments explored in the arrays, the wide range of hydrogel conditions explored in these studies revealed unique situations where vascular inhibiting compounds enhanced vascular network stability rather than prevent network formation. This study established techniques for systematically screening and analyzing vascular network formation in large numbers of three dimensional environments.

4.2 Abstract

Efficient biomaterial screening platforms can test a wide range of extracellular environments that modulate vascular growth. Here, we used synthetic hydrogel arrays to probe the combined effects of Cys-Arg-Gly-Asp-Ser (CRGDS) cell adhesion peptide concentration, shear modulus and vascular endothelial growth factor receptor 2 (VEGFR2) inhibition on human umbilical vein endothelial cell (HUVEC) viability, proliferation and tubulogenesis. HUVECs were encapsulated in degradable poly(ethylene glycol) (PEG) hydrogels with defined CRGDS concentration and shear modulus. VEGFR2 activity was modulated using the VEGFR2 inhibitor SU5416. We demonstrate that synergy exists between VEGFR2 activity and CRGDS ligand presentation in the context of maintaining HUVEC viability. However, excessive CRGDS disrupts this synergy. HUVEC proliferation significantly decreased with VEGFR2 inhibition and increased modulus, but did not vary monotonically with CRGDS concentration. Capillary-like structure (CLS) formation was highly modulated by CRGDS concentration and modulus, but was largely unaffected by VEGFR2 inhibition. We conclude that the characteristics of the ECM surrounding encapsulated HUVECs significantly influence cell viability, proliferation and CLS formation. Additionally, the ECM modulates the effects of VEGFR2 signaling, ranging from changing the effectiveness of synergistic interactions between integrins and VEGFR2 to determining whether VEGFR2 upregulates, downregulates or has no effect on proliferation and CLS formation.

4.3 Introduction

Angiogenesis is the growth of new vascular networks from existing blood vessels [1, 2], and controlling the growth of functional vasculature in biomaterials is critical to developing

functional tissue constructs. Perhaps the most well-studied mediator of angiogenesis is Vascular Endothelial Growth Factor (VEGF), which activates signaling cascades through VEGF receptor 2 (VEGFR2) that promote endothelial cell proliferation [3, 4] and survival [5]. When presented as a concentration gradient, VEGF directionally guides the formation of new vasculature through cell migration and tubule formation [1, 6]. An additional controller of cell viability [7-9], migration [10], proliferation [11] and tubulogenesis [12] is the extracellular matrix (ECM), but there is currently a limited understanding of how the ECM and VEGFR2 activity jointly modulate angiogenesis. Understanding how the extracellular matrix modulates VEGF-driven vascular growth is critical to understanding healing and developmental processes as well as evaluating the effectiveness of drugs designed to modulate angiogenesis.

Though the role of ECM in modulating VEGFR2 activity is not fully understood, there is evidence that VEGFR2 activity is influenced by integrin binding and extracellular matrix rigidity. Binding of $\alpha5\beta1$ as well as $\alpha v\beta3$ integrins to extracellular matrix proteins such as fibronectin and collagen elevates VEGF and VEGFR-2 activity in endothelial cells [13-16], and RhoA and ROCK phosphorylation increase VEGFR2 activity in endothelial cells that exist in stiffer environments [17, 18]. With these findings, it is reasonable to hypothesize that unusual extracellular environments such as growing tumors can lead to aberrant vascular growth. Tumor-associated endothelial cells have been shown to overexpress integrins relative to endothelial cells in normal tissue [19], and the ECM in cancerous breast tissue is stiffer than ECM in healthy breast tissue due to increased protein deposition [20-22]. These effects are likely to result in differing VEGFR2 activity between wound healing sites, developing tissues or tumors. Detailed studies of cell-ECM interactions during angiogenesis can be conducted via in-vitro experimentation, but so far most studies of in-vitro angiogenesis have limited control over

extracellular environments due to the use of naturally-derived materials as matrices. Additionally, in-vitro studies of angiogenesis are usually performed using low throughput experimentation techniques. These experimental formats result in a limited ability to control specific ECM properties and attribute specific, combinatorial modifications to the ECM directly to changes in cell behavior.

Much of what is known about cell-ECM interactions has been discovered in two-dimensional (2D) environments where surfaces can be made to present extracellular matrix proteins, cell adhesion molecules and growth factors. Common examples include protein-coated polymers [23], self-assembled monolayers (SAMs) [3, 11, 24, 25], patterned microwells [26, 27] and hydrogel surfaces [28-30]. While these substrates enable rapid analysis of cell interactions with specific ECM components, they do not approximate the three-dimensional (3D) extracellular environments that exist in vivo. Many important differences in cell behavior exist between 2D and 3D environments. For example, the expression of ECM-degrading matrix metalloproteinases (MMPs) is not required in the formation of capillary networks on surfaces, whereas MMP expression is critical for capillary growth in 3D matrices that restrict cell movement [31-34]. Matrix stiffness and cell adhesion ligand concentration affect endothelial cell migration [10, 35, 36] and network branching [37] differently in 2D and 3D environments. Additionally, it is well accepted that endothelial cells in 2D culture are directly exposed to soluble growth factors [3, 38] whereas growth factor and oxygen diffusion into hydrogels [39-41] play a role in spatially guiding vascularization in 3D environments. These previous studies emphasize not only the importance of 3D environments, but also the variety of parameters that can influence 3D capillary formation.

In order to culture endothelial cells in a variety of 3D environments, as well as investigate the specific effects of VEGF signaling in well-defined settings, we have developed an enhanced-throughput array format capable of 3D cell culture in poly(ethylene glycol) (PEG) hydrogels. PEG is a hydrophilic polymer that resists non-specific protein adsorption [42]. The use of this non-fouling material as the backbone of a hydrogel enables the investigation of how specific modifications to an otherwise "blank slate" extracellular microenvironment affect cell behavior. When multi-arm PEG molecules are functionalized with norbornene groups, the PEG can be controllably decorated with biomimetic signaling peptides and crosslinked into hydrogels through thiol-alkene (thiol-ene) coupling [43, 44]. Previously, screening formats have been utilized to investigate cell-ECM interactions in 2D environments. Examples include micropatterned hydrogel spots on silicon and glass [45], SAM arrays [3, 11, 24] and 24 well plates presenting self-assembling peptide hydrogels [30]. Screening platforms for investigating cell-ECM interactions in 3D environments have included microliter-scale hydrogels in 96 or 48 well plates, cell clusters cultured in isolation by photomasking [46, 47] and PEG-diacrylate hydrogel arrays [7-9]. While these screening platforms enable cell culture in fully 3D, customizable environments, they often consume large amounts of material, require specialized equipment and a high degree of technical proficiency to utilize, and place hydrogels in confined environments unable to support homogeneous swelling. The array developed here consists of 1-mm diameter, 200 μm thick spots protruding from a single hydrogel background. Thus, each hydrogel array spot was allowed to swell uniformly in an unconfined manner by virtue of their connection to a hydrogel base that was also allowed to swell (i.e. the hydrogel spots were neither confined nor linked to a rigid support).

Here we used an array of PEG hydrogels to screen the combined effects of adhesion ligand density, modulus and VEGFR2 signaling on pro-angiogenic cell behaviors using encapsulated human umbilical vein endothelial cells (HUVECs) as a model cell type. We hypothesized that cell adhesion, hydrogel modulus and VEGFR2-mediated signaling would synergistically modulate viability, proliferation and tubulogenesis of HUVECs. We also hypothesized that a VEGFR2 inhibitor modulates viability, proliferation and tubulogenesis differently depending on surrounding ECM contexts and therefore compared the effects of the inhibitor in our PEG hydrogels to effects in Matrigel, a standard platform for screening angiogenesis drugs in vitro [48].

4.4 Materials and methods

4.4.1 Cell culture

Human umbilical vein endothelial cells were purchased from Lonza (Walkersville, MD) and cultured in medium 199 (M199) (Mediatech Inc, Manassas, VA) supplemented with EGM-2 Bulletkit (Lonza). The medium supplement contained 2% bovine serum albumin as well as hydrocortisone, hFGF-B, VEGF, R3-IGF-1, Ascorbic Acid, Heparin, FBS, hEGF, and GA-1000. For simplicity M199 supplemented with EGM-2 will be referred to as “growth medium.” Growth medium was changed every other day and cells were passaged every 4 to 5 days. Cell passages were performed using 0.05% trypsin solution (HyClone, Logan, UT) and detached cells were recovered in M199 supplemented with 10% cosmic calf serum (HyClone). All media was supplemented with 100 U/mL Penicillin/ 100 μg/mL Streptomycin (HyClone). The cells were

maintained in a humidified 37˚C incubator with 5% CO_2 and used between 7 and 16 population doublings in all experiments.

4.4.2 PEG functionalization with norbornene

PEG-norbornene (PEGNB) was synthesized as previously described, with minor modifications during purification [43, 49]. Briefly, solid 8-arm PEG-OH (20 kDa molecular weight, tripentaerythritol core, Jenkem USA, Allen TX), dimethylaminopyridine and pyridine (Sigma Aldrich, St. Louis, MO) were dissolved in anhydrous dichloromethane (Fisher Scientific, Waltham, MA). In a separate reaction vessel, N,N′ -dicyclohexylcarbodiimide (Thermo Scientific, Waltham, MA) and norbornene carboxylic acid (Sigma Aldrich) were dissolved in anhydrous dichloromethane. Norbornene carboxylic acid was covalently coupled to the PEG-OH through the carboxyl group by combining the PEG solution and norbornene solutions and stirring the reaction mixture overnight under anhydrous conditions. Urea was removed from the reaction mixture using a glass fritted funnel and the filtrate was precipitated in cold diethyl ether (Fisher). The precipitated PEGNB was collected and dried overnight in a buchner funnel. To remove impurities, the PEGNB was dissolved in chloroform (Sigma Aldrich), precipitated in diethyl ether and dried a second time in a Buchner funnel. To remove excess norbornene carboxylic acid, PEGNB was dissolved in de-ionized H_2O, dialyzed in de-ionized H_2O for 1 week and filtered through a 0.4 μm pore-size syringe filter. The aqueous PEGNB solution was frozen using liquid nitrogen and lyophilized. Functionalization of PEG with norbornene groups (Fig. 1A) was quantified using proton nuclear magnetic resonance spectroscopy (NMR) to detect protons of the norbornene-associated alkene groups located at 6.8-7.2 PPM [43]. Functionalization efficiency

for norbornene coupling to PEG-OH arms was above 88% for all PEGNB used in these experiments.

4.4.3 Pre-coupling adhesion peptides to PEGNB

Lyophilized PEGNB was dissolved in 10 mM phosphate buffered saline (1x PBS) at 10 mM concentration (80 mM norbornene groups) and combined with 0.05% w/v Irgacure 2959 photoinitiator (I2959) (Ciba Specialty Chemicals, Tarrytown, NY) as well as 2x molar excess of either amidated Cys-Arg-Gly-Asp-Ser (CRGDS) adhesion peptide or amidated Cys-Arg-Asp-Gly-Ser (CRDGS), a scrambled nonfunctional peptide (Genscript, Piscataway, NJ). The mixture was reacted under 365 nm UV light for 3 minutes at a dose rate of 4.5 mW/cm^2 to covalently attach the peptides to norbornene groups (Fig. 1A) via the thiol-ene reaction [43]. To remove buffer salts and unreacted peptide from the decorated PEGNB, the reaction mixture was dialyzed in de-ionized H_2O for 2 days. The dialyzed solution was frozen in liquid nitrogen and lyophilized. The coupling efficiency of PEGNB to the peptides was quantified using proton NMR to detect disappearances of alkene protons at 6.8-7.2 PPM caused by covalent bonding of the peptides to the norbornene group. For simplicity, pre-coupled PEGNB molecules will be referenced as PEGNB-CRGDS and PEGNB-CRDGS.

4.4.4 Forming PEG hydrogels

Hydrogel array constructs were formed from 2 separate hydrogels: the inert hydrogel "background" (Fig. 1B) that is crosslinked using 3.4 kDa PEG-dithiol (PEGDT) (Fig. 1A) crosslinking molecule (Laysan Bio, Arab, AL), and "hydrogel spots" (Fig. 1C) that are decorated

with adhesion peptides and crosslinked using MMP-degradable KCGGPQGIWGQGCK peptide (Fig. 1A) (Genscript) [50]. All hydrogel solutions were created in serum-free M199 and consisted of PEGNB, 0.05% w/v I2959 and 2x molar excess crosslinking molecule to PEGNB to achieve 50% crosslinking density (Fig. 1). To vary cell adhesion to the hydrogels, precoupled-PEGNB-CRGDS and PEGNB-CRDGS molecules were added to the solutions to achieve desired adhesion peptide concentration with a total of 2 mM pendant peptide included in every solution. To vary the modulus of the background hydrogels the combined percent weight of PEGNB and PEGDT was varied between 4, 6 or 8% w/v. To vary the modulus of the hydrogel spots, the combined percent weight of the PEGNB, degradable crosslinking molecule and adhesion peptides was varied between 4.2, 5 and 7% w/v.

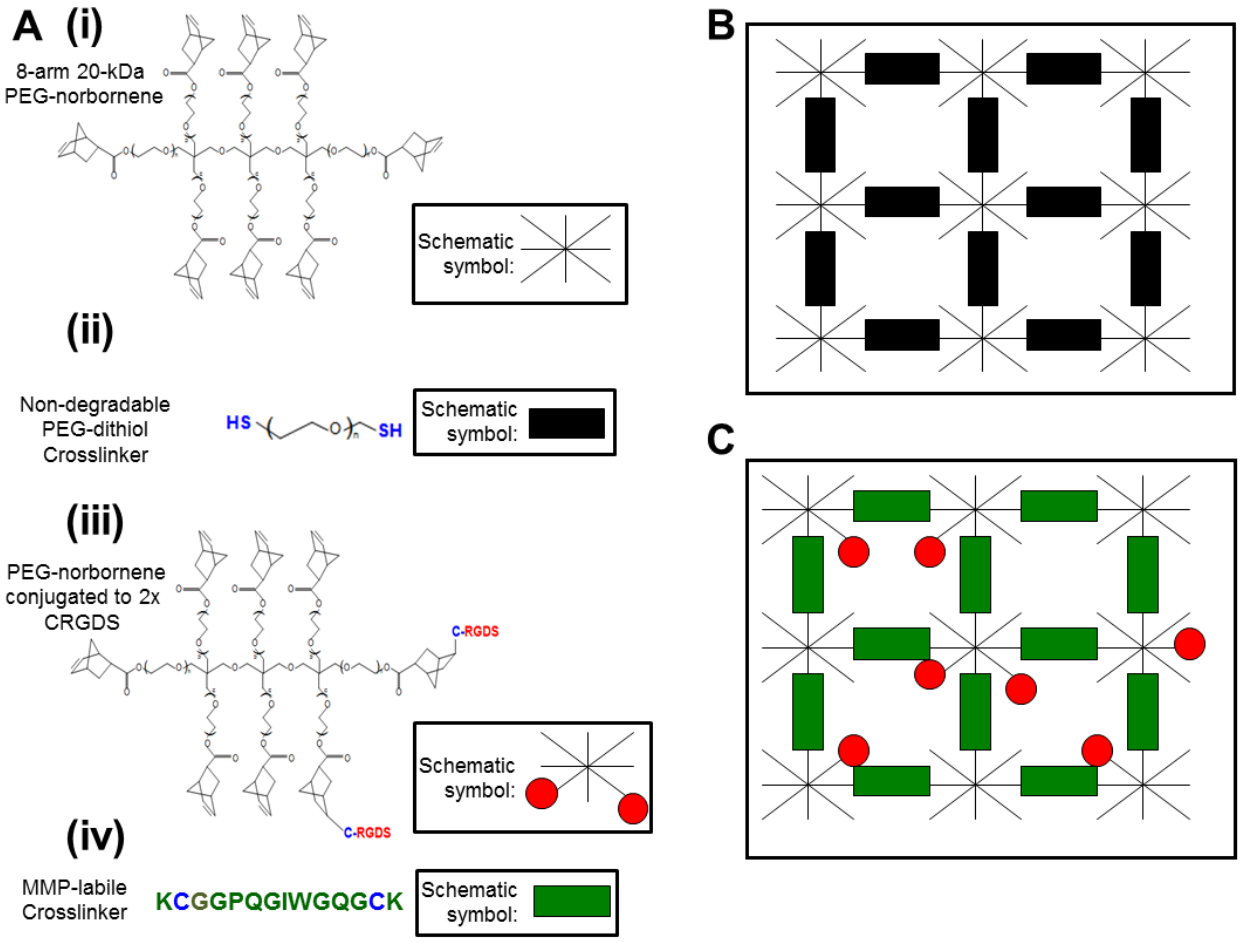

Chapter 4: Figure 1. Molecules included in PEG-norbornene hydrogels. **A)** The hydrogels are composed of (i) 8-arm PEG molecules, with each arm functionalized with a norbornene molecule; (ii) Di-thiolated PEG crosslinking molecules bridge multiple 8-arm PEG molecules together into an ordered polymer network. A di-thiolated PEG molecule acts as an inert crosslinking molecule that is not cell-degradable; (iii) In bioactive hydrogels, PEG molecules are decorated with CRGDS adhesion peptide or CR**DG**S scrambled peptide to modulate cell adhesion to the hydrogel; (iv) Di-thiolated matrix metalloproteinase (MMP) labile crosslinking peptides enable cell-driven hydrogel degradation. **B)** "Background" hydrogels are void of cell adhesion molecules and are not subject to cell-driven degradation. **C)** "Hydrogel spots" modulate cell behavior through covalently attached adhesion molecules and are biodegradable via MMP activity.

4.4.5 Mechanical properties of PEG hydrogels

Mass equilibrium swelling ratios and shear modulus were measured in background hydrogel samples and bulk samples of hydrogel spots. To measure mass equilibrium swelling ratios (Q), 20 µL droplets of hydrogel solutions were pipetted onto a flat Teflon surface and crosslinked under 365 nm UV light for 2 seconds at a dose rate of 90 mW/cm^2. The samples were swelled in serum-free M199 for 24 hours and weighed for swollen weight (WS). Afterward, the samples were washed in de-ionized H_2O overnight to remove M199 components from the hydrogel, frozen in -80˚C for 2 hours and lyophilized. The dried polymer was weighed for dry weight (WD) and mass equilibrium swelling ratio was calculated as per equation 1.

$$Q = \frac{W_S}{W_D}$$

Chapter 4: Equation 1. Mass equilibrium swelling ratio

To measure the shear modulus of the hydrogels, 660 µL of the above solutions were pipetted into 2.1cm diameter Teflon wells. The resulting hydrogels were swollen in 1x PBS for 24 hours before test samples of 8 mm diameter were retrieved using a hole punch with 3 replicates per condition. The samples were tested using an Ares-LS2 rheometer (TA Instruments, New Castle, DE). A 20 g force was applied to the samples and a strain sweep test at 10 Hz fixed frequency was performed from 0.1 to 20% strain. Complex shear modulus of each sample was as the average of measurements taken at 10 Hz, 1-10% strain.

4.4.6 Hydrogel array stencils

Hydrogel array stencils were fabricated using conventional photolithography techniques [51] and were formed from two separate elastomer parts: a 200 µm thick sheet of microwells and a 1mm thick base. Briefly, silicon master molds were fabricated by spin coating a 200 µm layer of SU-8 100 (Microchem, Newton, MA) onto a silicon wafer (University Wafer, Boston MA). Arrayed 1 mm diameter posts of photoresist were defined using a photomask (Imagesetter, Madison, WI). Poly(dimethyl siloxane) (PDMS) was prepared by combining Sylgard PDMS solution with crosslinking solution (Dow Corning, Midland, MI) at a 10:1 volume ratio. The solution was degassed under a vacuum for 45 minutes, poured onto the silicon master mold and crosslinked on a hot plate for 4 hours at 85˚C, forming the 200 µm thick sheet of microwells that penetrated the entire thickness of the sheet. To form the base of the hydrogel array stencil, the PDMS solution was poured between glass slides to form sheets of 1 mm thickness and cured on a hot plate for 4 hours at 85˚C. Both stencil components were cleaned in hexanes (Fisher) by soxhlet extraction [52] and placed in vacuo to remove residual solvent. The completed PDMS stencil was formed by laying the 200 µm thick sheet on top of the 1 mm thick base.

4.4.7 Forming PEG hydrogel arrays

Hydrogel spot solutions were added to the PDMS stencil wells as 0.4 µL droplets (Fig. 2). To solidify the hydrogel spots before dessication, the droplets were crosslinked under 365 nm UV light for 2 seconds at a dose rate of 90 mW/cm^2 after every 5 droplets were patterned. A photomask was used to prevent multiple UV exposures to previously cured spots.

Once all spots were crosslinked under UV light, a 1 mm-thick background hydrogel slab was formed by curing 230 µL background hydrogel solution under 365 nm UV light for 2 seconds at a dose rate of 90 mW/cm^2 between a flat 1 mm thick PDMS sheet and a 1" x 1" glass slide. After removing the PDMS sheet only, an additional 30 µL background hydrogel solution was pipetted on top of the hydrogel slab to anchor the spots to the background slab upon crosslinking. The background slab, still attached to the glass slide, was placed on top of the cured hydrogel spots and the entire array was cured for an additional 2 seconds under 365 nm UV light at a 90 mW/cm^2 dose rate. The hydrogel array was removed from the PDMS stencil and submerged in medium in a 6-well cell culture plate. The completed arrays were secured to the bottom of the wells by using magnets to hold the glass slides in place.

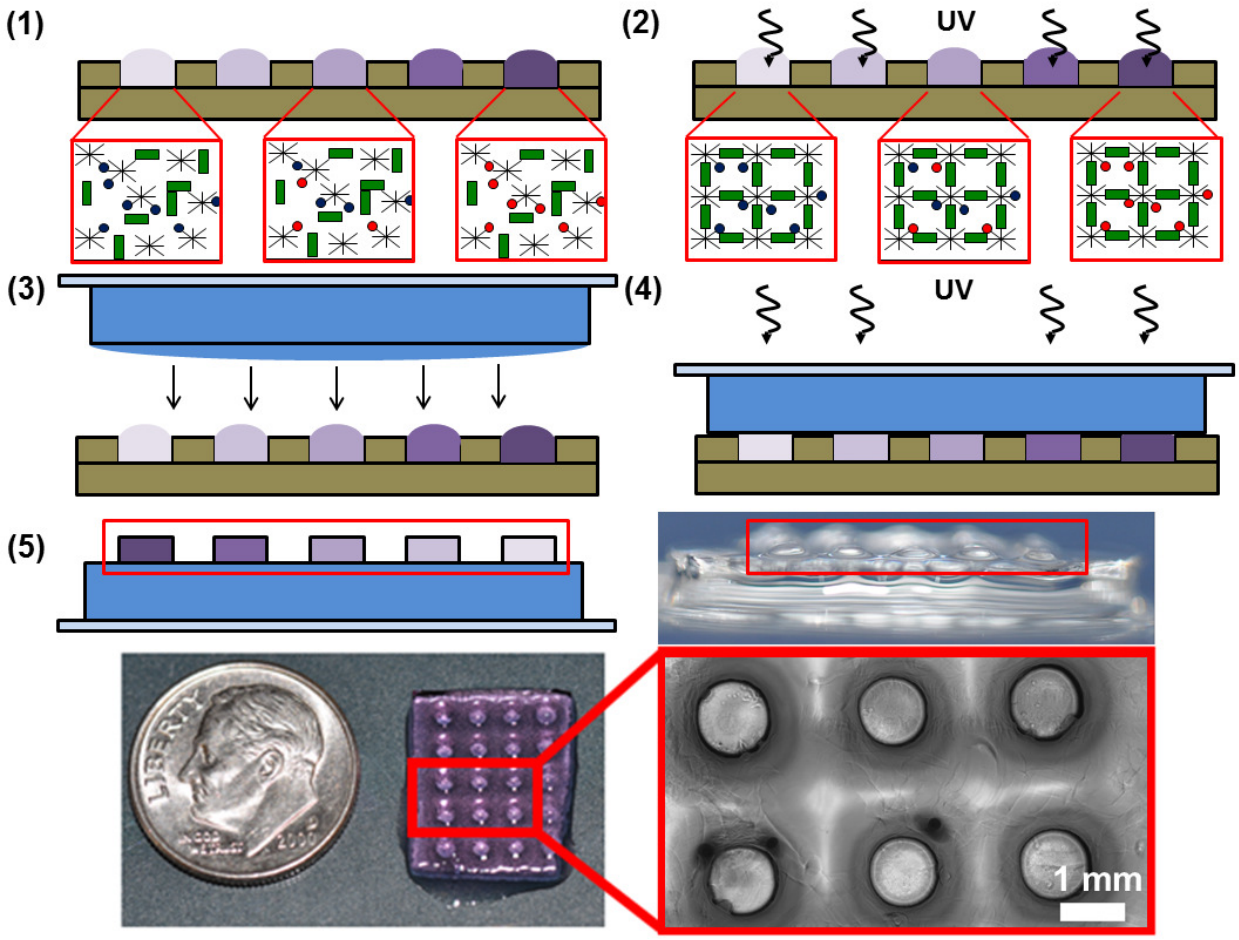

Chapter 4: Figure 2. Schematic representation of hydrogel array fabrication. **1)** Separate hydrogel spot solutions containing various ratios of CRGDS adhesion peptide (Red circles) and a scrambled CR**D**G**S** non-functional peptide (Blue circles) are pipetted into wells of a PDMS stencil. Total pendant peptide concentration is fixed at 2 mM in all solutions. **2)** The hydrogel spots are crosslinked in the stencil using UV light. **3)** A crosslinked 1-mm thick "background" hydrogel slab is laid on top of the crosslinked bioactive hydrogel spots. A thin layer of background hydrogel solution is added to the slab to anchor the cured spots to the background. **4)** The hydrogel spots are anchored to the background after treatment with UV light. **5)** The completed hydrogel array is removed from the stencil. Red boxes highlight the raised spots in the schematic and side view images of the arrays.

4.4.8 Peptide incorporation into hydrogel array spots

To verify controllable peptide incorporation into the hydrogel array spots, hydrogel solutions of 12% w/v total polymer consisting of PEGNB, a 2X molar excess of 3.4 kDa PEG dithiol to PEGNB, and PEGNB-CRGDS such that 0, 0.01, 0.1, 1, 2 mM concentrations of CRGDS were patterned into the array using the above procedure. The background hydrogels were compositionally identical to the spots but were lacking CRGDS. CRGDS concentration was verified by labeling the N-terminus of the peptide with fluorescein. Briefly, the arrays were treated with 3 μM solution of fluorescein-conjugated sulfodichlorophenol ester (Invitrogen, Grand Island, NY) in PBS, incubated for overnight, then rinsed for 24 hours in new PBS. The fluorescently labeled spots were photographed using a Nikon TI Eclipse microscope, and fluorescence intensity was quantified using ImageJ software.

4.4.9 HUVEC viability, tubulogenesis and proliferation in 3D hydrogel arrays

During hydrogel array fabrication, hydrogel spots contained HUVECs at a density of 2 x 10^7 cells/mL. The concentration of CRGDS adhesion peptide was adjusted to 0, 0.25, 0.5, 1.0 and 2.0 mM through the addition of PEGNB-CRGDS, with the total pendant peptide concentration in all hydrogel spots maintained at 2 mM by adding PEGNB-CRDGS. Total polymer percent weight was varied between 4.2, 5 and 7% w/v in the hydrogel spots and 4, 6 and 8% w/v in the backgrounds, with low percent weight hydrogel spots corresponding to low weight percent backgrounds and high percent weight hydrogel spots corresponding to high percent weight backgrounds. During viability experiments, arrays of encapsulated cells were cultured for 48 hours in growth medium alone or with 10 μM SU5416 (Sigma Aldrich), a known inhibitor of

VEGFR2 signaling [53]. Medium was replaced 24 hours after encapsulation. After 48 hours of culture, the arrays were washed with serum-free M199 and stained with 5 μM Cell Tracker Green (Invitrogen) for 45 minutes in M199. After 15 minutes of staining, the staining solution was supplemented with Hoescht nuclear stain (Invitrogen) to achieve a final concentration of 10 μg/mL. After staining, the arrays were washed with serum-free M199 and incubated for 30 minutes in growth medium containing 2 μM ethidium homodimer (Invitrogen). The arrays were then washed with 1X PBS and fixed for 30 minutes in 10% buffered formalin (Fisher). The arrays were soaked in 1X PBS overnight and photographed using a Nikon TE300 fluorescence microscope within 48 hours of fixation. Viability was quantified by dividing the number of live cell nuclei by total nuclei in the post.

During proliferation and tubulogenesis experiments, the arrays of encapsulated cells were cultured in growth medium alone or with 10 μM SU5416 for 24 hours only. Afterward, the cells were incubated for 5 hours in growth medium with 20 μM 5-ethynyl-2'-deoxyuridine (EdU) (Invitrogen) as a proliferation marker and, if appropriate, 10 μM SU5416. Afterward, the arrays were stained with Cell Tracker Green in the same manner as the viability assay, but without Hoescht nuclear stain or ethidium homodimer. The arrays were washed with 1X PBS, fixed for 30 minutes in 10% buffered formalin and stained using the Click-iT EdU 594 proliferation kit (Invitrogen). The staining procedure was slightly modified from the manufacturer's instructions, as Alexa Fluor® 594 was diluted to half the recommended concentration. The arrays were soaked in 1X PBS overnight and photographed using a Nikon TE300 fluorescence microscope. Proliferation was quantified by counting the number of EdU-positive cells and dividing by the total number of nuclei in the post. Tubulogenesis was quantified by manually measuring total capillary-like structure (CLS) length in each post as labeled by Cell Tracker Green. To obtain

confocal microscopy images, the hydrogel arrays were mounted in Prolong Gold antifade solution (Invitrogen) and photographed on a Nikon A1R-Si confocal microscope.

4.4.10 HUVEC proliferation and VEGFR2 inhibition

HUVECs were plated in tissue culture polystyrene (TCPS) 24-well plates at a density of 5.0 x 10^4 cells/cm^2. The cells were grown in growth medium alone or with 10 μM SU5416 for 24 hours. Afterward, the medium was changed to fresh growth medium with or without 10 μM SU5416 and 20 μM EdU. After 5 hours of incubation, the cells were fixed in 10% buffered formalin for 30 minutes and stained using the Click-iT EdU 488 proliferation kit (Invitrogen). The staining procedure was slightly modified from the manufacturer's instructions, as Alexa Fluor® 488 was diluted to half the recommended concentration. The cells were photographed using a Nikon TE300 fluorescence microscope and proliferation was quantified via by counting nuclei staining positive for EdU and normalizing the number to total nuclei.

4.4.11 HUVEC tubulogenesis in Matrigel

HUVECs were suspended in growth factor-reduced Matrigel (BD Biosciences, San Jose, CA) at a density of 2 x 10^7 cells/mL. A 200 μm thick PDMS sheet of microwells was placed on top of a glass slide and the Matrigel-cell suspension was pipetted as 0.4 μL droplets into the microwells. These arrays of Matrigel "spots" were incubated at 37˚C for 30 minutes and covered in growth medium alone or with 10 μM SU5416. After 48 hours of culture, the arrays were stained with Cell Tracker Green in the same manner as in the PEG hydrogel viability assay, but without Hoescht nuclear stain or ethidium homodimer. The arrays were washed with 1X PBS and fixed

for 30 minutes in 10% buffered formalin. A green fluorescence and phase contrast z-stack image of each spot was taken at 48 hours after encapsulation using a Nikon TI Eclipse microscope. Total CLS length in each individual spot was quantified manually.

4.4.12 HUVEC tubulogenesis in confined hydrogels

HUVEC tubulogenesis in 10 μL volume hydrogels was qualitatively assessed to determine the effects of hydrogel confinement on CLS formation. Here, the hydrogels contained 4.2% w/v total polymer, a 2X molar excess of cell-degradable crosslinking peptide to PEGNB, and PEGNB-CRGDS to establish a CRGDS concentration of 2 mM. The HUVECs used in these hydrogels were treated with 1 μM Cell Tracker Green prior to trypsinization. Briefly, the cells were washed with serum-free M199 and stained with Cell Tracker Green for 45 minutes in M199. After staining, the cells were washed with serum-free M199 and incubated for 30 minutes in growth medium. After trypsinization, the cells were resuspended in the PEG hydrogel solution at a density of at 2 x 10^7 cells/mL.

To observe tubulogenesis in confined hydrogels, the cell-containing hydrogel solutions were pipetted as 10 μL droplets on the bottoms of 48-well TCPS plates. The droplets were crosslinked under 365 nm UV light for 2 seconds at a dose rate of 90 mW/cm^2. To ensure that the droplets remained stationary throughout the duration of the experiment, 90 μL of 8% w/v background hydrogel solution was added around the solidified hydrogels and crosslinked under 365 nm UV light for 2 seconds at a dose rate of 90 mW/cm^2. The encapsulated cells were incubated in growth medium with 10 μM SU5416 for 24 hours. A green fluorescence and phase contrast z-

stack image of each sample was taken using a Nikon TI Eclipse microscope 24 hours after encapsulation.

To observe tubulogenesis in unconfined hydrogels, the cell-containing hydrogel solutions were pipetted as 10 µL droplets on a flat PDMS sheet and crosslinked under 365 nm UV light for 2 seconds at a dose rate of 90 mW/cm^2. The resulting hydrogels were transferred to a 24-well TCPS plate containing growth medium with 10 µM SU5416. After 24 hours of incubation, the gels were pinned using a 24-well culture inserts (Becton Dickinson, Franklin Lakes, NJ) to keep them stationary during photography. A green fluorescence and phase contrast z-stack image of each sample was taken using a Nikon TI Eclipse microscope 24 hours after encapsulation.

4.4.13 Statistical analysis

Statistical differences were calculated using the two-sided Student's T-test assuming equal variances. Statistical significance was denoted as $p < 0.05$.

4.5 Results

4.5.1 Hydrogel equilibrium swelling ratio and complex shear modulus

The swelling properties and moduli of degradable hydrogel spots and inert background hydrogels were controlled by adjusting the percent weight of polymer included in the formulations. Hydrogel spot formulations containing 4.2, 5 and 7% w/v polymer had mass equilibrium swelling ratios of 42.1 ± 2.1, 28.7 ± 2.9, and 21.6 ± 0.4, respectively. Background hydrogels containing 4, 6 and 8% w/v polymer had equilibrium swelling ratios of 34.9 ± 0.9, 23.9 ± 0.9

and 21.3 ± 1.1, respectively (Fig. 3A). The background hydrogels were designed to have similar but slightly lower swelling ratios than the hydrogel spots in order to provide a more stable substrate for anchoring the spots during culture. Hydrogel spot formulations containing 4.2, 5 and 7% w/v polymer had moduli of 260 ± 140 Pa, 980 ± 210 Pa and 3220 ± 610 Pa, respectively. Therefore, the 4.2, 5 and 7% w/v hydrogels were designated as "low", "medium" and "high" modulus hydrogels for the duration of the study to clarify the presentation of the data. The moduli of the 4, 6 and 8% w/v background hydrogels were 1040 ± 100 Pa, 3100 ± 220 Pa and 4160 ± 350 Pa, respectively (Fig. 3B). The range of moduli chosen for this study (~260-3220 Pa) spans a wide range of tissues, including soft tissues such as the vocal fold lamina [54], as well as normal breast tissue and cancerous breast tissue, two examples of tissues that differ in mechanical properties as well as extent of vascularization [55, 56].

4.5.2 Hydrogel array fabrication and peptide incorporation

The hydrogel constructs in this study consisted of arrayed PEG hydrogel spots that contained controlled concentrations of CRGDS. Functionalization efficiency of PEGNB with CRGDS or CRDGS was confirmed using NMR. The adhesion peptides CRGDS and CRDGS were reacted to PEGNB at 2x molar excess to decorate, on average, two of the eight arms of the PEGNB molecule with the cell adhesion peptides. The presence of CRGDS at 2x molar excess to PEGNB resulted in a 24.8 ± 4.1% reduction of alkene protons present on the PEG molecule, and the presence of CRDGS at 2x molar excess to PEGNB resulted in a 25.7 ± 4.9% reduction of alkene protons (Fig. 3C). This indicates that approximately 2 of the 8 available norbornene groups on a given PEGNB molecule were coupled to the adhesion peptide, as expected.

Incorporation of peptide-decorated PEG macromers into the hydrogel arrays was also visualized using fluorescein staining via a sulfodichlorophenol-ester linkage. Fluorescent signals from the array were directly proportional to the amount of peptide added to the arrayed hydrogel spots. Additionally, only background fluorescence was detected between the spots, indicating that the peptides were present in the spots only (Fig. 3D). These results demonstrate that PEG hydrogels can be used to provide synthetic control over incorporation of thiol-containing ligands, in this case, the cell adhesion peptide CRGDS.

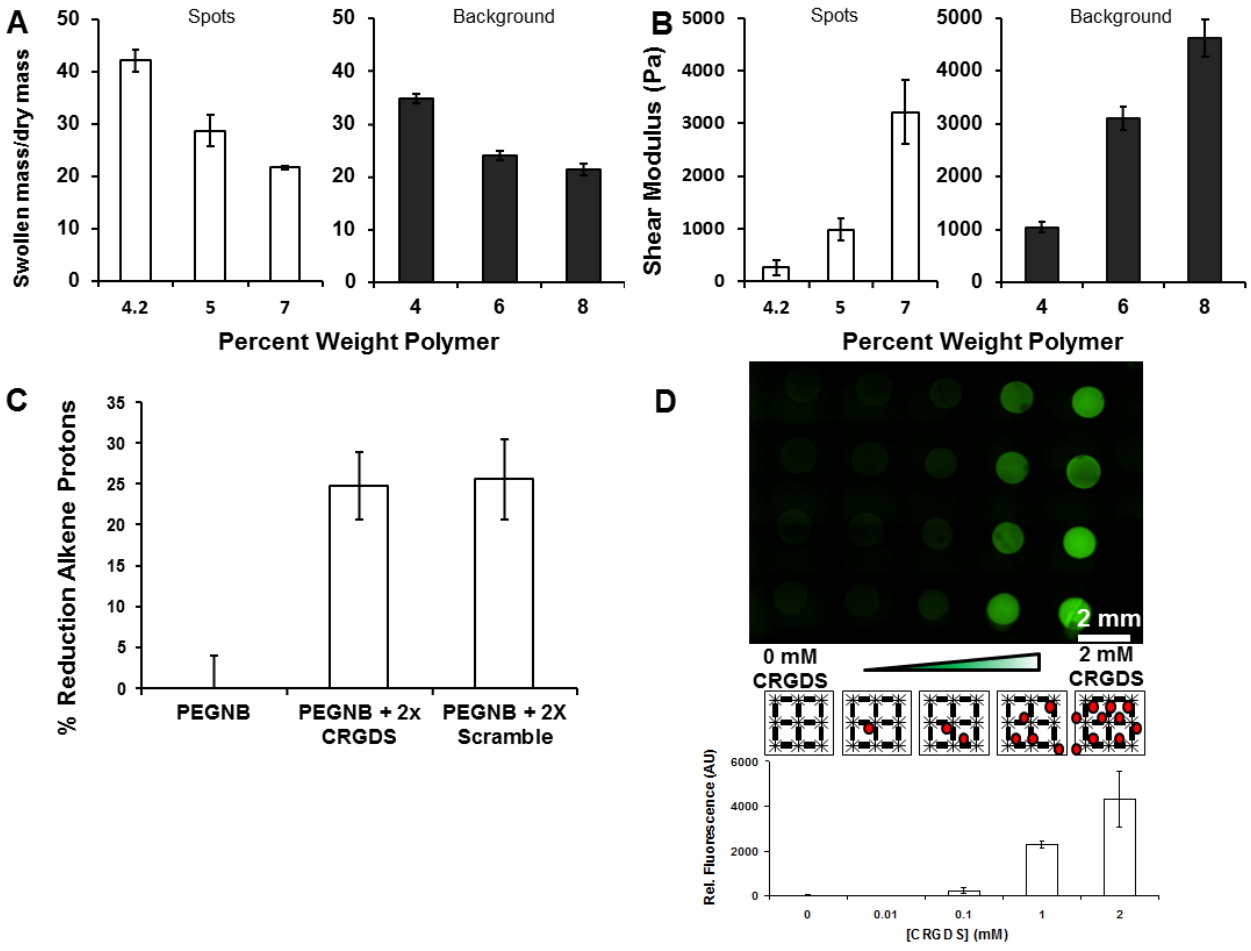

Chapter 4: Figure 3. Characterizing mechanical properties and pendant peptide incorporation into the hydrogel array. **A)** Equilibrium swelling ratios of degradable (left) and background

(right) and hydrogels used in low, medium and high hydrogel modulus conditions. **B)** Complex shear modulus of degradable (left) and background (right) hydrogels using in low, medium and high hydrogel modulus conditions. Error bars indicate standard deviation. **C)** Reduction in norbornene alkene protons due to covalent coupling of CRGDS and CRDGS as measured using NMR. **D)** N-terminal amines of CRGDS were labeled with Alexa Fluor® 488 (Green). Green fluorescence intensity was quantified from the left to right columns (Black lines: PEG polymer and crosslinker. Red circles: CRGDS).

4.5.3 Three-dimensional cell viability in PEG hydrogel arrays

We quantified viability of encapsulated HUVECs to verify that the cells withstood the encapsulation and array patterning processes, and to evaluate the effects of adhesion ligand density and stiffness on maintaining cell survival. Cell viability generally increased with increasing CRGDS, and high modulus conditions suppressed viability. In all conditions HUVECs displayed viability levels at or above 40% of total encapsulated cells, with the lowest viability levels observed in spots containing 0 mM CRGDS. Increased CRGDS concentration increased viability in all modulus conditions, with maximal viability observed at 0.5 and 1.0 mM CRGDS. At these optimal CRGDS concentrations, low modulus hydrogels promoted the highest viability levels compared to equivalent CRGDS concentrations in higher modulus conditions. However, viability in the low and medium modulus hydrogels decreased when CRGDS concentration was increased from 1.0 to 2.0 mM. This decrease did not reduce viability below levels observed at 0 mM CRGDS concentrations, indicating that the 2.0 mM CRGDS concentration was suboptimal, but not detrimental to HUVEC viability relative to non-adhesive conditions. In the high modulus condition, there was no significant decrease in HUVEC viability at 2.0 mM when compared to 1.0 mM CRGDS, suggesting a role of stiffness in maintaining viability in the presence of high CRGDS concentrations (Fig. 4A).

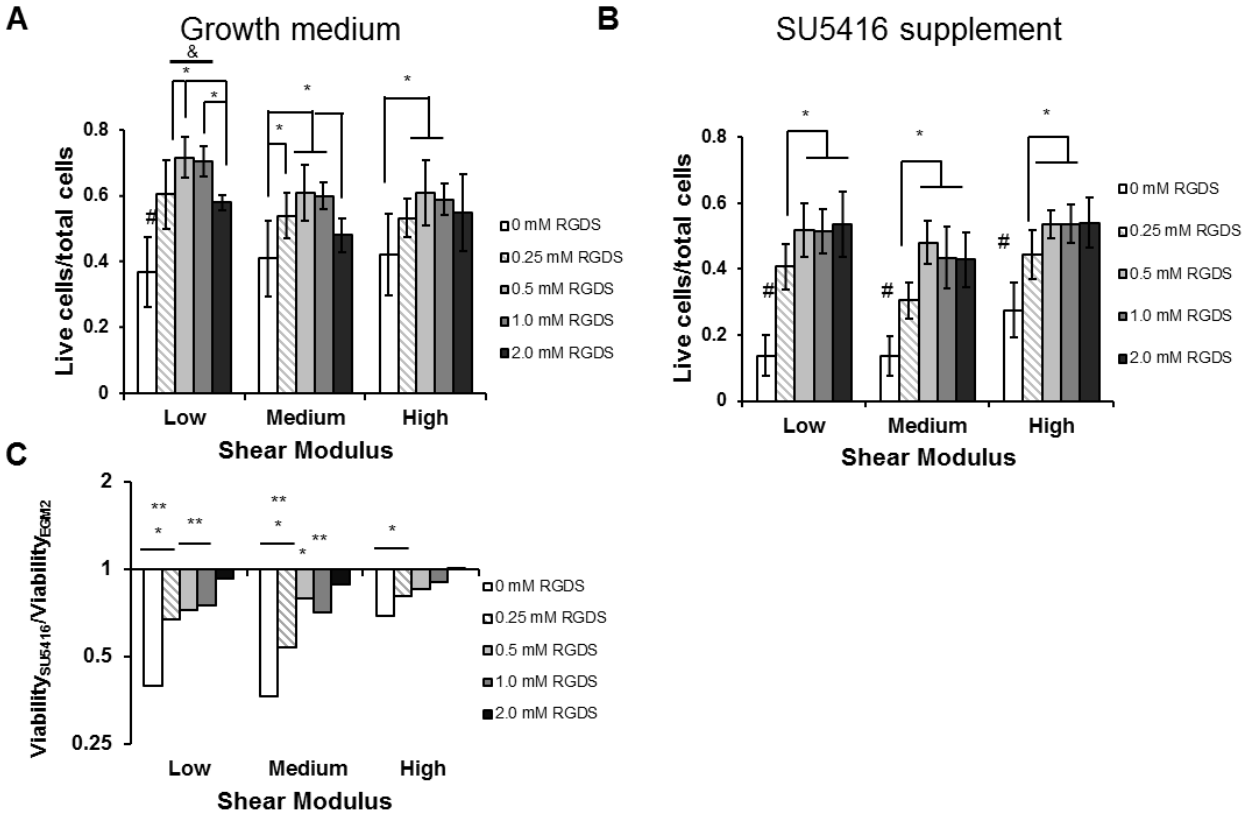

Chapter 4: Figure 4. Viability of HUVECs encapsulated inside the hydrogel array spots. **A)** Cell viability as determined by counting live cell and dead cell nuclei 48 hours after encapsulation. **B)** Cell viability measured when VEGFR2 was inhibited by 10 μM SU5416 supplementation. *, $p < 0.05$. &, $p < 0.05$ compared to all equivalent CRGDS concentration in other modulus conditions **C)** Viability of SU5416-treated HUVECs normalized to HUVEC viability in growth medium. *, $p < 0.05$; **, $p < 0.01$; ***, $p < 0.001$ compared to growth medium control.

4.5.4 Three-dimensional cell proliferation in PEG hydrogel arrays

The effects of cell adhesion and stiffness on proliferation were determined by labeling and quantifying the nuclei of encapsulated HUVECs in S-phase. In all modulus conditions, the addition of CRGDS to the hydrogel increased cell proliferation beyond spots lacking CRGDS

(Fig. 5A). Proliferation did not follow a monotonic trend with increasing CRGDS, and high modulus hydrogels suppressed proliferation relative to low and medium modulus conditions. In particular, proliferation in the low and medium modulus conditions displayed a biphasic response to increasing CRGDS. Proliferation was lower at 0.5 mM CRGDS compared to 0.25 and 2.0 mM CRGDS in the low modulus condition and lower at both 0.5 and 1.0 mM CRGDS compared to 2.0 mM CRGDS in the medium modulus condition. In the high modulus condition, the overall proliferation rate was significantly lower than proliferation rates in the low and medium modulus conditions, and no significant differences in proliferation existed between any conditions containing CRGDS. In addition to ECM effects on proliferation, we also qualitatively noted that a majority of proliferating cells co-localized with multicellular structures (Fig. 5D).

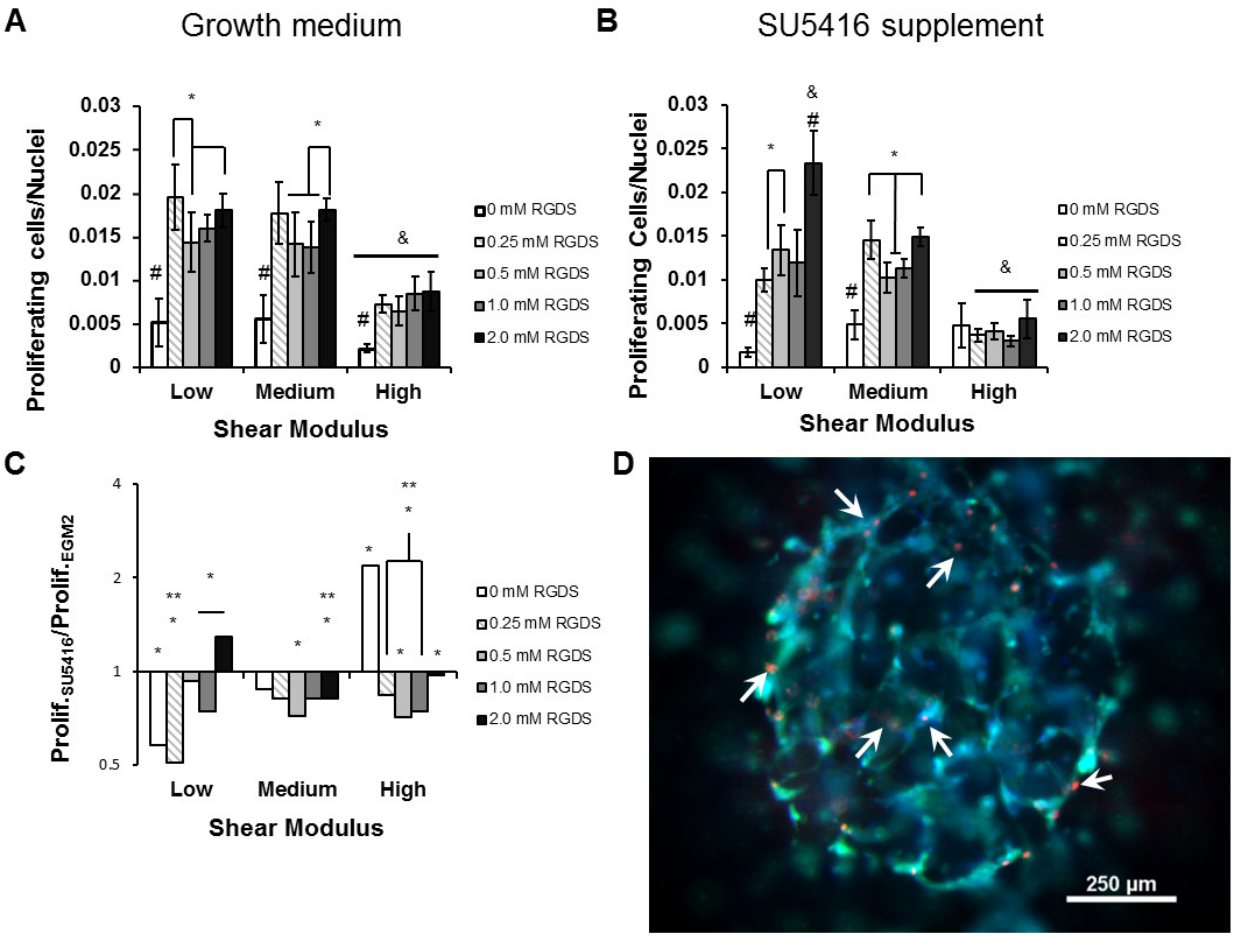

Chapter 4: Figure 5. Proliferation of HUVECs encapsulated inside the hydrogel array spots. **A)** Cell proliferation as determined by Click-it EdU staining 24 hours after encapsulation **B)** Cell proliferation measured when VEGFR2 was inhibited by 10 µM SU5416 supplementation. *, $p < 0.05$. &, $p < 0.05$ compared to all equivalent CRGDS concentration in other modulus conditions **C)** Cell proliferation during SU5416 treatment normalized to proliferation in growth medium. *, $p < 0.05$; **, $p < 0.01$; ***, $p < 0.001$ compared to growth medium control. **D)** Proliferating cells (arrowheads) were localized to multicellular structures. Green: Cell Tracker Green. Blue: Hoescht nuclear stain. Red: Alexa Fluor® 594 labeling nuclei of cells in S-phase.

4.5.5 Three-dimensional tubulogenesis in PEG hydrogel arrays

Cell adhesion and hydrogel stiffness significantly influenced total capillary-like structure (CLS) length in the hydrogel spots, and optimal levels of CRGDS concentration and modulus

maximized CLS formation in the range of conditions tested. In all modulus conditions, CLS formation was rare in the absence of CRGDS. In the low modulus condition, CLS formation increased with increasing CRGDS up to 1.0 mM concentration and decreased at 2.0 mM CRGDS. This trend was not observed in the medium modulus condition where CLS formation remained elevated at 2.0 mM CRGDS (Fig. 6A). In the high modulus condition CLS formation was significantly increased at 0.25, 0.5 and 1.0 mM CRGDS compared to the condition lacking CRGDS, but this increase was no longer significant at 2.0 mM CRGDS. CLS formation at 0.5 mM CRGDS was significantly lower in the high modulus condition compared the low modulus condition and CLS formation at 1.0 and 2.0 mM CRGDS was lower in the high modulus condition compared to the medium modulus condition, indicating that high stiffness interfered with CLS formation in these hydrogels. Taken together, these results suggest that tubulogenesis increases with increasing CRGDS, but the most significant increases were observed in an optimal, medium modulus condition that was not excessively compliant or stiff.

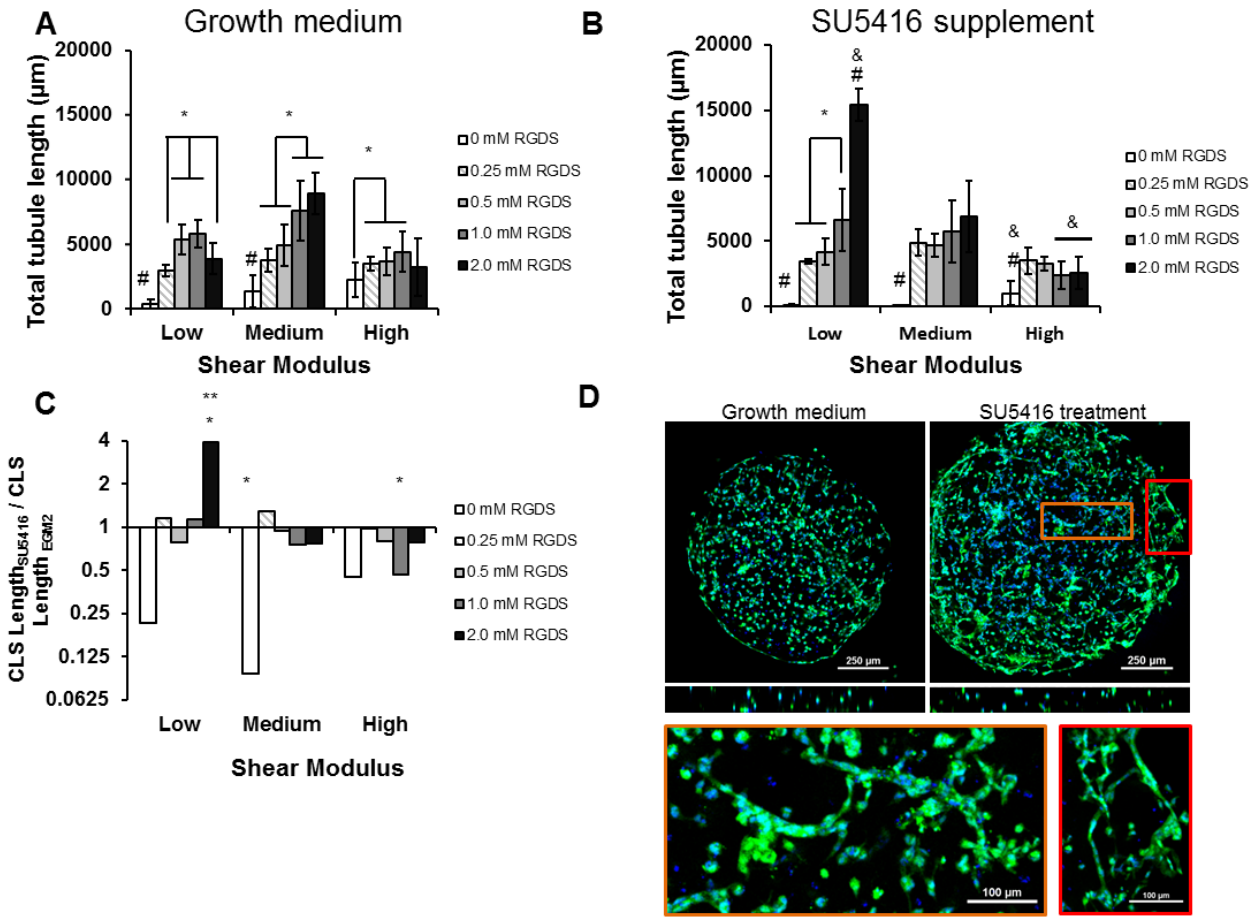

Chapter 4: Figure 6. Tubulogenesis of HUVECs encapsulated inside the hydrogel array spots. **A)** Total tubule length was determined by manually measuring tubule lengths throughout the spots from epifluorescence Z-stack images. The cells were stained using Cell Tracker Green and Hoescht nuclear stain 24 hours after encapsulation. **B)** Tubulogenesis when VEGFR2 was inhibited by 10 μM SU5416 supplementation. *, $p < 0.05$. &, $p < 0.05$ compared to all equivalent CRGDS concentration in other modulus conditions **C)** Tubulogenesis during SU5416 treatment normalized to tubulogenesis in growth medium. *, $p < 0.05$; **, $p < 0.01$; ***, $p < 0.001$ compared to growth medium. **D)** Confocal microscopy images of low tubulogenesis in low modulus, 2 mM RGDS spots and increased tubulogenesis levels with SU5416 treatment. Bottom: Enlarged examples of capillary-like structures seen in the VEGFR2-inhibited condition. Scale bars: 100 μm. Green: Cell Tracker Green. Blue: Hoescht nuclear stain.

4.5.6 HUVEC viability, proliferation and tubulogenesis with VEGFR2 inhibition

SU5416 is an inhibitor to VEGFR2 phosphorylation [53], and we confirmed that inhibiting VEGF signaling by adding SU5416 to growth medium reduced HUVEC proliferation and tubulogenesis in traditional cell culture systems in our hands. When HUVECs were seeded on TCPS surfaces and assayed for proliferation, VEGFR2 inhibition resulted in a 20% decrease in proliferation compared to the growth medium control (Fig. 7A). When HUVECs were encapsulated in growth factor-reduced Matrigel and assayed for CLS formation, VEGFR2 inhibition resulted in a 50% decrease in total tubule length compared to HUVECs incubated with growth medium only (Fig. 7B,C).

To explore the combinatorial roles of VEGFR2 signaling, controlled adhesion ligand density and stiffness in synthetic environments, we encapsulated HUVECs in hydrogel array spots, inhibited VEGFR2 signaling and assayed for viability, proliferation and tubulogenesis. VEGFR2 inhibition significantly reduced cell viability in conditions that did not contain the CRGDS cell adhesion peptide (Fig. 4B). In all modulus conditions viability plateaued at 0.5 mM CRGDS, indicating a limited role of CRGDS in maintaining cell viability when VEGFR2 was inhibited. This also suggests a synergistic interaction between VEGFR2 and integrin-mediated cell adhesion in the context of HUVEC viability. However, while normal VEGFR2 generally increased viability levels when compared to inhibited VEGFR2, the difference between normal VEGFR2 conditions and inhibited conditions decreased as the CRGDS concentration increased. In all modulus conditions, the reduction of viability with VEGFR2 inhibition was insignificant in spots containing 2 mM CRGDS, indicating a diminishing role of VEGFR2 in modulating viability in the presence of increased CRGDS. Additionally, the effect of VEGFR2 inhibition on

viability was not significant in the high modulus condition when CRGDS concentration was at or above 0.5 mM CRGDS (Fig. 4C), indicating that the role of VEGFR2 was not as substantial in high modulus compared to lower modulus hydrogels. These results indicated that synergy possibly exists between VEGFR2 and integrin binding, but that the role of VEGFR2 was modulated by CRGDS levels and stiffness. In essence, the importance of VEGF signaling during 3D HUVEC culture was context-dependent.

HUVEC proliferation was decreased by VEGFR2 inhibition in a majority of hydrogel conditions. In the low and medium modulus conditions, all spots containing CRGDS had cell proliferation levels elevated beyond the 0 CRGDS condition, but proliferation levels did not increase with CRGDS in the high modulus condition (Fig. 5B). In the low modulus condition, VEGFR2 inhibition caused a significant decrease in proliferation levels at 0, 0.25 and 1 mM CRGDS conditions. Interestingly, proliferation levels in the 2 mM CRGDS condition increased significantly with VEGFR2 inhibition at low modulus. In the medium modulus condition, VEGFR2 inhibition caused significant proliferation decreases in the 0.5 and 2 mM CRGDS conditions, and no increases in proliferation were observed. Interestingly, this response of proliferation to CRGDS at medium modulus remained the same as when VEGFR2 was not inhibited, suggesting an insignificant role of VEGFR2 at this modulus. In the high modulus condition, significant decreases in proliferation with VEGFR2 inhibition were observed in all CRGDS concentrations except the 0 mM RGDS condition. Though there was a significant increase in proliferation in the absence of CRGDS, this proliferation level was less than proliferation levels observed with CRGDS in the other modulus conditions (Fig. 5C). Taken together, the surrounding context of synthetic hydrogel conditions dramatically changes HUVEC responses to VEGFR2 inhibition, as measured by cell proliferation.

Inhibition of VEGFR2 with SU5416 also significantly changed the CRGDS-dependent trends in tubulogenesis in all the shear modulus conditions tested. In the low shear modulus conditions, CLS length increased monotonically with CRGDS concentration and increased dramatically at 2.0 mM CRGDS (Fig. 6B,C,D). In the medium modulus condition, CLS length in spots containing CRGDS was significantly greater than lengths observed in the absence of CRGDS. However, with VEGFR2 inhibition CLS length no longer changed with CRGDS concentration at medium modulus (Fig. 6B). In the high modulus condition, CLS length in all spots containing CRGDS was significantly greater than lengths observed in the absence of CRGDS. Again, changing CRGDS concentrations did not change CLS length, and CLS lengths at all CRGDS concentrations were lower than CLS lengths in the medium modulus condition. Remarkably, despite these changes in CLS trends, VEGFR2 inhibition did not cause significant changes to CLS length in most hydrogel conditions when compared to growth medium controls (Fig. 6C). Only 3 hydrogel conditions saw any significant effects with VEGFR2 inhibition: increased CLS length in low modulus, 2 mM CRGDS spots, decreased CLS length in medium modulus, 0 mM CRGDS spots, and decreased CLS length in high modulus, 1 mM CRGDS spots. These data are in stark contrast to VEGFR2 inhibition in Matrigel, which resulted in a clear decrease in CLS length. Taken together, our data demonstrated that the context of surrounding hydrogel conditions dramatically change HUVEC responses to VEGFR2 inhibition, as measured by HUVEC viability, proliferation, and tubulogenesis.

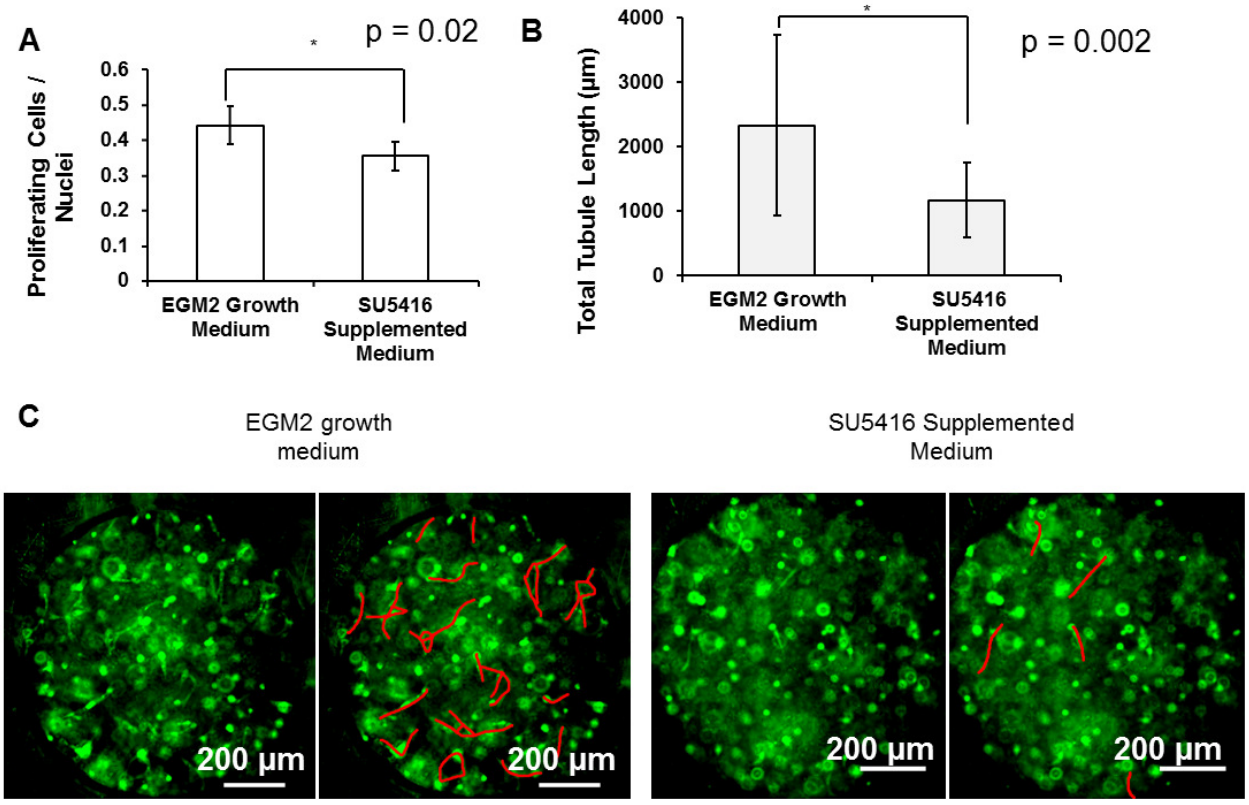

Chapter 4: Figure 7. Effects of VEGFR2 inhibition in standard model systems. **A)** HUVEC proliferation with and without SU5416 supplementation on tissue culture-treated polystyrene (TCPS). *, $p < 0.05$. **B)** HUVEC tubulogenesis with and without SU5416 supplementation in growth factor-reduced Matrigel. **C)** HUVEC CLS formation in 0.4 µL Matrigel spots. In each pair of pictures, the tubules in the right hand copy were highlighted. Green: Cell Tracker Green. *, $p < 0.05$ between EGM2 and SU5416-treated conditions.

4.5.7 Tubulogenesis in confined and non-confined hydrogels

One distinction of the hydrogel array presented in this study when compared to many prior studies is the degree to which the hydrogel is physically confined. For example, hydrogels formed in standard plastic well-plates, or elastomeric devices are typically highly confined, while the hydrogel spots in our array platform are allowed to swell in concert with the background hydrogel. To further understand the comparison between CLS formation in hydrogels confined

to rigid substrates versus unconfined hydrogels, we qualitatively observed the spatial distribution of CLS formation in hydrogels that were either confined to 48 well plates or detached from substrates and allowed to freely swell in medium. The confined hydrogels were susceptible to physical "buckling" during swelling, resulting in an out-of-focus area in the middle of the hydrogels (Supp. Fig. 1A). Buckling caused heterogeneity in CLS formation, with most of the structures forming around the edge of the buckled hydrogel area. In contrast, CLS formation in the non-confined hydrogels occurred homogeneously throughout the volume of the hydrogel (Supp. Fig. 1B), similar to our observations in hydrogel array spots in this study. These observations suggest that cell encapsulation in confined hydrogels can introduce lurking variables upon swelling that significantly affect the outcome of a 3D neovascularization experiment.

4.6 Discussion

In this study we simultaneously adjusted cell adhesion ligand concentration, shear modulus and VEGF signaling in an arrayed hydrogel construct that enabled comprehensive screening of HUVEC viability, proliferation, and tubulogenesis. Over the course of these studies, we were able to form and analyze HUVEC behavior in over 900 hydrogel spots total. Previous studies have often modulated cell interactions with extracellular environments by including or not including biological signaling molecules in the matrix [28, 57] as well as using antibodies or siRNA to activate or inactivate receptors to external signals [16]. In contrast, here we modulated cell adhesion to the matrix by tuning CRGDS concentrations over a range of values rather than completely activating or inactivating integrin signaling. Simultaneously modulating CRGDS concentration in concert with hydrogel modulus, while also toggling VEGFR2 signaling, enabled

us to study how changing levels of ECM cues affects synergy between multiple signaling sources. This task would not be readily achievable in larger-scale hydrogels or naturally-derived ECMs due to the number of distinct variables and outcomes of interest. We can generally conclude that combinatorially varied ECM cues affect the outcomes of HUVEC viability, proliferation and tubulogenesis, and that hydrogel conditions change HUVEC responses to VEGFR2 inhibition. A series of more focused conclusions can be drawn from the data. Specifically, excessive CRGDS concentrations in PEG hydrogels removed apparent synergy between VEGFR2 and integrin-mediated cell adhesion in the context of maintaining cell viability, proliferation in 3D culture depended on modulus and VEGFR2 inhibition but did not correlate linearly with CRGDS concentration, and ECM properties generally played a larger role in dictating CLS formation than VEGFR2 inhibition.

Previous studies have defined AKT-mediated signaling pathways that promoted increased cell viability [58] and were initiated by VEGFR2 phosphorylation and binding of αVβ3 integrin to cell adhesion ligands [59]. VEGFR2 and αVβ3 integrins are also known to behave synergistically, as binding of αVβ3 integrins to adhesion ligands enhances VEGFR2 activity and vice-versa [16]. The proposed mechanism behind this synergy was that the β3 integrin subunit must bind directly to the VEGFR2 via the cytoplasmic domain [60]. Our cell viability data were consistent with these previous studies, as non-inhibited VEGFR2 signaling and increased CRGDS concentration in the hydrogels individually and cooperatively increased HUVEC viability (Fig. 4A,B). However, we also found that VEGFR2 signaling did not contribute to increased cell viability in environments that contained the highest concentrations of CRGDS (Fig. 4A). This result suggests that, while VEGFR2 and cell adhesion to the ECM work together to

promote cell viability, excessive adhesion to the surrounding ECM may interfere with this synergy.

We evaluated HUVEC proliferation levels in the hydrogel arrays and found that adhesion, modulus and VEGFR2 modulated proliferation differently than viability. Proliferation levels increased beyond baseline levels in hydrogels containing CRGDS and generally decreased with VEGFR2 inhibition (Fig. 5). These results were predictable given previously established dependences of proliferation on αVβ3 integrin [11] and VEGFR2 signaling [3], as well as our experiment where VEGFR2 inhibition reduced proliferation in standard 2D HUVEC culture (Fig. 7A). However, once CRGDS was included in the hydrogels we commonly observed biphasic trends in proliferation relating to CRGDS rather than monotonic increases in proliferation with increased CRGDS. Our group and others have previously demonstrated that increased RGD density on well-defined surfaces increased cell proliferation monotonically for multiple cell types, including HUVECs [3, 11, 30]. The fact that our results here contradicted previous studies are understandable in view of the known differences in cell-ECM interactions in 2D versus 3D environments [61]. We also observed significantly different effects of VEGFR2 inhibition between the different modulus conditions, indicating a role of the ECM in determining how VEGFR2 modulates proliferation. However, beyond combinatorial receptor-ligand interactions which require further characterization in 3D contexts, it is likely that other factors such as cell-cell contact and matrix degradation played major roles in modulating proliferation in our synthetic 3D environments. For example, we observed that proliferating cells were always associated with multicellular structures (Fig. 5D), indicating that cell-cell contact is an important parameter.

We evaluated capillary-like structure (CLS) formation by HUVECs in our hydrogels and first observed that optimized CRGDS concentrations and hydrogel modulus maximized structure formation while VEGFR2 was not inhibited (Fig. 6A). These results agree with results of previous studies in literature. For example, moderate concentrations of RGD permitted optimal angiogenic sprouting from aortic ring explants into fibrin hydrogels, while excessive RGD inhibited endothelial cell migration and vascular growth [10]. In other studies vascular growth of human dermal microvascular ECs and bovine pulmonary microvascular ECs into collagen hydrogels were inhibited when stiffness was too low to support tubule stability or too high to permit cell migration [41, 62]. It should be noted that the low end of the stiffness ranges in these prior studies fell below our low modulus condition and the high end of the ranges was equivalent to our medium modulus condition. Yamamura et al proposed that increasing collagen hydrogel stiffness by increasing collagen fibril density encourages cell aggregation and network formation rather than migration and invasion of individual cells [62]. The increased CLS formation observed in our medium modulus hydrogels corroborates this finding, and we also showed that our high modulus hydrogels inhibits CLS formation.

Multiple results here demonstrated that the effects of VEGFR2 inhibition are highly context-dependent. For example, VEGFR2 inhibition increased proliferation in the 2.0 mM CRGDS, low modulus PEG hydrogels, but decreased proliferation in 2D culture on tissue-culture polystyrene. Interestingly, the context-dependence of VEGFR2 inhibition in some cases even showed trends that contrast with the expected effects of a VEGFR2 inhibitor. For example, we found that there was no significant effect of VEGFR2 inhibition on CLS formation in synthetic hydrogel networks (Fig. 6C). The notable exception to this finding was the low modulus hydrogel containing 2.0 mM CRGDS. Whereas CLS formation in the other CRGDS concentrations was

largely unchanged by VEGFR2 inhibition, CLS formation dramatically increased with VEGFR2 inhibition. This suggests that normal VEGFR2 can have an inhibitory effect on CLS formation in particular extracellular environments.

Though the roles of cell adhesion and modulus during vascularization in 3D hydrogels are well-defined, the role of VEGFR2 in dictating de novo CLS formation has been unclear. Particularly, conflicting evidence exists as to whether VEGFR2 promotes or inhibits CLS formation. Hayashi et al suggested an inhibitory role of VEGFR2 in blood vessel formation by demonstrating that decreased VEGFR2 phosphorylation is necessary for lumen formation by endothelial stalk cells in mouse embryoid bodies, mouse teratomas and zebrafish models. Additionally, a previous study by our group demonstrated that VEGFR2 activation via soluble VEGF stimulation disrupted in-vitro tubule network formation by HUVECs under a Matrigel overlay [3]. Conversely, Roberts et al suggested a stimulatory role of VEGFR2 by demonstrating that ERK5 activation by VEGFR2 is necessary for in-vitro tubular network formation by human dermal microvascular endothelial cells in collagen hydrogels [58], and Stratman et al demonstrated that VEGF and bFGF signaling prime HUVECs to receive signals from hematopoietic cytokines and undergo in-vitro tubule network formation in collagen hydrogels [63]. In these examples, experiments were conducted either in vivo or in naturally-derived collagen or Matrigel models, making it difficult to assess how ECM cues and VEGFR2 activity combinatorially modulated CLS formation. To determine the extent to which our results were due to the use of synthetic, controlled hydrogels rather than naturally-derived ECM, we also subjected HUVECs to VEGFR2 inhibition in Matrigel and found a clear reduction of tubulogenesis observed in Matrigel, contrasting with our results in PEG (Fig. 7B,C). It is well known that Matrigel, derived from a mouse sarcoma, consists of over 1000 distinct protein species at unspecified

concentrations [64]. Since Matrigel is a poorly defined and variable material, it is difficult to speculate on the mechanism behind the difference in the role of VEGF. Our results have clearly demonstrated, however, that the surrounding ECM context can determine how VEGFR2 modulates CLS formation.

The combined data from the proliferation and tubulogenesis assays demonstrated that proliferation did in part correlate with CLS formation. This was especially evident in the low modulus hydrogels, where VEGFR2 inhibition resulted in monotonic increases of both proliferation and CLS formation, and where proliferation and CLS formation increased dramatically with VEGFR2 inhibition in the 2.0 mM CRGDS conditions (Fig. 5A,6A). Interestingly, while VEGFR2 activity combined with a high CRGDS concentration lowered both CLS formation and cell viability in low modulus hydrogels (Fig. 4A,6A), cell proliferation remained high in that condition (Fig. 5A). Additionally, in medium modulus hydrogels we observed no significant changes to CLS formation and few significant changes in proliferation when VEGFR2 was inhibited (Fig. 5, Fig. 6). These data collectively demonstrate that other mechanisms besides integrin-mediated cell adhesion, VEGFR2 signaling, and associated synergy are active in determining angiogenic cell behavior. Two potential candidate mechanisms could be cell-cell contact and hydrogel degradability. Chen et al had previously studied the proliferative activity of HUVECs in a number of 2D spreading and cell-cell contact contexts and noted that the extent of cell spreading dictates whether cell-cell contact increases or decreases proliferation. Specifically, VE-Cadherin engagement increased proliferation when cell spreading was restricted [65]. Based on this type of mechanism, we could speculate that the biphasic trends we observed between HUVEC proliferation and CRGDS concentration could possibly be attributable to a transition between a state where low cell attachment to the ECM promotes high

proliferation and a state where sufficient CRGDS concentrations promote CLS formation and increased cell-cell contacts (Fig. 5A). However, if polymer density is high enough to restrict cell migration and cytokinesis, as was likely the case in the high modulus hydrogels, proliferation and CLS formation (Fig. 5A, 6A) would be diminished as well. The disparity between low CLS formation and high proliferation in the low modulus, 2.0 mM CRGDS condition (Fig. 4A, 6A) could also be explained by increased matrix degradation as a result of VEGFR2 signaling [66, 67], leading to CLS network destabilization. We previously demonstrated that excessive hydrogel degradation via hydrolysis lowered the viability of encapsulated cells [7], which supports the notion that protease-mediated degradability of hydrogels could also affect cell viability in the current study. Each of these speculative discussion points highlight the need for detailed characterization of mechanisms that drive endothelial cell behavior in 3D environments. The array-based approach described herein and similar enhanced throughput approaches are needed to provide further mechanistic insights in future studies.

The system designed in these studies encapsulated cells in well-defined PEG hydrogels prior to cell settling, resulting in a homogeneous cell distribution throughout the dimensions of spots. The resulting hydrogel spots were mounted to an inert background hydrogel (Fig. 2). Importantly, anchoring the degradable hydrogels to a swelling substrate is critical to observing encapsulated cells in the array construct. If, alternatively, similar hydrogel formulations were allowed to form in a confined environment, such as within a rigid well-plate, swelling issues rendered the hydrogels not observable. In particular, we observed that within 24 hours of incubation many of the hydrogels formed in polystyrene well plates buckled due to high degrees of swelling (Supp. Fig 1A), making long-term imaging and maintenance of the 3D cell cultures impossible. Buckling was especially problematic, as it could act as a lurking variable that promotes non-

homogenous CLS formation in the hydrogels, not to mention adding difficulty to imaging. Anchorage to a swelling substrate stabilized the hydrogel spots throughout the swelling process, being flexible enough to allow homogeneous volumetric swelling of the spots without buckling. The distribution of CLS formation in the array spots was more similar to the non-confined hydrogels rather than the confined hydrogels. Any structures that formed in the hydrogel array spots were distributed homogeneously throughout the gel by 24 hours after encapsulation (Fig. 6D). This suggests that attachment of hydrogel spots to a swelling substrate effectively nullifies the effects of confinement.

4.7 Conclusion

Using a hydrogel array, we have combinatorially manipulated cell adhesion and stiffness to examine critical endothelial cell behaviors – viability, proliferation, and capillary-like structure (CLS) formation. The screening system designed here analyzed HUVEC behavior in over 900 spots total. The characteristics of the 3D ECM surrounding encapsulated HUVECs significantly influenced cell viability, proliferation and CLS formation. Further, the context provided by the surrounding ECM modulated the effects of VEGFR2 signaling, ranging from changing the effectiveness of synergistic interactions between integrins and VEGFR2 to determining whether VEGFR2 upregulates, downregulates or has no effect on proliferation and CLS formation. The differences in cell behavior due to combinatorially manipulated environmental parameters shown here highlight the need for additional characterization of 3D cell-matrix interactions, as well as further mechanistic studies of how these interactions modulate cell behavior.

4.8 Acknowledgements

The authors would like to acknowledge funding from the National Institutes of Health (NIH R01 HL093282-01A1, NIH R21 EB016381-01, NIH 1UH2 TR000506-01 and the Biotechnology Training Program NIGMS 5T32GM08349) as well as the UW Madison Graduate Engineering Research Scholars program. We would like to thank Justin Williams and David Beebe for their assistance with soft lithography techniques. This study made use of the National Magnetic Resonance Facility at Madison, which is supported by NIH grants P41RR02301 (BRTP/ NCRR) and P41GM10399 (NIGMS). Additional equipment was purchased with funds from the University of Wisconsin, the NIH (RR02781, RR08438), the NSF (DMB-8415048, OIA-9977486, BIR-9214394), the DOE, and the USDA. Small angle X-ray scattering (SAXS) equipment was purchased with funds from NIH grant S100RR027000 (NCRR). Mechanical testing data was obtained using the Ares LS2 rheometer at the UW Madison Soft Materials Laboratory. Confocal Microscopy images were taken using the Nikon A1R-Si Confocal Microscope at the Waisman Center Cellular & Molecular Neuroscience Core facility in Madison, WI. Special thanks go Justin Koepsel for helpful discussions and technical instruction throughout the course of these studies.

4.9 Supplemental Information

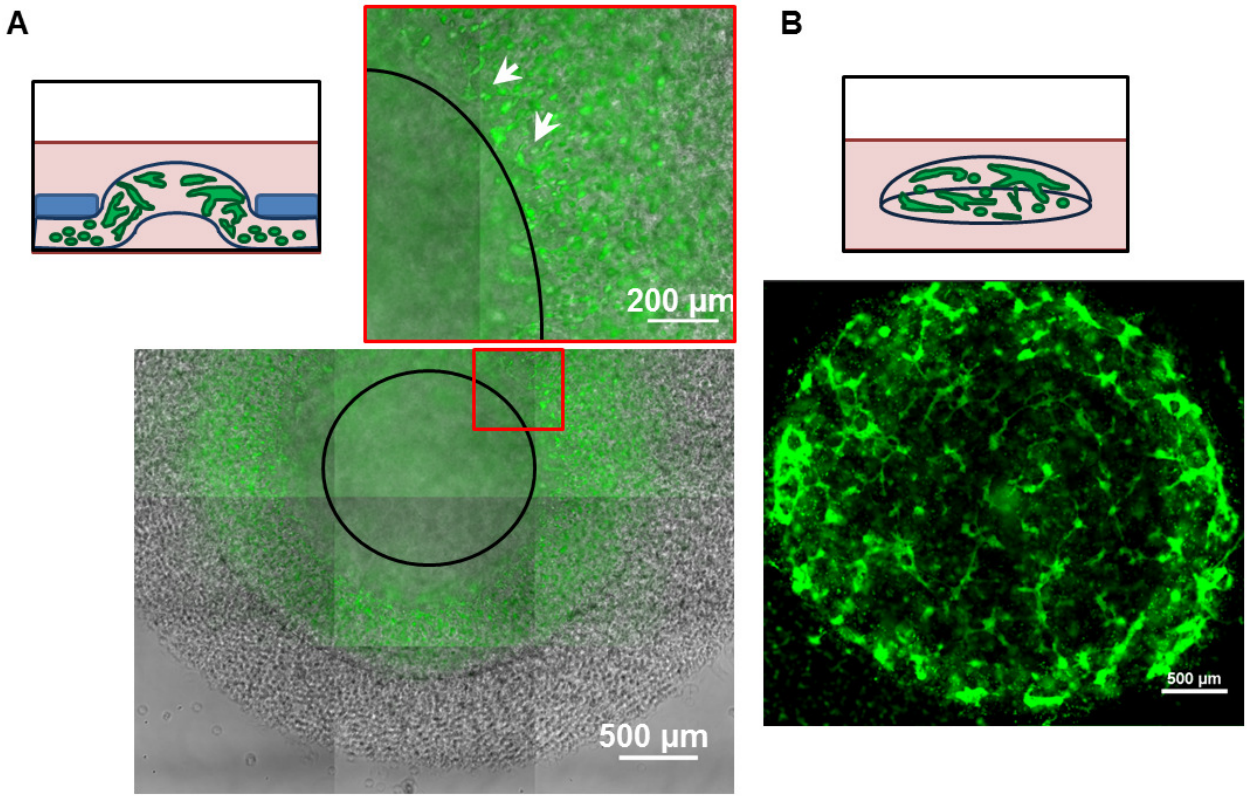

Chapter 4: Supplemental figure 1. Hydrogel homogeneity and heterogeneity in confined vs. non-confined PEGNB hydrogels. **A)** Hydrogels confined to a 48 well plate at 24 hours after encapsulation. Schematic: Cell-containing hydrogel is anchored by the edges by a background hydrogel (blue rectangles) in order to prevent complete detachment of the hydrogel into medium during swelling. Black circle: buckling area. Arrowheads: CLS formation. **B)** Freely-swollen hydrogels at 24 hours after encapsulation.

4.10 References

[1] De Smet F, Segura I, De Bock K, Hohensinner P, Carmeliet P. Mechanisms of vessel branching filopodia on endothelial tip cells lead the way. Arterioscl Thromb Vas. 2009;29:639-49.

[2] Risau W. Mechanisms of angiogenesis. Nature. 1997;386:671-4.

[3] Koepsel J, Nguyen E, Murphy W. Differential effects of a soluble or immobilized VEGFR-binding peptide. Integr Biol. 2012;4:914-24.

[4] Murphy J, Fitzgerald D. Vascular endothelial cell growth factor (VEGF) induces cyclooxygenase (COX)-dependent proliferation of endothelial cells (EC) via the VEGF-2 receptor. Faseb J. 2001;15:1667-69.

[5] Gerber H, McMurtrey A, Kowalski J, Yan M, Keyt B, Dixit V, et al. Vascular endothelial growth factor regulates endothelial cell survival through the phosphatidylinositol 3 '-kinase AKT signal transduction pathway - requirement for FLK-1/KDR activation. J Biol Chem. 1998;273:30336-43.

[6] Barkefors I, Le Jan S, Jakobsson L, Hejll E, Carlson G, Johansson H, et al. Endothelial cell migration in stable gradients of vascular endothelial growth factor a and fibroblast growth factor 2 - effects on chemotaxis and chemokinesis. J Biol Chem. 2008;283:13905-12.

[7] Jongpaiboonkit L, King WJ, Lyons GE, Paguirigan AL, Warrick JW, Beebe DJ, et al. An adaptable hydrogel array format for 3-dimensional cell culture and analysis. Biomaterials. 2008;29:3346-56.

[8] Jongpaiboonkit L, King WJ, Murphy WL. Screening for 3D environments that support human mesenchymal stem cell viability using hydrogel arrays. Tissue Eng Pt A. 2009;15:343-53.

[9] King WJ, Jongpaiboonkit L, Murphy WL. Influence of FGF2 and PEG hydrogel matrix properties on hMSC viability and spreading. J Biomed Mater Res A. 2010;93A:1110-23.

[10] Shen C, Raghavan S, Xu Z, Baranski J, Yu X, Wozniak M, et al. Decreased cell adhesion promotes angiogenesis in a PYK2-dependent manner. Exp Cell Res. 2011;317:1860-71.

[11] Koepsel J, Loveland S, Schwartz M, Zorn S, Belair D, Le N, et al. A chemically-defined screening platform reveals behavioral similarities between primary human mesenchymal stem cells and endothelial cells. Integr Biol. 2012;4:1508-21.

[12] Moon JJ, Saik JE, Poche RA, Leslie-Barbick JE, Lee SH, Smith AA, et al. Biomimetic hydrogels with pro-angiogenic properties. Biomaterials. 2010;31:3840-7.

[13] Mahabeleshwar G, Feng W, Reddy K, Plow E, Byzova T. Mechanisms of integrin-vascular endothelial growth factor receptor cross-activation in angiogenesis. Circ Res. 2007;101:570-80.

[14] Hodivala-Dilke K. Alpha v beta 3 integrin and angiogenesis: a moody integrin in a changing environment. Curr Opin Cell Biol. 2008;20:514-9.

[15] Khan ZA, Chan BM, Uniyal S, Barbin YP, Farhangkhoee H, Chen S, et al. EDB fibronectin and angiogenesis -- a novel mechanistic pathway. Angiogenesis. 2005;8:183-96.

[16] Soldi R, Mitola S, Strasly M, Defilippi P, Tarone G, Bussolino F. Role of alpha(v)beta(3) integrin in the activation of vascular endothelial growth factor receptor-2. Embo J. 1999;18:882-92.

[17] Mammoto A, Connor K, Mammoto T, Yung C, Huh D, Aderman C, et al. A mechanosensitive transcriptional mechanism that controls angiogenesis. Nature. 2009;457:1103-08.

[18] Bryan B, Dennstedt E, Mitchell D, Walshe T, Noma K, Loureiro R, et al. RhoA/ROCK signaling is essential for multiple aspects of VEGF-mediated angiogenesis. Faseb J. 2010;24:3186-95.

[19] Beer A, Lorenzen S, Metz S, Herrmann K, Watzlowikl P, Wester H, et al. Comparison of integrin alpha(v)beta(3) expression and glucose metabolism in primary and metastatic lesions in cancer patients: a PET study using F-18-galacto-RGD and F-18-FDG. J Nucl Med. 2008;49:22-9.

[20] Cox T, Erler J. Remodeling and homeostasis of the extracellular matrix: implications for fibrotic diseases and cancer. Dis Model Mech. 2011;4:165-78.

[21] Provenzano P, Inman D, Eliceiri K, Knittel J, Yan L, Rueden C, et al. Collagen density promotes mammary tumor initiation and progression. Bmc Med. 2008;6. Available from URL: http://www.biomedcentral.com/1741-7015/6/11 (doi:10.1186/1741-7015-6-11)

[22] Conklin M, Eickhoff J, Riching K, Pehlke C, Eliceiri K, Provenzano P, et al. Aligned collagen is a prognostic signature for survival in human breast carcinoma. Am J of Pathol. 2011;178:1221-32.

[23] Kaehler J, Zilla P, Fasol R, Deutsch M, Kadletz M. Precoating substrate and surface configuration determine adherence and spreading of seeded endothelial-cells on polytetrafluoroehtylene grafts. J Vasc Surg. 1989;9:535-41.

[24] Koepsel JT, Murphy WL. Patterning discrete stem cell culture environments via localized self-assembled monolayer replacement. Langmuir. 2009;25:12825-34.

[25] Hudalla G, Koepsel J, Murphy W. Surfaces that sequester serum-borne heparin amplify growth factor activity. Adv Mater. 2011;23:5415-8.

[26] Ochsner M, Dusseiller M, Grandin H, Luna-Morris S, Textor M, Vogel V, et al. Micro-well arrays for 3D shape control and high resolution analysis of single cells. Lab Chip. 2007;7:1074-7.

[27] Charnley M, Textor M, Khademhosseini A, Lutolf M. Integration column: microwell arrays for mammalian cell culture. Integr Biol. 2009;1:625-34.

[28] Leslie-Barbick JE, Moon JJ, West JL. Covalently-immobilized vascular endothelial growth factor promotes endothelial cell tubulogenesis in poly(ethylene glycol) diacrylate hydrogels. J Biomater Sci Polym Ed. 2009;20:1763-79.

[29] Saunders R, Hammer D. Assembly of human umbilical vein endothelial cells on compliant hydrogels. Cell Mol Bioeng. 2010;3:60-7.

[30] Jung J, Moyano J, Collier J. Multifactorial optimization of endothelial cell growth using modular synthetic extracellular matrices. Integr Biol. 2011;3:185-96.

[31] Stratman A, Saunders W, Sacharidou A, Koh W, Fisher K, Zawieja D, et al. Endothelial cell lumen and vascular guidance tunnel formation requires MT1-MMP-dependent proteolysis in 3-dimensional collagen matrices. Blood. 2009;114:237-47.

[32] Sacharidou A, Koh W, Stratman A, Mayo A, Fisher K, Davis G. Endothelial lumen signaling complexes control 3D matrix-specific tubulogenesis through interdependent CDC42- and MT1-MMP-mediated events. Blood. 2010;115:5259-69.

[33] Hanjaya-Putra D, Yee J, Ceci D, Truitt R, Yee D, Gerecht S. Vascular endothelial growth factor and substrate mechanics regulate in vitro tubulogenesis of endothelial progenitor cells. J Cell Mol Med. 2010;14:2436-47.

[34] Lafleur M, Handsley M, Knauper V, Murphy G, Edwards D. Endothelial tubulogenesis within fibrin gels specifically requires the activity of membrane-type-matrix metalloproteinases (MT-MMPs). J Cell Sci. 2002;115:3427-38.

[35] Le Saux G, Magenau A, Gunaratnam K, Kilian K, Bocking T, Gooding J, et al. Spacing of integrin ligands influences signal transduction in endothelial cells. Biophys J. 2011;101:764-73.

[36] Liu J, Tirrell D. Cell response to RGD density in cross-linked artificial extracellular matrix protein films. Biomacromolecules. 2008;9:2984-8.

[37] Myers K, Applegate K, Danuser G, Fischer R, Waterman C. Distinct ECM mechanosensing pathways regulate microtubule dynamics to control endothelial cell branching morphogenesis. J Cell Biol. 2011;192:321-34.

[38] Baker B, Chen C. Deconstructing the third dimension – how 3D culture microenvironments alter cellular cues. J Cell Sci. 2012;125:1-10.

[39] Abaci H, Truitt R, Tan S, Gerecht S. Unforeseen decreases in dissolved oxygen levels affect tube formation kinetics in collagen gels. Am J Physiol-Cell Ph. 2011;301:C431-40.

[40] Calvani M, Rapisarda A, Uranchimeg B, Shoemaker R, Melillo G. Hypoxic induction of an HIF-1 alpha-dependent bFGF autocrine loop drives angiogenesis in human endothelial cells. Blood. 2006;107:2705-12.

[41] Shamloo A, Heilshorn S. Matrix density mediates polarization and lumen formation of endothelial sprouts in VEGF gradients. Lab Chip. 2010;10:3061-8.

[42] Lutolf MP, Hubbell JA. Synthetic biomaterials as instructive extracellular microenvironments for morphogenesis in tissue engineering. Nat Biotechnol. 2005;23:47-55.

[43] Fairbanks BD, Schwartz MP, Halevi AE, Nuttelman CR, Bowman CN, Anseth KS. A versatile synthetic extracellular matrix mimic via thiol-norbornene photopolymerization. Adv Mater. 2009;21:5005-10.

[44] Hoyle C, Bowman C. Thiol-ene click chemistry. Angew Chem Int Ed. 2010;49:1540-73.

[45] Gobaa S, Hoehnel S, Roccio M, Negro A, Kobel S, Lutolf M. Artificial niche microarrays for probing single stem cell fate in high throughput. Nat Methods. 2011;8:949-55.

[46] Albrecht D, Tsang V, Sah R, Bhatia S. Photo- and electropatterning of hydrogel-encapsulated living cell arrays. Lab Chip. 2005:111-8.

[47] Albrecht D, Underhill G, Wassermann T, Sah R, Bhatia S. Probing the role of multicellular organization in three-dimensional microenvironments. Nat Methods. 2006;3:369-75.

[48] Khoo C, Micklem K, Watt S. A Comparison of Methods for Quantifying Angiogenesis in the matrigel assay in vitro. Tissue Eng Pt C-Meth. 2011;17:895-906.

[49] Toepke MW, Impellitteri NA, Theisen JM, Murphy WL. Characterization of thiol-ene crosslinked PEG hydrogels. Macromol Mater Eng. 2013;298:699-703.

[50] Nagase H, Fields GB. Human matrix metalloproteinase specificity studies using collagen sequence-based synthetic peptides. Biopolymers. 1996;40:399-416.

[51] Jo BH, Van Lerberghe LM, Motsegood KM, Beebe DJ. Three-dimensional micro-channel fabrication in polydimethylsiloxane (PDMS) elastomer. J Microelectromech S. 2000;9:76-81.

[52] Thibault C, Severac C, Mingotaud A, Vieu C, Mauzac M. Poly(dimethylsiloxane) contamination in microcontact printing and its influence on patterning oligonucleotides. Langmuir. 2007;23:10706-14.

[53] Mendel D, Schreck R, West D, Li G, Strawn L, Tanciongco S, et al. The angiogenesis inhibitor SU5416 has long-lasting effects on vascular endothelial growth factor receptor phosphorylation and function. Clin Cancer Res. 2000;6:4848-58.

[54] Chan R, Titze I. Viscoelastic shear properties of human vocal fold mucosa: Measurement methodology and empirical results. J Acoust Soc Am. 1999;106:2008-21.

[55] Sinkus R, Tanter M, Xydeas T, Catheline S, Bercoff J, Fink M. Viscoelastic shear properties of in vivo breast lesions measured by MR elastography. Magn Reson Imaging. 2005;23:159-65.

[56] Schneider B, Miller K. Angiogenesis of breast cancer. J Clin Oncol. 2005;23:1782-90.

[57] Leslie-Barbick J, Saik J, Gould D, Dickinson M, West J. The promotion of microvasculature formation in poly(ethylene glycol) diacrylate hydrogels by an immobilized VEGF-mimetic peptide. Biomaterials. 2011;32:5782-9.

[58] Roberts O, Holmes K, Muller J, Cross D, Cross M. ERK5 is required for VEGF-mediated survival and tubular morphogenesis of primary human microvascular endothelial cells. J Cell Sci. 2010;123:3189-200.

[59] Han S, Jung Y, Lee E, Park H, Kim G, Jeong J, et al. DICAM inhibits angiogenesis via suppression of AKT and p38 MAP kinase signalling. Cardiovasc Res. 2013;98:73-82.

[60] Cebe-Suarez S, Zehnder-Fjallman A, Ballmer-Hofer K. The role of VEGF receptors in angiogenesis; complex partnerships. Cell Mol Life Sci. 2006;63:601-15.

[61] Cukierman E, Pankov R, Stevens D, Yamada K. Taking cell-matrix adhesions to the third dimension. Science. 2001;294:1708-12.

[62] Yamamura N, Sudo R, Ikeda M, Tanishita K. Effects of the mechanical properties of collagen gel on the in vitro formation of microvessel networks by endothelial cells. Tissue Eng. 2007;13:1443-53.

[63] Stratman A, Davis M, Davis G. VEGF and FGF prime vascular tube morphogenesis and sprouting directed by hematopoietic stem cell cytokines. Blood. 2011;117:3709-19.

[64] Hughes C, Postovit L, Lajoie G. Matrigel: A complex protein mixture required for optimal growth of cell culture. Proteomics. 2010;10:1886-90.

[65] Nelson C, Chen C. VE-cadherin simultaneously stimulates and inhibits cell proliferation by altering cytoskeletal structure and tension. J Cell Sci. 2003;116:3571-81.

[66] Xu Z, Yu Y, Duh E. Vascular endothelial growth factor upregulates expression of ADAMTS1 in endothelial cells through protein kinase C signaling. Invest Ophth Vis Sci. 2006;47:4059-66.

[67] Funahashi Y, Shawber CJ, Sharma A, Kanamaru E, Choi YK, Kitajewski J. Notch modulates VEGF action in endothelial cells by inducing matrix metalloprotease activity. Vasc Cell. 2011;3. Available from URL: http://www.ncbi.nlm.nih.gov/pubmed/21349159 (doi:10.1186/2040-2384-2-3).

Chapter 5:

Endothelial cell responses to TGF-β signaling in 2D and 3D cell culture environments with defined mechanical properties

Eric H. Nguyen, William L. Murphy. Endothelial cell responses to TGF-β signaling in 2D and 3D cell culture environments with defined mechanical properties. *In preparation*.

5.1 Preface

Chapters 3 and 4 established techniques to culture cells on hydrogel surfaces (2D) and inside hydrogels (3D) where hydrogel stiffness was tuned orthogonally with cell adhesivity. The purpose of studies in this chapter was to demonstrate the utility of defined hydrogels to determine the effects of substrate parameters on TGFβ-mediated changes in endothelial cell phenotype. Here, human umbilical vein endothelial cells were seeded onto fibronectin-coated tissue culture polystyrene, seeded onto surfaces of PEG hydrogels of varying moduli (2D) and encapsulated in PEG hydrogels (3D) while treated with TGF-β. Results demonstrated that culture context and hydrogel modulus have significant impacts on the overall consequences of TGF-β signaling. This work also suggested that culture substrates containing only an integrin binding ligand and culture environments containing only TGF-β may be insufficient to induce a phenotypic change of Endothelial-Mesenchymal transformation.

5.2 Abstract

Phenotypic changes in endothelial cells that result in the loss of homeostatic activity can potentially give rise to vascular dysfunction and tissue pathology. A common mediator in the transformation of cell phenotypes is transforming growth factor beta (TGF-β), though the role of

the extracellular environment in dictating the outcomes of TGF-β signaling are not well understood. These studies investigated differential effects of TGF-β signaling on endothelial cell phenotype in various cell culture environments including monolayer culture on fibronectin-coated tissue culture polystyrene (TCPS), monolayer culture on poly(ethylene glycol) (PEG) hydrogel surfaces (2D), and three-dimensional (3D) culture inside degradable PEG hydrogels. These studies demonstrate that treating human umbilical vein endothelial cells (HUVECs) with TGF-β1 or 2 induces differential changes in the expression of endothelial and mesenchymal cell markers depending on the culture environment and mechanical stiffness of the extracellular environment. Specifically, TGF-β treatment induces a state of quiescence and partial loss of endothelial phenotype in HUVECs seeded on TCPS and encapsulated in PEG hydrogels while similar growth factor treatment induces a state of vascular stability in HUVECs seeded on PEG hydrogel surfaces. Additionally, the cell culture in 2D and 3D environments of varying modulus revealed that the regulation of endothelial cell markers by TGF-β may be independent of modulus in 2D culture but dependent on modulus in 3D culture.

5.3 Introduction

Endothelial cells, characterized as lining the interior surfaces of blood vessels and microvasculature, perform critical actions to facilitate tissue viability including the perfusion of blood and the regulation of material transport between blood and interstitial fluid [1]. A variety of changes in endothelial cell phenotype such as delamination, cell death, and quiescence can lead to loss of tissue function and progression of numerous disorders including cancer metastasis, tissue ischemia, diabetic ulcer formation, diabetic retinopathy, cardiovascular disease and

embryonic lethality [1, 2]. A notable example of a pathological change in phenotype is endothelial-mesenchymal transition (EndMT), characterized as the disappearance of endothelial cell phenotype in exchange for a mesenchymal cell phenotype [3]. While known to facilitate embryonic development, particularly in the development of cardiac tissue [4, 5], EndMT is particularly implicated in numerous complications such as tissue fibrosis [6], myocardial infarction [7-9], and the onset of cancer metastasis [3, 6, 10].

A common inducer of phenotypic changes in endothelial cells is transforming growth factor β (TGF-β) [11-14]. TGF-β has been characterized as promoting a diverse range of endothelial cell behaviors including apoptosis [15, 16], increased proliferation [17], and the promotion [18, 19] and inhibition [20] of angiogenesis. While a plethora of cell responses to TGF-β are known, the factors that drive endothelial cells to execute particular responses over others is not well understood. Several factors have been reported as modulating the outcomes of TGF-β signaling including expression of numerous co-receptors to type-1 and type-2 TGF-β receptors [21, 22], TGF-β concentration [18, 20], differential potencies of TGF-β1 and 2 [23], and the presence of other growth factors such as VEGF that potentially attenuate TGF-β activity [24].

A potentially critical influence on TGF-β signaling outcomes is the extracellular matrix (ECM), which provides environmental signaling cues to cells including cell adhesion molecules and mechanical stiffness [25-27]. Based on the association between pathological endothelial cell phenotypes and environments of increased stiffness, such as in blood vessel stiffening [28] and cancer tumors [29], we hypothesize that the elastic modulus of the ECM is critical for the onset of pathological endothelial cell phenotypes driven by TGF-β signaling. Poly(ethylene glycol) (PEG) hydrogels are versatile tools for exploring how ECM properties and TGF-β signaling simultaneously affect endothelial cell phenotype. The chemically-defined nature of PEG

hydrogels and the ability to resist protein fouling provide an appropriate material to study how specific changes in biomolecule presentation and mechanical properties impact endothelial cell behavior [27]. Specifically a photoinitiated thiol-ene reaction [30] was leveraged here to control polymer network density, modes of degradation, and the inclusion of a Arg-Gly-Asp (RGD) peptide sequence to facilitate integrin-mediated cell adhesion [31]. Notably, the mechanical properties of PEG can recapitulate the water content and mechanics of numerous tissues in the body, ranging from neural tissue to diseased arteries [32-34].

In this study human umbilical vein endothelial cells (HUVECs) were cultured in numerous cell culture environments including fibronectin-coated tissue culture polystyrene (TCPS) as well as the surfaces and interiors of RGD-functionalized PEG hydrogels of varying stiffness. Here cells are treated with TGF-β1 and 2 in order to observe the impact of culture contexts on the phenotypic outcomes of TGF-β signaling. HUVECs responded to TGF-β signaling with differential outcomes including entering quiescent states and increasing vascular stability when cultured in the different contexts, suggesting a major role of the environment in dictating cell responses to growth factor stimuli.

5.4 Experimental Section

5.4.1 Materials

Human umbilical vein endothelial cells and EGM-2 Bulletkit were purchased from Lonza (Walkersville, MD). Medium 199 (M199) was purchased from Mediatech Inc (Manassas, VA). Trypsin, Cosmic Calf Serum and Penicillin/Steptomycin were purchased from HyClone (Logan,

UT). PEG was purchased as a non-functionalized, 10 or 20 kDa molecular weight, 8-arm star molecule with a tripentaerythritol core from Jenkem USA (PEG-OH, Allen TX). Dimethylaminopyridine, pyridine, norbornene carboxylic acid, dichloromethane, chloroform, 3-mercatopropyl trimethoxylsilane (3-MPTS), toluene and dithiothreitol were purchased from Sigma Aldrich (St. Louis, MO). 0.4 μm pore-size syringe filters were purchased from Millipore (Billerica, MA). Anhydrous dichloromethane, diethyl ether, hexanes, methanol, phosphate buffered saline (10 mM, 1x PBS) Triton-X-100 and bovine serum albumin (BSA) were purchased from Fisher Scientific (Waltham, MA). N,N'-dicyclohexylcarbodiimide was purchased from Thermo Scientific (Waltham, MA). Irgacure 2959 photoinitiator (I2959) was purchased from Ciba Specialty Chemicals (Tarrytown, NY). Costar 6-well and 96-well plates were purchased from Corning (Corning, NY). Human Plasma Fibronectin (FN) was purchased from Gibco (Gaithersburg, MD). Amidated peptides Cys-Arg-Gly-Asp-Ser (CRGDS), Cys-Arg-Asp-Gly-Ser (CRDGS), Arg-Gly-Asp-dPhe-Cys (cyclic RGD) and KCGGPWQGCK (MMPDP) were purchased from Genscript (Piscataway, NJ). Dithiolized PEG crosslinking molecule of 3.4 kDa molecular weight (PEGDT) was purchased from Laysan Bio (Arab, AL). SU-8 100 was purchased from Microchem (Newton, MA). Silicon wafers were purchased from University Wafer (Boston MA). Patterned transparencies were purchased from Imagesetter (Madison, WI). Sylgard Poly(dimethyl siloxane) (PDMS) solution was purchased from Dow Corning (Midland, MI). Gold coated glass slides were purchased from EMF (Ithaca, NY). FlouroSAM ($HS\text{-}C_{11}\text{-}O\text{-}C_2\text{-}(CF_2)_5\text{-}CF_3$) was purchased from Pro Chimia (Sopot, Poland). Three chamber Proplate Isolator assemblies were purchased from Grace Bio-labs (Bend, OR). Soluble recombinant human growth factors VEGF, TGF-β1 and TGF-β2 were purchased from R&D Systems (Minneapolis, MN). Calcein AM, ethidium homodimer and hoescht nuclear stain were purchased

from Life Technologies (Carlsbad, CA). Primary antibodies Mouse anti-CD31 and Rabbit anti-SNAIL were purchased from Millipore (Billerica, MA). Rabbit anti-Von Willebrand Factor (VWF) and Mouse anti-CD34 were purchased from Dako (Carpinteria, CA). Mouse anti-α-Smooth Muscle Actin (αSMA) was purchased from Sigma-aldrich. Rabbit anti-pSMAD3 was purchased from Thermo-Fisher Scientific (Waltham, MA). Rabbit Anti-Collagen I (Col-I) was purchased from Novus Biologicals (Littleton, CO). Secondary antibodies Alexafluor 488 goat anti-mouse and Alexafluor 594 goat anti-rabbit were purchased from Life Technologies.

5.4.2 Cell culture

Human umbilical vein endothelial cells were cultured in growth medium consisting of M199 supplemented with EGM-2 Bulletkit, which contains 2% BSA as well as hydrocortisone, hFGF-B, VEGF, R3-IGF-1, Ascorbic Acid, Heparin, FBS, hEGF, and GA-1000. Growth medium was changed every other day and cells were passaged every 4 to 7 days. Cell passages were performed using 0.05% trypsin solution and detached cells were recovered in M199 supplemented with 10% cosmic calf serum. All media was supplemented with 100 U/mL Penicillin/ 100 µg/mL Streptomycin. The cells were maintained in a humidified 37˚C incubator with 5% CO2 and used between 5 and 16 population doublings in all experiments.

5.4.3 PEG functionalization with norbornene

PEG-norbornene (PEGNB) was synthesized as previously described [27, 35, 36]. PEGOH of 10 or 20 kDa molecular weight, dimethylaminopyridine and pyridine were dissolved in anhydrous dichloromethane. In a separate reaction vessel, N,N'-dicyclohexylcarbodiimide and norbornene

carboxylic acid were dissolved in anhydrous dichloromethane. Norbornene carboxylic acid was covalently coupled to the PEGOH through the carboxyl group by combining the PEG solution and norbornene solutions and stirring the reaction mixture overnight under anhydrous conditions. Urea was removed from the reaction mixture using a glass fritted funnel and the filtrate was precipitated in cold diethyl ether. The precipitated PEGNB was collected and dried overnight in a buchner funnel. To remove impurities, the PEGNB was dissolved in chloroform, precipitated in diethyl ether and dried a second time in a Buchner funnel. To remove excess norbornene carboxylic acid, PEGNB was dissolved in de-ionized H_2O, dialyzed in de-ionized H_2O for 1 week and filtered through a 0.4 μm pore-size syringe filter. The aqueous PEGNB solution was frozen using liquid nitrogen and lyophilized. Functionalization of PEG with norbornene groups (Fig. 1A) was quantified using proton nuclear magnetic resonance spectroscopy (NMR) to detect protons of the norbornene-associated alkene groups located at 6.8-7.2 PPM [35]. Functionalization efficiency for norbornene coupling to PEGOH arms was above 90% for PEGNB used in all experiments (Figure 1A).

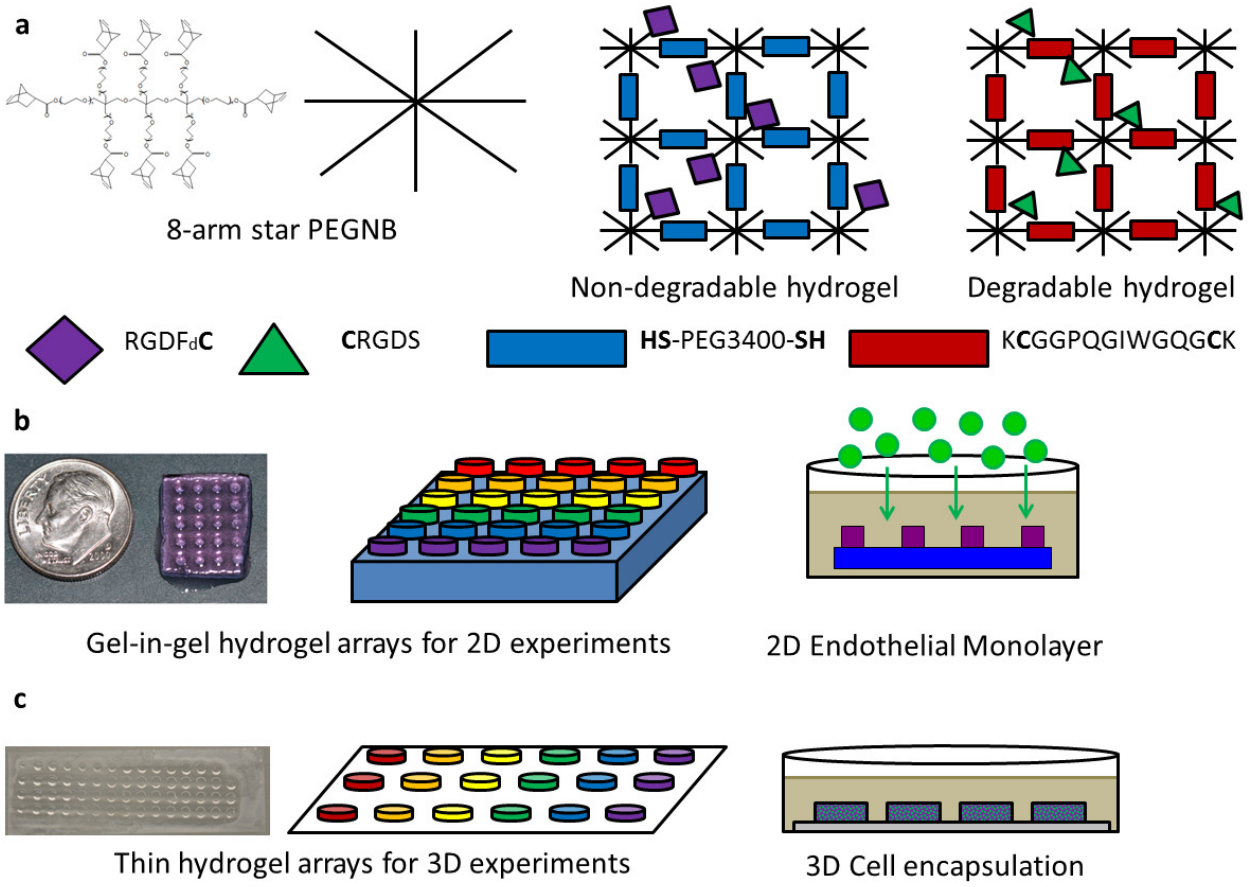

Chapter 5: Figure 1. Cell culture systems to investigate phenotypic changes in HUVECs. (**a**) Schematic of hydrogel networks for cell culture. (**b**) Gel-in-gel hydrogel array and transformation experiments on cell-adhesive PEG hydrogels. (**c**) Thin hydrogel array and transformation experiments in degradable PEG hydrogels.

5.4.4 Pre-coupling adhesion peptides to PEGNB

Peptide coupling to PEGNB was performed as previously described [27]. Lyophilized PEGNB was dissolved in DIH_2O at 1 mM concentration (8 mM norbornene groups) and combined with 0.05% w/v I2959 as well as 2x molar excess of either CRGDS adhesion peptide, CRDGS as scrambled nonfunctional peptide or cyclized RGD for increased affinity to HUVEC integrins. The mixture was reacted under 365 nm UV light for 15 minutes at a dose rate of 4.5 mW/cm^2 to covalently attach the peptides to norbornene groups via the thiol-ene reaction [35]. To remove

buffer salts and unreacted peptide from the decorated PEGNB, the reaction mixture was dialyzed in de-ionized H_2O for 2 days. The dialyzed solution was frozen in liquid nitrogen and lyophilized. The coupling efficiency of PEGNB to the peptides was quantified using proton NMR to detect disappearances of alkene protons at 6.8-7.2 PPM caused by covalent bonding of the peptides to the norbornene group. Pre-coupled PEGNB molecules will be referenced as PEGNB-CRGDS, PEGNB-CRDGS and PEGNB-CycRGD.

5.4.5 Mechanical properties of PEG hydrogels

Hydrogel compressive modulus was measured using 8 mm diameter hydrogel disks as previously described [37]. Non-degradable hydrogels for HUVEC monolayer culture contained PEGNB concentrations ranging from 40 mg/mL to 150 mg/mL as well as dithiolized PEG crosslinking molecule to crosslink 30% to 70% available norbornene groups in solution. Degradable hydrogels for culture of encapsulated HUVECs contained PEGNB concentrations ranging from 30 mg/mL to 70 mg/mL as well as MMPDP to crosslink 50 to 70% available norbornene groups in solution. To create the sample disks 72 µL of hydrogel precursor solution was pipetted into 8 mm diameter, 1.2 mm deep Teflon wells. The resulting hydrogels were swollen in 10 mM PBS (1x PBS) for 24 hours and an 8 mm diameter hole punch was used to trim highly swollen samples as needed. The samples were tested in triplicate using an Ares-LS2 dynamic mechanical analysis instrument (TA Instruments, New Castle, DE). A 20 g force was applied to the samples and a strain sweep test at 10 Hz fixed frequency was performed from 0.005 to 1% strain. The compressive modulus of each sample was as the average of measurements taken at 10 Hz, 0.2-1% strain.

5.4.6 HUVEC culture on Fibronectin-coated TCPS

Costar 96 well plates were coated using a 100 uL of 3.125% FN solution in 1x PBS and incubated for 45 minutes prior to air drying. Each well of the 96 well plates were given 100 uL M199 + EGM2 prior to adding 100 uL HUVEC suspension in M199 + EGM2 at a cell density of 5.0 x 10^4 cells/cm^2. Media was changed every 2 days until cells grew to 70% confluence.

5.4.7 Hydrogel array stencils

Hydrogel array stencils were fabricated using conventional photolithography techniques [38] as described previously [27]. Stencils were formed from two separate elastomer parts: a 200 µm thick sheet of microwells and a 1mm thick base. Silicon master molds were fabricated by spin coating a 200 µm layer of SU-8 100 onto a silicon wafer. Arrayed 1 mm diameter posts of photoresist were defined using a photomask. PDMS was prepared by combining Sylgard PDMS solution with crosslinking solution at a 10:1 volume ratio. The solution was degassed under a vacuum for 45 minutes, poured onto the silicon master mold and crosslinked on a hot plate for 4 hours at 85˚C, forming the 200 µm thick sheet of microwells that penetrated the entire thickness of the sheet. To form the base of the hydrogel array stencil, the PDMS solution was poured between glass slides to form sheets of 1 mm thickness and cured on a hot plate for 4 hours at 85˚C. Both stencil components were cleaned in hexanes by soxhlet extraction [39] and placed in vacuo to remove residual solvent. The completed PDMS stencil was formed by laying the 200 µm thick sheet on top of the 1 mm thick base.

5.4.8 Forming PEG hydrogel arrays for HUVEC monolayer culture

Hydrogel array constructs were formed from 2 separate hydrogels as described previously [27]: an inert hydrogel "background" consisting of 80 mg/mL 20 kDa PEGNB and PEGDT to crosslink 50% available norbornene groups in solution, and "hydrogel spots" consisting of 10 or 20 kDa PEGNB, PEGDT, and PEGNB-cycRGD to provide cell-adhesive PEG surfaces that present 4 mM cyclic RGD and span a range of moduli from 24 to 493 kPa (Figure 1A). Hydrogel spot solutions were added to the PDMS stencil wells as 0.4 μL droplets. Hydrogel spots were crosslinked under 365 nm UV light for 3 seconds at a dose rate of 90 mW/cm2 after all droplets were pipetted into the stencil.

Once all spots were crosslinked under UV light, a 1 mm-thick background hydrogel slab was formed by curing 230 μL background hydrogel solution under 365 nm UV light for 3 seconds at a dose rate of 90 mW/cm2 between a flat 1 mm thick PDMS sheet and a 1" x 1" glass slide. After removing the PDMS sheet only, an additional 30 μL background hydrogel solution was pipetted on top of the hydrogel slab to anchor the spots to the background slab upon crosslinking. The background slab, still attached to the glass slide, was placed on top of the cured hydrogel spots and the entire array was cured for an additional 2 seconds under 365 nm UV light at a 90 mW/cm^2 dose rate. The hydrogel array was removed from the PDMS stencil and secured to the bottom of Costar 6-well plates by using magnets to hold the glass slides in place. The arrays were submerged in 4 mL 1x PBS and incubated overnight at 37˚C to swell the arrays to equilibrium.

Prior to cell seeding 1x PBS was replaced with 4 mL M199 + EGM2. HUVECs were seeded onto arrays at a density of 2.5 x 10^4 cells/cm^2. For a nuclear colocalization quantification test

cells were seeded at a density of 1.0 x 10^5 cells/cm^2. Cells were incubated for 24 hours prior to treatment with experimental media (Figure 1B).

5.4.9 Preparing patterned gold slides with differential wettability

Gold coated glass slides were patterned with hydrophobic and hydrophilic regions as previously described [40]. Briefly, goat coated slides were sonicated in 100% ethanol for 5 minutes and immersed in a 0.1 mM FlouroSAM solution prepared in ethanol for 2 hours at room temperature while protected from light. This created a hydrophobic region on the surface of the glass. A PDMS mask consisting of 64 holes arranged in a 4 x 16 pattern was aligned with the gold slide and adhered to the surface. The exposed hydrophobic regions of the mask were etched by surface plasma treatment using a Diener Plasma Treatment Chamber (Diener Electronic, Ebhausen, Germany) at 40 sccm and 50 W for approximately two minutes. After etching, the PDMS mask was removed and slides were rinsed in ethanol. The etched gold slide was placed into a 0.25 mM solution of [$HS–C_{11}–(O–CH_2–CH_2)_3–OH$] ($EG_3$-OH) in ethanol overnight at room temperature to create hydrophilic surfaces in the etched regions of the gold slide.

5.4.10 Silanizing glass slides for thin hydrogel arrays

Glass microscope slides were functionalized with silane monolayers as previously described [40]. Slides were sonicated for 45 minutes in 50 % HCL in methanol to remove any surface impurities and rinsed in methanol followed by two rinses in ethanol to remove excess acetone from the surface. Cleaned glass slides were surface plasma treated using the Diener Plasma Treatment Chamber on both sides of slides for 5 minutes at 40 sccm and 50 W. The activated slides were

transferred to a toluene solution containing 2.5% 3-MPTS and incubated overnight. After retrieval, samples were cleaned by subsequent rinses of toluene, 1:1 toluene: ethanol and three rinses of ethanol. Slides were cured in a nitrogen-purged pressure chamber at 100 °C for 1 hour to crosslink the 3-MPTS monolayer. After curing, the silanized glass slides were placed in an airtight container and protected from light until use.

5.4.11 Preparing thin hydrogel arrays for HUVEC encapsulation

To prepare the silanized glass slides for formation of the thin hydrogel arrays, glass slides were treated in 10 mM dithiothreitol in 1x PBS at 37°C for 30 minutes to increase the number of free thiols on the surface of the slide. After incubation, slides were rinsed in 1x PBS. Patterned gold slides were rinsed with ethanol and dried using N2 gas. The glass and gold slides were sterilized in 70% ethanol at room temperature for 30 minutes. A PDMS spacer was applied to the surface of the gold slide to control the height of the hydrogels. Hydrogel solutions were prepared to consist of 20 kDa PEGNB, MMPDP, and PEG-CRGDS to provide cell-adhesive PEG matrices that present 2 mM CRGDS and span a range of moduli from 14 to 44 kPa (Figure 1A). For encapsulation the hydrogel solutions conatined HUVECs at a density of 5.0 x 10^6 cells/mL. 0.75 µL of the prepared PEG solutions were pipetted onto the hydrophilic regions of the glass slide in a humidity chamber. A silanized glass slide was slowly placed onto the surface of the gold slide and placed under a UV lamp. The hydrogel spots were exposed to 365 nm ultraviolet light at 90 mW/cm^2 for 2 seconds. Following polymerization, the glass slide was removed from the underlying gold slide. This resulted in a patterned hydrogel array on the surface of the glass slide. Following retrieval of the hydrogel arrays a three chamber Proplate® Isolator was assembled on top of the array to separate media conditions between assigned groups of spots. The individual

wells were given 2.5 mL M199 + EGM2 and incubated at 37˚C for 24 hours prior to the addition of experimental media conditions (Figure 1C).

5.4.12 Treating HUVECs with TGF-β

In all culture systems M199 + EGM2 was replaced with 1x PBS prior to replacement with M199 containing either 0.25% Fetal Bovine Serum alone or 0.25% serum with 5 ng/mL TGF-β1(R&D Systems, 240-B-002) or TGF-β2 (R&D Systems, 302-B2-002). In experiments investigating effects of combinatorial treatment of VEGF and TGF-β all above conditions contained either 0.5, 2 or 5 ng/mL VEGF (R&D Systems, 293-VE-010). HUVECs seeded on fibronectin-coated TCPS were treated using 200 uL experimental medium per well. HUVECs seeded on non-degradable hydrogel arrays were treated using 4 mL experimental medium per array. HUVECs encapsulated in degradable hydrogel arrays were treated using 2.5 mL experimental medium per well of the Proplate® isolator system. Cells were incubated in experimental medium for 72 hours in all culture systems prior to rinsing cells with 1x PBS and 30 minutes of fixation in buffered formalin solution.

5.4.13 HUVEC viability after encapsulation in PEG hydrogels

HUVECs were encapsulated in degradable thin-hydrogel arrays as previously described. All conditions were incubated in M199 + EGM2 for 24 hours prior to treatment with experimental media. In one condition growth medium was replaced with M199 + EGM2 containing 0.2% Calcein AM, 0.1% ethidium homodimer and 0.1% hoescht nuclear stain prior to incubation at 37˚C for 20 minutes. Afterward the cells were rinsed with 1x PBS and fixed in buffered formalin

for 30 minutes. The remaining conditions were treated for 72 hours using either M199 + 0.25% fetal bovine serum alone or 0.25% serum with 5 ng/mL TGF-β1 or 2. After treatment the cells were treated with Calcein AM, ethidium homodimer and hoescht nuclear stain as previously described. The cells were rinsed using 1x PBS prior to 30 minute fixation with buffered formalin solution. All hydrogel spots were photographed within 24 hours of fixation using a Nikon TE300 fluorescence microscope. Viability was quantified by dividing the number of live cell nuclei by total nuclei in the post.

5.4.14 Antibody staining

With exception of samples used in viability studies, all fixed cell samples were incubated in 1x PBS overnight after removal of formalin buffer. Cells were permeabilized in 1x PBS containing 0.25% Triton-X-100 and 1% Bovine Serum Albumin for 30 minutes. Following Permeabilization cells were incubated for 2 hours in 1x PBS containing 0.05% Triton-X-100 and 0.1% BSA along with antibodies consisting of 1:500 mouse anti-CD31 (Millipore, MAB2148), 1:200 rabbit anti-VWF (Dako, A0082), 1:600 mouse anti-αSMA (Sigma, A2547), 1:200 rabbit anti-pSMAD3 (Thermo-Pierce, PA5-12693), 1:200 mouse anti-CD34 (Dako, M7165) or rabbit anti-SNAIL (Millipore, ABD38). Note that cells were treated with 1:100 rabbit anti-SNAIL in TCPS culture and 1:200 rabbit anti-SNAIL in PEG monolayer culture. In 3D hydrogel cultures the antibody treatment consisted of 1:500 mouse anti-CD31 (Millipore, MAB2148), 1:200 rabbit anti-VWF (Dako, A0082), 1:600 mouse anti-αSMA (Sigma, A2547) or 1:500 rabbit anti-Collagen I (Novus Biologicals, NB600-408). After two 15-minute rinses with wash buffer consisting of 1x PBS and 0.05% Triton-X-100, samples were incubated for 2 hours in 1x PBS, 0.05% Triton-X-100, and 1:300 both of Alexafluor 488 goat anti-mouse secondary antibody

(Life Technologies) and 1:300 Alexafluor 594 goat anti-rabbit secondary antibody (Life Technologies). Samples were rinsed once for 15 minutes in 1x PBS and 0.05% Triton-X-100, then treated with 1:1000 Hoescht nuclear stain in 1x PBS for 30 minutes. Afterward the cells were rinsed twice in 1X PBS and stored in 1X PBS overnight. Samples were imaged using a Nikon TI Eclipse fluorescence microscope. A nuclear co-localization quantification method was used to quantify the level of overlap between expressed cell markers and the stained nuclei of all cells (Supplementary Fig. 1).

5.4.15 Statistical analysis

All values are presented as mean ± standard deviation unless otherwise noted. Statistical differences were calculated using the two-sided Student's T-test assuming equal variances with Bonferroni corrections when comparing differences in endothelial cell marker expression on TCPS and differences in marker expression during the nuclear co-localization quantification test. All other statistical differences were calculated using two-way ANOVA and Tukey's Multiple Comparisons tests. Statistical significance is denoted as $p < 0.05$.

5.5 Results

5.5.1 Hydrogel modulus

The compressive modulus of PEG hydrogels was controlled based on modifications to crosslinking density and polymer concentration in hydrogel precursor solutions. Non-degradable hydrogels used to culture HUVECs in monolayer culture were crosslinked using PEGDT. The

various concentrations of PEGNB and PEGDT in hydrogel solutions resulted in compressive moduli of 24 ± 4, 44 ± 2, 69 ± 6, 142 ± 16, 244 ± 26, and 493 ± 54 kPa (Figure 2A). In particular the highest modulus of 493 kPa was achieved by substituting 20 kDa PEGNB molecule with a 10 kDa molecule to increase crosslinking density in the hydrogels [41]. Degradable hydrogels used to encapsulate HUVECs were crosslinked using MMPDP in order to enable cell migration and environmental remodeling. The various concentrations of PEGNB and MMPDP in hydrogel solutions resulted in compressive moduli ranging from 13.8 kPa in the softest hydrogel formulation to 26 ± 4, 37 ± 5, and 44 ± 7 kPa (Figure 2B). The lowest modulus hydrogel was only analyzed as a single sample as only one sample was mechanically stable enough to withstand the forces associated with dynamic mechanical analysis.

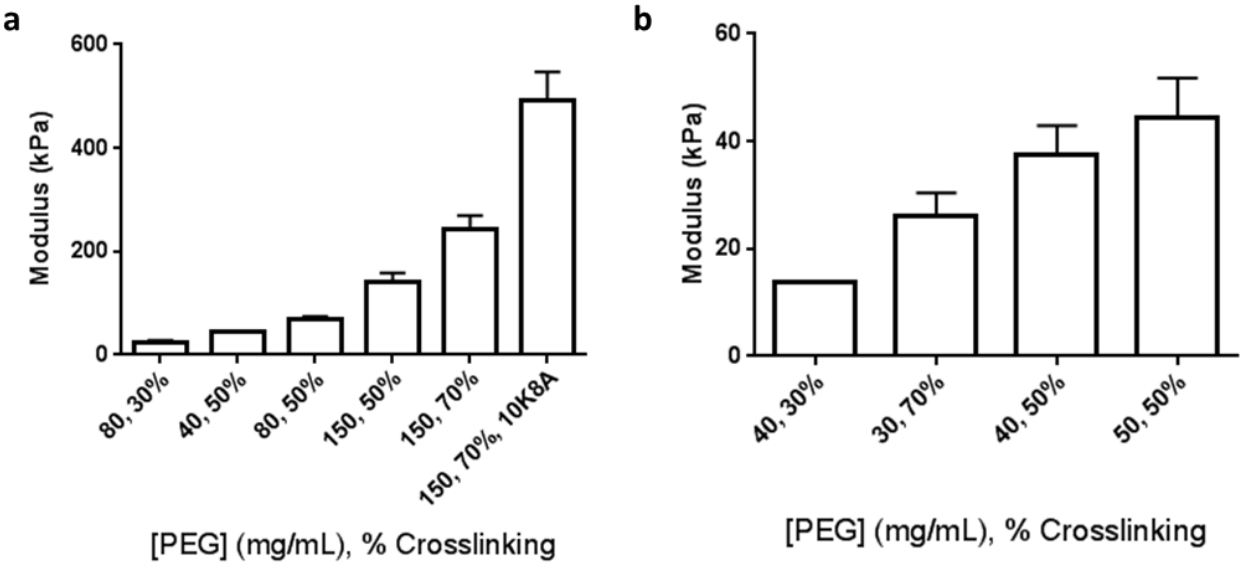

Chapter 5: Figure 2. Hydrogel modulus and corresponding PEG concentration and thiol-ene crosslinking in precursor solutions. (**a**) Non-degradable PEG hydrogels for 2D environments. (**b**) Degradable PEG hydrogels in 3D environments.

5.5.2 Marker quantification by nuclear colocalization

HUVECs were seeded on non-degradable PEG hydrogels and treated with medium containing 0.25% FBS alone or with 5 ng/mL TGF-β2 to explore the efficacy of quantifying cell marker expression using automated nuclear colocalization. Size exclusion and fluorescence intensity thresholding were performed using Nikon Elements image analysis software to highlight nuclei of fixed cells and α-SMA labeled with Alexafluor 488. α-SMA expression was quantified by counting the number of cells positive for α-SMA and by determining the percentage of colocalization detected between α-SMA and nuclei. Both quantification methods demonstrated similar results of high α-SMA expression by HUVECs in serum-only conditions. Additionally, in both quantification methods HUVECs treated with TGF-β2 demonstrated decreased α-SMA expression on low modulus hydrogels followed by increased α-SMA expression with increasing modulus. However, quantification with nuclear colocalization detected statistically significant differences in α-SMA expression between cells treated with serum and cells treated with TGF-β2 in all hydrogel modulus conditions. Conversely, quantification with cell number only highlighted significant differences on low modulus hydrogels (Supplemental Figure 1). This may be attributed to the fact that nuclear colocalization accounts for relative levels of expression in individual cells instead of only quantifying the number of cells that are positive and negative for α-SMA expression.

5.5.3 TGF-β signaling – HUVECs on TCPS

HUVECs seeded on human plasma fibronectin-coated TCPS responded to TGF-β signaling by increasing SMAD3 phosphorylation and SNAIL expression while downregulating expression of

common endothelial cell markers CD31 and VWF. After treatment with medium containing 0.25% FBS alone or with 5 ng/mL TGF-β1 or 2 all HUVEC populations on TCPS were fixed and immunostained for phosphorylated SMAD3 (pSMAD3), SNAIL, CD31, VWF, α-SMA and CD34. Compared to the serum-only condition HUVECs treated with TGF-β1 or 2 demonstrated respective 4 and 5-fold increases in pSMAD3 levels (Figure 3A) as well as respective 20 and 17-fold increases in SNAIL expression (Figure 3B). These data suggest that TGF-β treatment initiated SMAD signaling as well as expression of transcription factors associated with the endothelial-mesenchymal transition [13, 28]. We next observed changes in CD31 and VWF expression to determine the state of endothelial cell marker expression in the treated cells. Compared to the serum-only condition HUVECs treated with TGF-β1 and 2 demonstrated respective 3 and 2-fold decreases in CD31 expression (Figure 3C) and statistically significant-but-marginal decreases in VWF expression (Figure 3D). These data suggest a diminishing endothelial cell phenotype in the HUVECs [13]. We next observed changes in α-SMA and CD34 expression to clarify the cell phenotype resulting from TGF-β treatment, with α-SMA expression signifying a transformation to a mesenchymal phenotype [13] and CD34 signifying a transformation to a endothelial progenitor cell phenotype [42, 43]. However, there were no statistically significant changes in either marker compared to the serum-only condition, suggesting that neither a complete endothelial-mesenchymal transition nor a reversion to a progenitor cell type occurred with TGF-β treatment. Moreover CD34 expression levels remained below 5% colocalization with nuclei throughout the duration of the experiments, indicating a negligible presence of progenitor cell types in the tested cell population (Figure 3E,F).

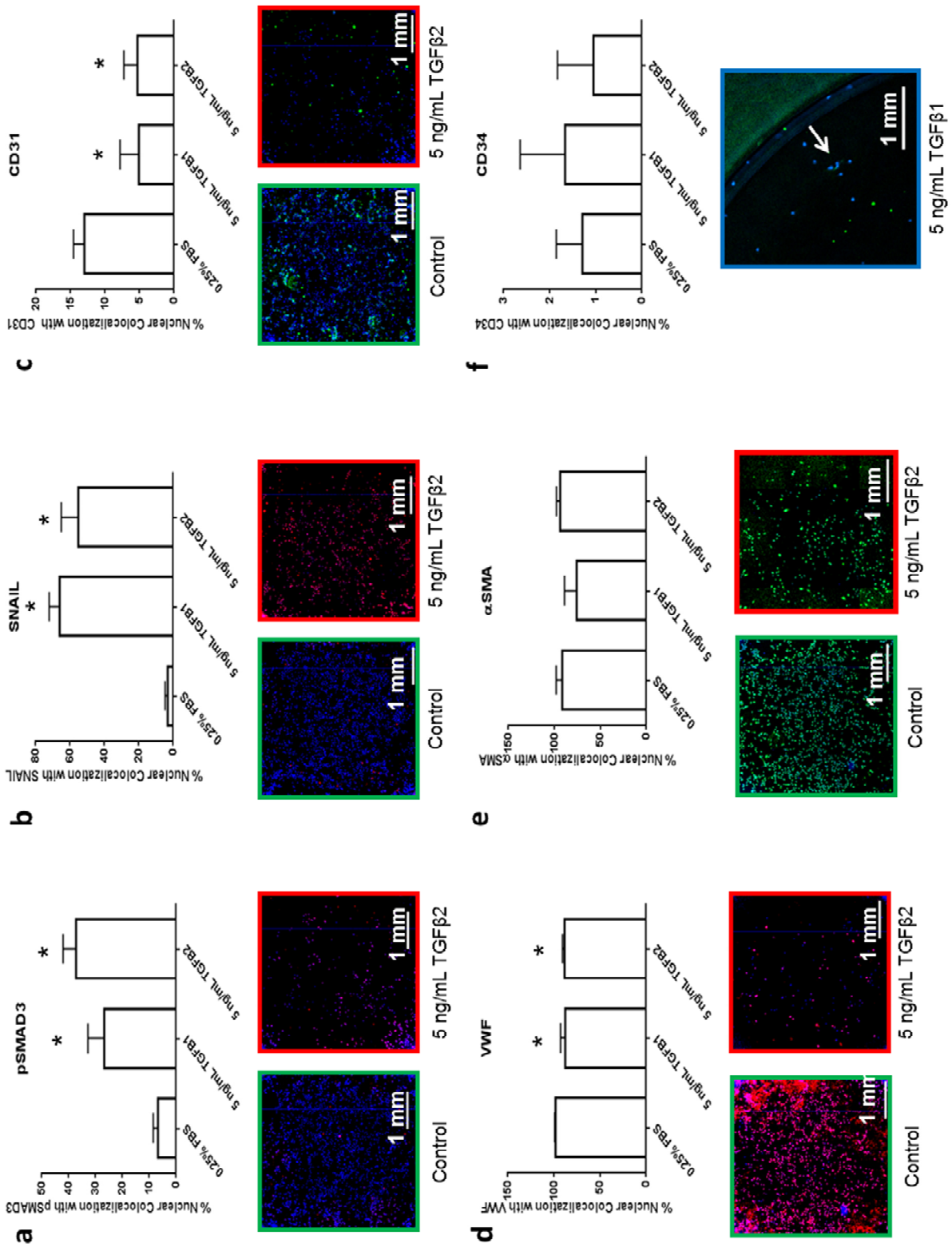
a
pSMAD3
% Nuclear Colocalization with pSMAD3
0.25% FBS
5 ng/mL TGFB1
5 ng/mL TGFB2
Control
5 ng/mL TGFβ2
1 mm
b
SNAIL
% Nuclear Colocalization with SNAIL
c
CD31
% Nuclear Colocalization with CD31
d
VWF
% Nuclear Colocalization with VWF
e
αSMA
% Nuclear Colocalization with αSMA
f
CD34
% Nuclear Colocalization with CD34
5 ng/mL TGFβ1

Chapter 5: Figure 3. Changes in HUVEC marker expression with TGF-β treatment on fibronectin-coated TCPS. (**a**) Phosphorylated SMAD3 immunostaining. Red: pSMAD3. Blue: Hoescht nuclear stain. (**b**) SNAIL expression and immunostaining. Red: SNAIL. Blue: Hoescht nuclear stain. (**c**) CD31 expression and immunostaining. Green: CD31. Blue: Hoescht nuclear stain. (**d**) Von willebrand factor expression and immunostaining. Red: VWF. Blue: Hoescht nuclear stain. (**e**) Smooth muscle actin expression and immunostaining. Green: αSMA. Blue: Hoescht nuclear stain. (**f**) CD34 expression and immunostaining. Green, Arrowhead: CD34+-positive HUVEC. Blue: Hoescht nuclear stain. *, $p < 0.05$ compared to 0.25% FBS control media.

5.5.4 Concurrent VEGF and TGF-β treatment on TCPS

VEGF, a known inhibitor of TGF-β signaling [24], attenuated TGF-β-induced changes in pSMAD3, SNAIL, and CD31 in a dose-dependent manner. TGF-β1 and 2 treatment was performed on HUVECs cultured on TCPS as previously described, but all media conditions including serum controls now contained 0.5, 2 or 5 ng/mL VEGF. TGF-β1 and 2 increased SNAIL expression above expression levels in medium containing only serum and VEGF. However in the case of pSMAD3 only treatment with 0.5 ng/mL VEGF and 5 ng/mL TGF-β2 resulted in significant increases in pSMAD3 levels over those observed in conditions containing only serum and VEGF. This indicates that SMAD signaling is only increased by high concentrations of TGF-β in conditions containing low concentrations of VEGF. VEGF increased CD31 expression in a dose dependent manner in all TGF-β treated conditions, while only TGF-β1 decreased CD31 expression compared to conditions containing only serum and VEGF. Concurrent treatment with VEGF and TGF-β resulted in marginal changes in VWF and α-SMA expression. VEGF significantly increased CD34 expression in a dose dependent manner, but as % colocalization of CD34 with nuclei was still below 5% this change was insufficient to signify a significant reversion of HUVECs to progenitor cells (Figure 4).

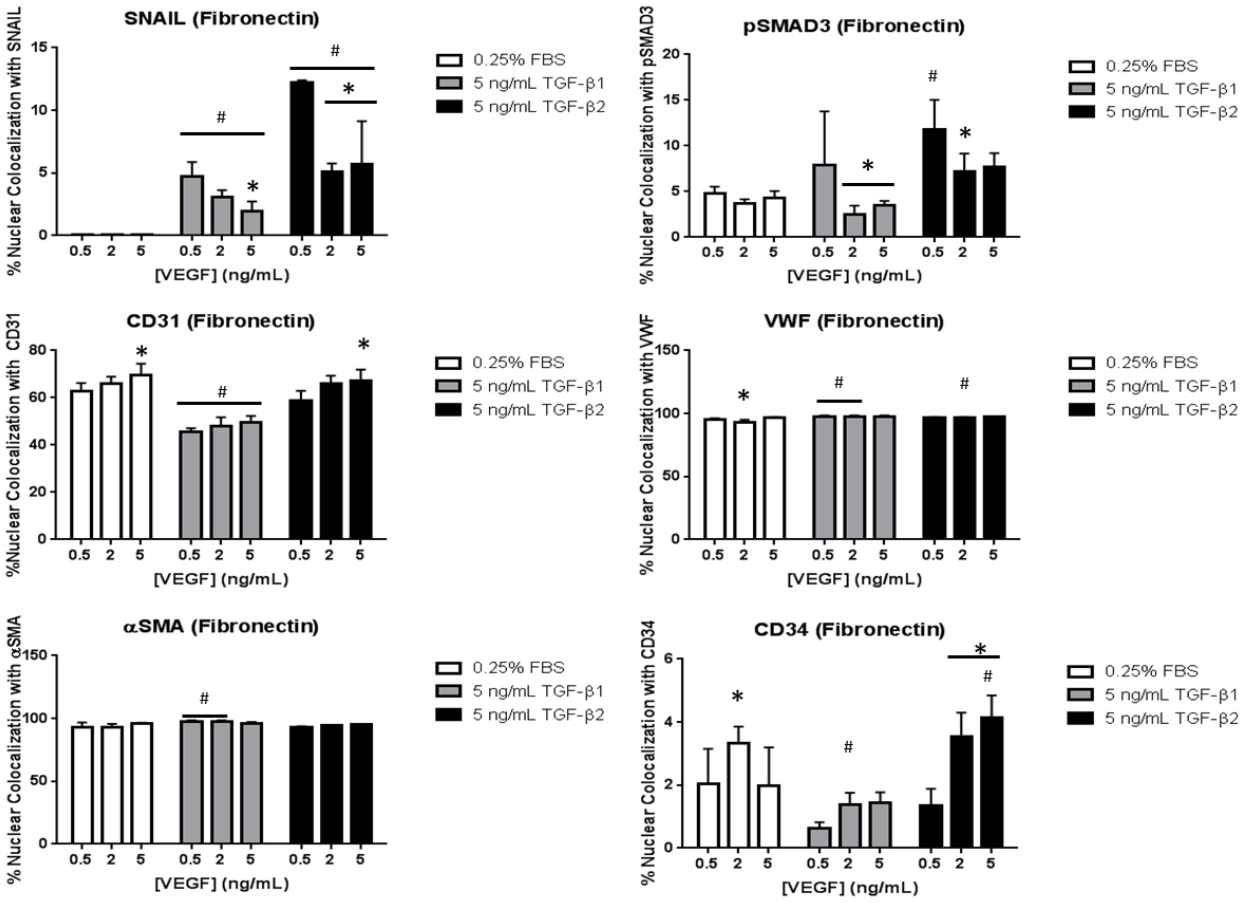

Chapter 5: Figure 4. Changes in HUVEC marker expression with concurrent TGF-β and VEGF treatment on fibronectin-coated TCPS. *, $p < 0.05$ compared to 0.5 ng/mL VEGF treatment. #, $p < 0.05$ compared to 0.25% FBS control media.

5.5.5 TGF-β signaling – HUVECs on PEG hydrogels

HUVECs seeded on PEG hydrogels demonstrated dissimilar responses to TGF-β treatment compared to HUVECs seeded on FN-coated TCPS. HUVECs were seeded at low population densities to mimick endothelial cell dispersion in situations such as tissue development and wound healing. After treatment with TGF-β1 and 2, HUVECs were fixed and immunostained for

all markers investigated on TCPS. HUVECs on PEG hydrogels displayed a high baseline level of SNAIL expression of 40-50% colocalization in media containing serum only, which was higher than colocalization levels of 3% observed in equivalent media conditions on TCPS. TGF-β treatment significantly decreased SNAIL expression from serum controls only on low modulus hydrogels. Levels of pSMAD3 remained at low levels of 10% or less in all media and modulus conditions, though TGF-β1 significantly increased pSMAD3 levels from serum controls in low modulus conditions. pSMAD3 significantly increased with increasing modulus with TGF-β2 treatment only. These results suggest that pSMAD3 levels depend on both TGF-β signaling and substrate modulus. CD31 expression increased with TGF-β treatment at all modulus levels, an effect unlike the decreased in expression observed on TCPS. α-SMA expression increased significantly with increasing substrate stiffness, suggesting that changes in α-SMA expression is driven by substrate modulus rather than TGF-β signaling. As an exception to this is finding TGF-β2 treatment maintained a low α-SMA expression level at all modulus conditions. Taken together, these results suggest that in HUVECs seeded on PEG hydrogels, TGF-β acts through signaling pathways dissimilar to those that promote a mesenchymal transition, and that TGF-β acts to stabilize a pro-endothelial phenotype instead of driving EndMT on PEG hydrogels. Additionally, TGF-β is possibly promoting a stable endothelial phenotype mainly through signaling pathways that are independent of substrate stiffness, as TGF-β-mediated changes in CD31 and αSMA expression were largely independent of stiffness despite stiffness-dependence of SNAIL and pSMAD3. CD34 did not have high levels of expression in any condition, suggesting that HUVECs were not reverting to progenitor cells in these studies (Figure 5).

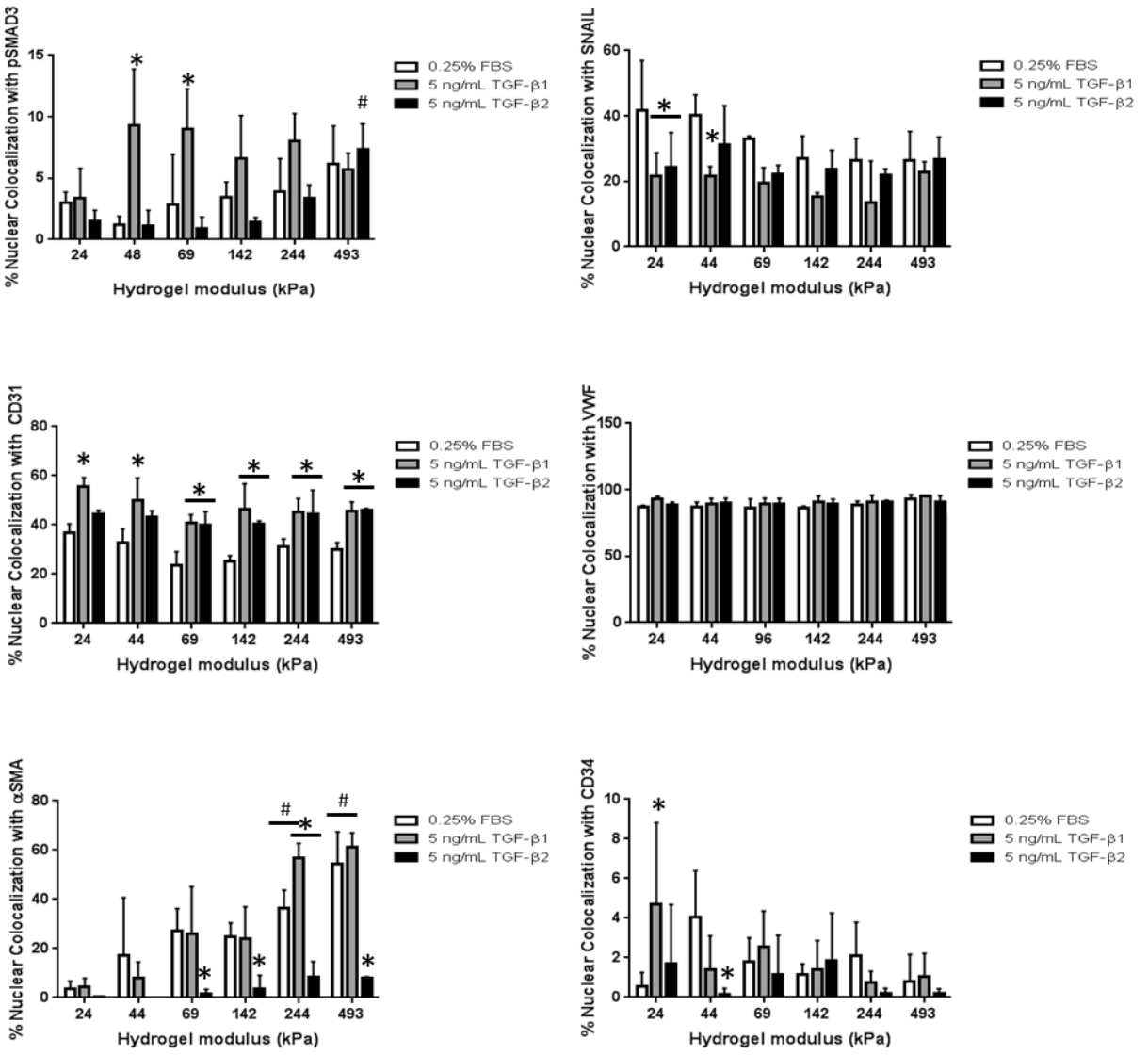

Chapter 5: Figure 5. Changes in HUVEC marker expression with TGF-β treatment on cell adhesive PEG hydrogels of varying modulus. *, $p < 0.05$ compared to 0.25% FBS control media. #, $p < 0.05$ compared to 24, 44 or 69 kPa hydrogels.

5.5.6 TGF-β treatment – HUVECs encapsulated in PEG hydrogels

HUVECs encapsulated in PEG hydrogels demonstrated decreased expression of CD31, α-SMA and ECM protein Col-I with increased hydrogel modulus, and further decreases in all tested markers were observed with TGF-β1 treatment. HUVECs were encapsulated at relatively low

densities to mimic cell dispersion in situations such as tissue development and wound healing. After treatment with media containing 0.25% FBS alone or with 5 ng/mL TGF-β1 or 2 all encapsulated HUVEC populations were fixed and immunostained for CD31, VWF, α-SMA and Col-I. Increased hydrogel modulus decreased expression of all observed markers by at least 2-fold compared to cells in the 14 kPa condition, with exception to VWF which did not see a 2-fold decrease in expression at any hydrogel modulus. TGF-β1 treatment further decreased expression of CD31, α-SMA and Col-I in most hydrogel moduli compared to serum-only control conditions. However, TGF-β1-mediated decreases in CD31 and VWF required hydrogel moduli to reach at least 26 and 44 kPa, respectively. Compared with TGF-β1, TGF-β2 activity was mostly insignificant except with α-SMA, where expression was significantly decreased from serum-only controls in 26 and 44 kPa conditions (Figure 6).

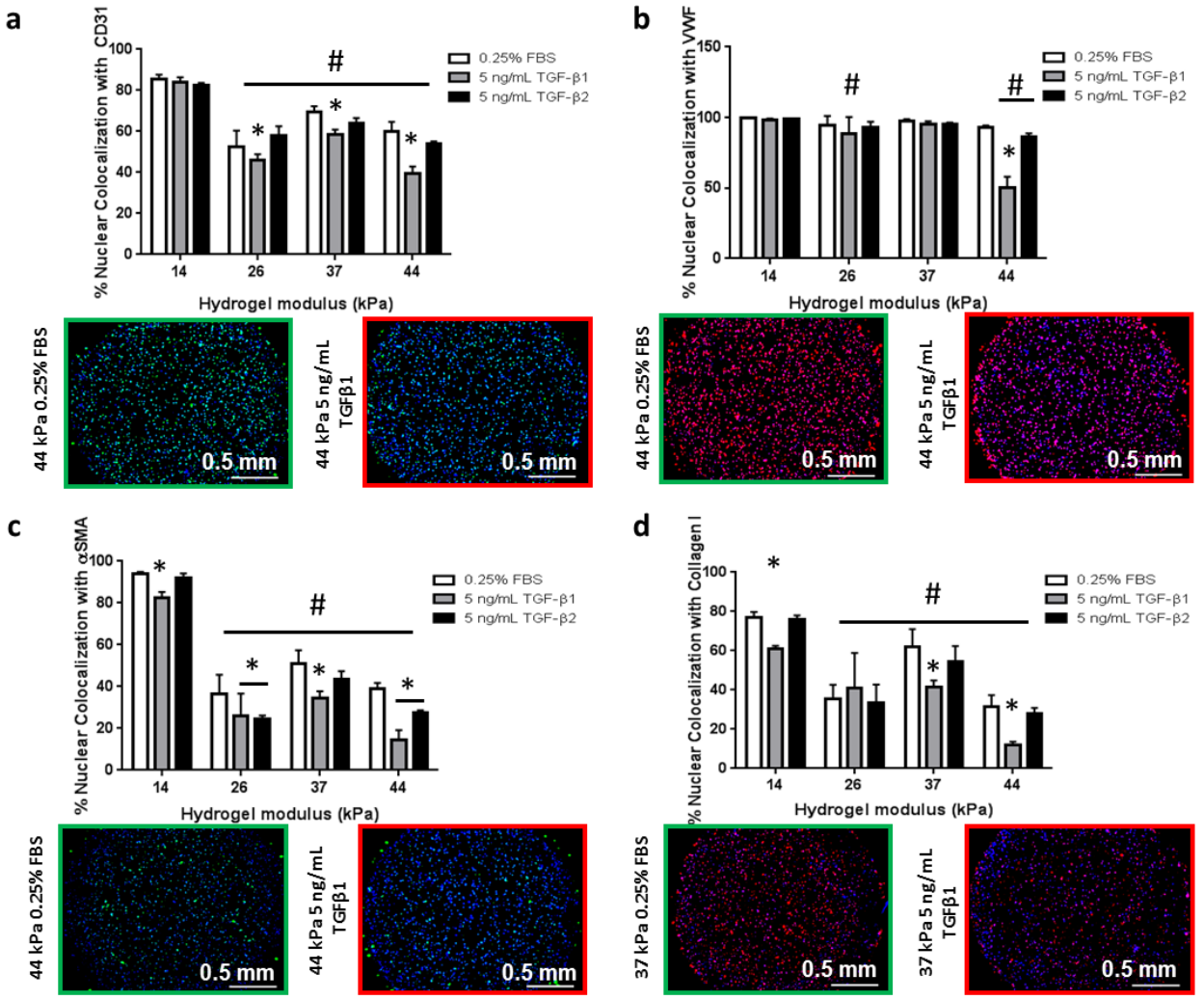

Chapter 5: Figure 6. Changes in HUVEC marker expression with TGF-β treatment in degradable PEG hydrogels of varying modulus. (**a**) CD31 expression and immunostaining. Green: CD31. Blue: Hoescht nuclear stain. (**b**) Von willebrand factor expression and immunostaining. Red: VWF. Blue: Hoescht nuclear stain. (**c**) Smooth muscle actin expression and immunostaining. Green: αSMA. Blue: Hoescht nuclear stain. (**d**) Collage I expression and immunostaining. Red: Col I. Blue: Hoescht nuclear stain. *, $p < 0.05$ compared to 0.25% FBS control media. #, $p < 0.05$ compared to 14 kPa hydrogel.

We investigated whether changes in cell marker expression occurred due to TGF-β-mediated reductions in cell viability. Viability levels in all modulus and TGF-β treatment conditions were sustained near 40-50% of encapsulated HUVECs. This suggests that reductions in marker

expression due to hydrogel stiffness and growth factor treatment were not due to decreased cell viability (Figure 7). The universal reduction in marker expression seen here may imply a phenotypic change of encapsulated HUVECs to a quiescent state, unlike results observed during monolayer culture on hydrogel surfaces. Additionally, the fact that TGF-β1 modulates α-SMA and Col-I at most hydrogel moduli and that it only modulates CD31 and VWF above minimum threshold moduli suggests that it acts through multiple signaling pathways that may be independent and dependent on substrate stiffness. Finally, the results concerning TGF-β2 only modulating α-SMA expression may suggest that it lacks the potency of TGF-β1 in this 3D culture scenario.

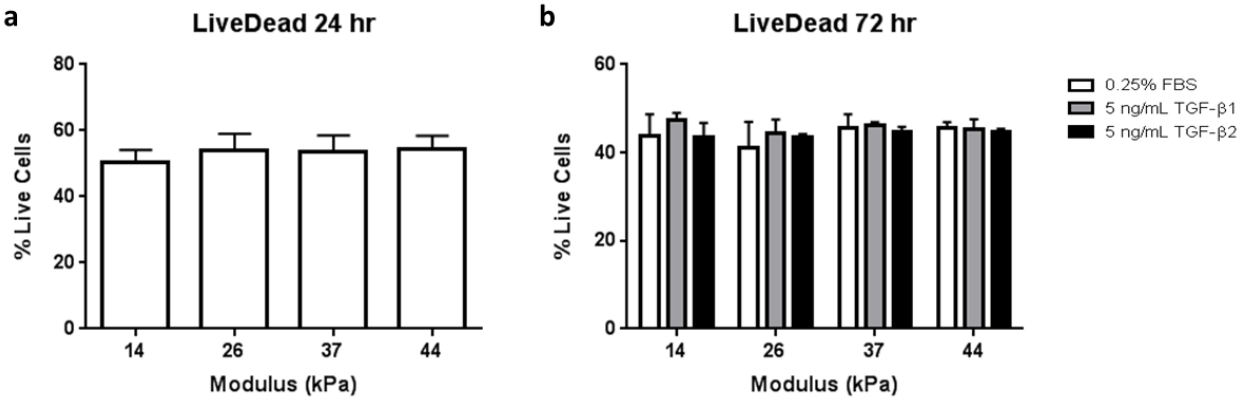

Chapter 5: Figure 7. Viability of HUVECs cultured in degradable PEG hydrogels. (**a**) Viability in PEG hydrogels of varying modulus 24 hours after encapsulation. (**b**) Viability of HUVECs with TGF-β treatment 72 hours after encapsulation.

5.6 Discussion

These studies demonstrated that endothelial cell responses to TGF-β signaling are mediated by cell culture contexts and substrate stiffness. Specifically, while HUVECs on fibronectin-coated TCPS upregulated expression of SNAIL and increased SMAD3 activity with TGF-β treatment,

HUVECs cultured on PEG hydrogels downregulated SNAIL expression with treatment and demonstrated a low baseline activity of SMAD3. Additionally, TGF-β signaling decreased CD31 expression in HUVECs seeded on TCPS and encapsulated in PEG hydrogels, but increased CD31 expression in HUVECs on PEG hydrogel surfaces. Our results here suggest that the composition and mechanics of the PEG hydrogels determine different phenotypic outcomes of TGF-β treatment, specifically between quiescent phenotypes where expression of most cell markers decreases, and pro-endothelial phenotypes where cell-cell junction proteins increase in expression levels.

The factors determining how endothelial cells respond to TGF-β signaling are not well understood, as TGF-β signaling has been known to enhance [18, 19] or inhibit [20] angiogenesis in different cases. An initial distinction between the divergent effects of TGF-β is the families of SMAD proteins activated during TGF-β signaling. Specifically, the activation of SMADs 1,5 and 8 promote proliferation and angiogenesis, while SMADs 2 and 3 inhibits angiogenesis [44]. The different SMADs are activated by different TGF-β receptors. For example, the TGF-β type-1 receptor Alk1 and endoglin initiate signaling cascades mediated by SMADs 1,5 and 8 while Alk2, Alk5 and betaglycan initiate signaling cascades mediated by SMADs 2 and 3 [13, 17]. Differential expression of TGF-β receptors would determine the activities of TGF-β [45], though the mechanisms governing differential receptor expression are not well understood. Other possibilities for determining signaling pathway activation during TGF-β signaling may relate to integrin binding and substrate stiffness. Interactions between TGF-β receptors and α_v integrins are known to modulate TGF-β activity [22], and the occupation of those integrins by adhesion ligands in the ECM may affect their propensity to bind to TGF-β receptors. Taken together, integrin activity on endothelial cells may drive pro-angiogenic or pro-apoptotic effects of TGF-β

signaling by modulating growth factor activity [18]. However, other signaling pathways such as stiffness-mediated P13K/AKT signaling can drive TGF-β to drive EndMT rather than apoptosis [46]. As demonstrated by HUVECs encapsulated in PEG hydrogels in the current studies, it is also possible that multiple stiffness-dependent and stiffness-independent signaling pathways are simultaneously activated by TGF-β. Further characterization of growth factor receptor expression and integrin activity on endothelial cells as well as the role of stiffness-mediated signaling cascades is necessary to mechanistically determine how the extracellular environment modulates the effects of TGF-β signaling.

A notable behavior demonstrated by HUVECs during these studies included the constitutive expression of α-SMA in 0.25% FBS control conditions, as well as the decreased α-SMA expression in response to TGF-β. This was not an expected result given that previous studies demonstrated the onset of α-SMA expression by TGF-β signaling in endothelial cells that previously did not express the marker [13]. α-SMA expression in primary endothelial cells has been reported in endothelial cells in the absence of TGF-β, and this was due to either increasing passage numbers [47] or the application of mechanical stress and strain [48]. In the present study HUVECs were purchased from a commercial source, possibly leading to inflated passage numbers prior to experimentation, and the results of this the current study suggest that substrate stiffness plays a critical role in α-SMA expression in the absence of TGF-β signaling. This principle may also be applied to HUVECs cultured on fibronectin-coated TCPS, which has greater elastic modulus than the PEG hydrogels.

A recent study by Zhang *et al* revealed that the stiffness of hyaluronic acid films dictated whether HUVECs underwent TGF-β1-mediated EndMT, and that HUVECs expressed low levels of α-SMA in control conditions. A number of differences exist between the studies performed

here and the studies performed by Zhang *et al*. In experiments by Zhang, HUVECs were isolated rather than purchased from a commercial source, and a naturally-derived substrate was used to culture the endothelial cells rather than synthetic PEG hydrogels. Additionally, successful transitions occurred in media containing 20% FBS rather than 0.25% FBS as used in the present study [49]. This large amount of extra protein and protein binding to a naturally-derived substrate may have contained sufficient concentrations of other transition-inducing factors that were functionally absent from the present study. For example, a previous study demonstrated that the simultaneous addition of TGF-β2 and Interleukin 1-β induced EndMT in HUVECs while TGF-β2 alone did not [50]. The lack of defined IL-1β in the present system may have induced an "incomplete" transition and consequent quiescent phenotype, denoted partially by the reduction of α-SMA, in the HUVECs from the current study. Future studies should employ IL-1β to confirm this hypothesis.

An initial objective of this study was to determine relationships between PEG hydrogel properties and possibly determine candidate materials for efficiently executing EndMT *in vitro*. While we demonstrated that culturing HUVECs on RGD-functionalized PEG hydrogels or encapsulating them inside PEG hydrogels significantly changed overall HUVEC response to TGF-β signaling, our data suggests that PEG hydrogels functionalized with RGD alone are insufficient to induce signaling pathways necessary to induce EndMT. The differential effects of TGF-β signaling on pSMAD3 and SNAIL levels on fibronectin-coated TCPS and PEG hydrogels suggest two possible conclusions: that the elevated substrate mechanics of TCPS encouraged a TGF-β-mediated EndMT, or that a substrate consisting of full-length proteins as opposed to integrin-binding peptides alone contains the molecular signals necessary to drive EndMT. Whether the differences are determined by one possibility or both should be addressed

in future studies functionalizing PEG hydrogels with additional biomolecules including synergistic cell binding motifs such as PHSRN [51] to promote migratory cell phenotypes often demonstrated by mesenchymal cell types [52], or molecules binding soluble heparin to modulate TGF-β signaling dynamics [53, 54]. Additional functionalities such as these are present in full-length proteins such as fibronectin, but are absent on PEG hydrogels presenting only an integrin-binding molecule.

5.7 Conclusion

In this study HUVECs cultured on fibronectin-coated TCPS, on non-degradable PEG hydrogel surfaces of varying elastic modulus and in degradable PEG hydrogels of varying density demonstrated differential outcomes of TGF-β signaling depending on culture contexts. TGF-β treatment induced changes in HUVEC expression of pSMAD3, SNAIL, CD31, VWF on TCPS as well as CD31, VWF, α-SMA and Col-I in degradable PEG hydrogels to indicate a loss of endothelial cell phenotype and the onset of quiescence. Conversely, HUVEC expression of pSMAD3, SNAIL, CD31, VWF and α-SMA on non-degradable PEG hydrogels indicated a stabilization of an endothelial cell phenotype with TGF-β treatment. While the pathways mediating TGF-β-induced changes in CD31 and α-SMA expression appear to be largely independent of modulus on PEG surfaces, endothelial marker regulation by TGF-β was differentially affected by modulus in 3D cell culture. The differential cell behaviors with varying culture contexts highlight the need for well-defined materials to study how substrate properties such as modulus and the presence of additional insoluble signaling molecules specifically affect endothelial cell phenotype. The inclusion of additional soluble signals including those associated

with inflammation is necessary to more accurately model TGF-β-driven endothelial cell pathology.

5.8 Acknowledgements

The authors would like to acknowledge funding from the National Institutes of Health (NIH R01 HL093282-01A1, NIH R21 EB016381-01, NIH 1UH2 TR000506-01, the UW-Madison Biotechnology Training Program NIGMS 5T32GM08349, and the UW-Madison Cardiovascular Research Center T32-HL 07936) as well as the UW Madison Graduate Engineering Research Scholars program. We would like to thank Justin Williams and David Beebe for their assistance with soft lithography techniques. This study made use of the National Magnetic Resonance Facility at Madison, which is supported by NIH grants P41RR02301 (BRTP/ NCRR) and P41GM10399 (NIGMS). Additional equipment was purchased with funds from the University of Wisconsin, the NIH (RR02781, RR08438), the NSF (DMB-8415048, OIA-9977486, BIR-9214394), the DOE, and the USDA. Small angle X-ray scattering (SAXS) equipment was purchased with funds from NIH grant S100RR027000 (NCRR). Mechanical testing data was obtained using the Ares LS2 rheometer at the UW Madison Soft Materials Laboratory. Special thanks go to William Daly for helpful discussions and technical instruction throughout the course of these studies and Ngoc Nhi Le for providing materials for hydrogel array patterning.

5.9 Supplemental information

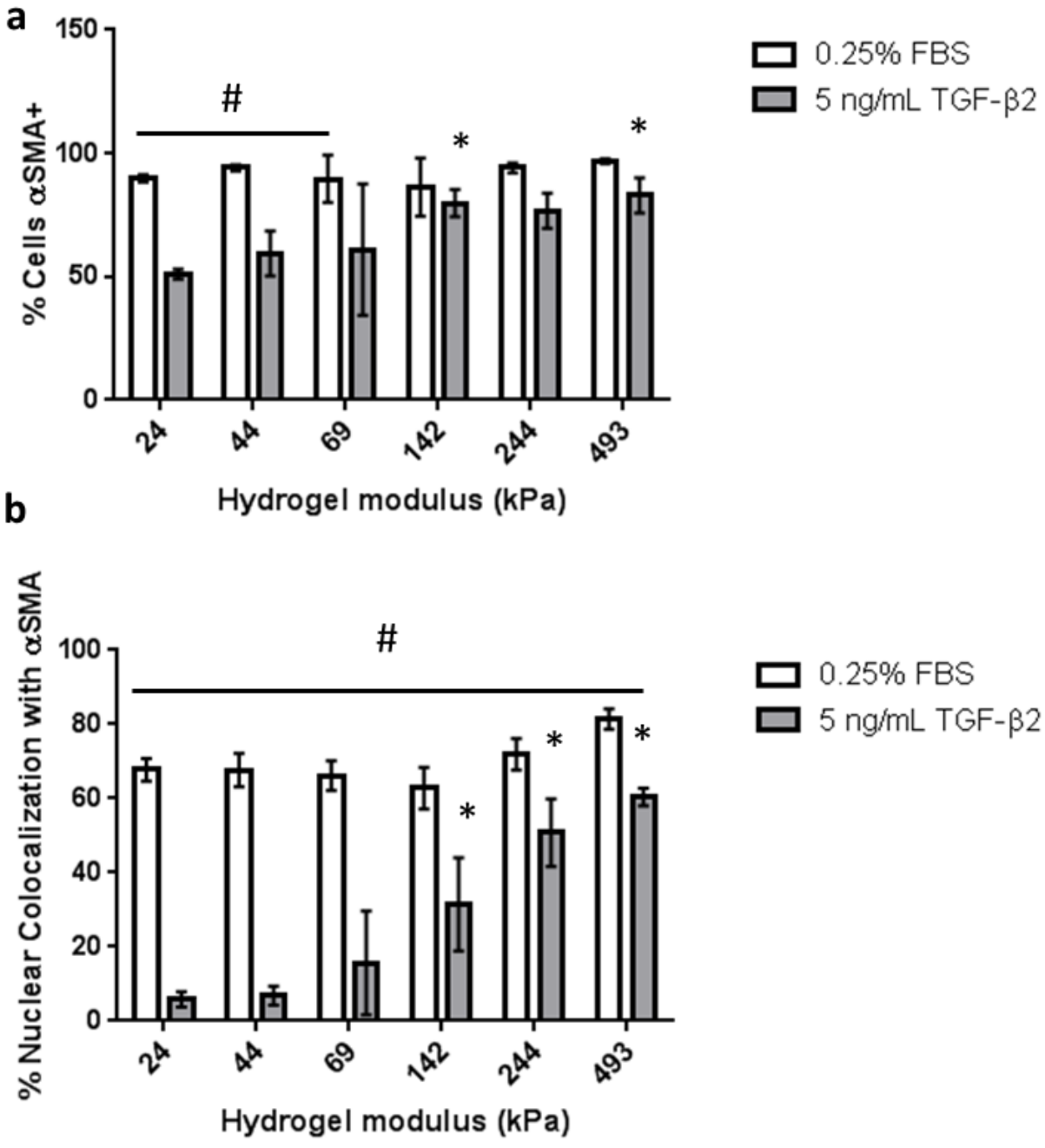

Chapter 5: Supplemental Figure 1. Comparison of cell marker quantification methods. (**a**) Number of cells positive for α-SMA. (**b**) % nuclear co-localization with α-SMA stain. *, $p < 0.05$ compared to 24 kPa hydrogel. #, $p < 0.05$ compared to 0.25% FBS control media.

5.10 References

[1] Sumpio BE, Riley JT, Dardik A. Cells in focus: endothelial cell. Int J Biochem Cell Biol. 2002;34:1508-12.

[2] Kolluru GK, Bir SC, Kevil CG. Endothelial dysfunction and diabetes: effects on angiogenesis, vascular remodeling, and wound healing. Int J Vasc Med. 2012;2012:918267.

[3] Lin F, Wang N, Zhang TC. The role of endothelial-mesenchymal transition in development and pathological process. IUBMB Life. 2012;64:717-23.

[4] Nakajima Y, Yamagishi T, Hokari S, Nakamura H. Mechanisms involved in valvuloseptal endocardial cushion formation in early cardiogenesis: Roles of transforming growth factor (TGF)-beta and bone morphogenetic protein (BMP). Anatomical Record. 2000;258:119-27.

[5] Liebner S, Cattelino A, Gallini R, Rudini N, Iurlaro M, Piccolo S, et al. beta-Catenin is required for endothelial-mesenchymal transformation during heart cushion development in the mouse. Journal of Cell Biology. 2004;166:359-67.

[6] Piera-Velazquez S, Li Z, Jimenez S. Role of Endothelial-Mesenchymal Transition (EndoMT) in the Pathogenesis of Fibrotic Disorders. American Journal of Pathology. 2011;179:1074-80.

[7] Zeisberg E, Tarnavski O, Zeisberg M, Dorfman A, McMullen J, Gustafsson E, et al. Endothelial-to-mesenchymal transition contributes to cardiac fibrosis. Nature Medicine. 2007;13:952-61.

[8] Zhang Z, Wang J, Xu Y, Jiang Z, Wu R, Wang L, et al. Menstrual blood derived mesenchymal cells ameliorate cardiac fibrosis via inhibition of endothelial to mesenchymal transition in myocardial infarction. International Journal of Cardiology. 2013;168:1711-4.

[9] Aisagbonhi O, Rai M, Ryzhov S, Atria N, Feoktistov I, Hatzopoulos A. Experimental myocardial infarction triggers canonical Wnt signaling and endothelial-to-mesenchymal transition. Disease Models & Mechanisms. 2011;4:469-83.

[10] Potenta S, Zeisberg E, Kalluri R. The role of endothelial-to-mesenchymal transition in cancer progression. British Journal of Cancer. 2008;99:1375-9.

[11] Arciniegas E, Sutton A, Allen T, Schor A. Transforming growth factor-beta-1 promotes the differentiation of endothelial cells into smooth muscle-like cells-invitro. Journal of Cell Science. 1992;103:521-9.

[12] Diez M, Musri M, Ferrer E, Barbera J, Peinado V. Endothelial progenitor cells undergo an endothelial-to-mesenchymal transition-like process mediated by TGF beta RI. Cardiovascular Research. 2010;88:502-11.

[13] Medici D, Shore E, Lounev V, Kaplan F, Kalluri R, Olsen B. Conversion of vascular endothelial cells into multipotent stem-like cells. Nature Medicine. 2010;16:1400-6.

[14] Medici D, Potenta S, Kalluri R. Transforming growth factor-beta 2 promotes Snail-mediated endothelial-mesenchymal transition through convergence of Smad-dependent and Smad-independent signalling. Biochemical Journal. 2011;437:515-20.

[15] Leksa V, Godar S, Schiller HB, Fuertbauer E, Muhammad A, Slezakova K, et al. TGF-beta-induced apoptosis in endothelial cells mediated by M6P/IGFII-R and mini-plasminogen. J Cell Sci. 2005;118:4577-86.

[16] Ferrari G, Cook BD, Terushkin V, Pintucci G, Mignatti P. Transforming growth factor-beta 1 (TGF-beta1) induces angiogenesis through vascular endothelial growth factor (VEGF)-mediated apoptosis. J Cell Physiol. 2009;219:449-58.

[17] Kubiczkova L, Sedlarikova L, Hajek R, Sevcikova S. TGF-β - an excellent servant but a bad master. J Transl Med. 2012;10:183.

[18] Goumans MJ, Lebrin F, Valdimarsdottir G. Controlling the angiogenic switch: a balance between two distinct TGF-b receptor signaling pathways. Trends Cardiovasc Med. 2003;13:301-7.

[19] Pepper MS. Transforming growth factor-beta: vasculogenesis, angiogenesis, and vessel wall integrity. Cytokine Growth Factor Rev. 1997;8:21-43.

[20] Pepper MS, Vassalli JD, Orci L, Montesano R. Biphasic effect of transforming growth factor-beta 1 on in vitro angiogenesis. Exp Cell Res. 1993;204:356-63.

[21] Lebrin F, Goumans MJ, Jonker L, Carvalho RL, Valdimarsdottir G, Thorikay M, et al. Endoglin promotes endothelial cell proliferation and TGF-beta/ALK1 signal transduction. EMBO J. 2004;23:4018-28.

[22] Mamuya FA, Duncan MK. aV integrins and TGF-β-induced EMT: a circle of regulation. J Cell Mol Med. 2012;16:445-55.

[23] Jennings JC, Mohan S, Linkhart TA, Widstrom R, Baylink DJ. Comparison of the biological actions of TGF beta-1 and TGF beta-2: differential activity in endothelial cells. J Cell Physiol. 1988;137:167-72.

[24] Yamauchi K, Nishimura Y, Shigematsu S, Takeuchi Y, Nakamura J, Aizawa T, et al. Vascular endothelial cell growth factor attenuates actions of transforming growth factor-beta in human endothelial cells. J Biol Chem. 2004;279:55104-8.

[25] Griffith LG, Swartz MA. Capturing complex 3D tissue physiology in vitro. Nature Reviews Molecular Cell Biology. 2006;7:211-24.

[26] Bryan B, Dennstedt E, Mitchell D, Walshe T, Noma K, Loureiro R, et al. RhoA/ROCK signaling is essential for multiple aspects of VEGF-mediated angiogenesis. Faseb Journal. 2010;24:3186-95.

[27] Nguyen EH, Zanotelli MR, Schwartz MP, Murphy WL. Differential effects of cell adhesion, modulus and VEGFR-2 inhibition on capillary network formation in synthetic hydrogel arrays. Biomaterials. 2014;35:2149-61.

[28] Cooley BC, Nevado J, Mellad J, Yang D, St Hilaire C, Negro A, et al. TGF-β signaling mediates endothelial-to-mesenchymal transition (EndMT) during vein graft remodeling. Sci Transl Med. 2014;6:227ra34.

[29] Fang M, Yuan J, Peng C, Li Y. Collagen as a double-edged sword in tumor progression. Tumour Biol. 2014;35:2871-82.

[30] Fairbanks BD, Schwartz MP, Halevi AE, Nuttelman CR, Bowman CN, Anseth KS. Versatile, bioresponsive hydrogels via thiol-ene photopolymerization. Advanced Materials.DOI: 10.1002/adma.200901808.

[31] Bellis SL. Advantages of RGD peptides for directing cell association with biomaterials. Biomaterials. 2011;32:4205-10.

[32] Sinkus R, Tanter M, Xydeas T, Catheline S, Bercoff J, Fink M. Viscoelastic shear properties of in vivo breast lesions measured by MR elastography. Magnetic Resonance Imaging. 2005;23:159-65.

[33] Schneider B, Miller K. Angiogenesis of breast cancer. Journal of Clinical Oncology. 2005;23:1782-90.

[34] Levental I, Georges P, Janmey P. Soft biological materials and their impact on cell function. Soft Matter. 2007;3:299-306.

[35] Fairbanks BD, Schwartz MP, Halevi AE, Nuttelman CR, Bowman CN, Anseth KS. A Versatile Synthetic Extracellular Matrix Mimic via Thiol-Norbornene Photopolymerization. Advanced Materials. 2009;21:5005-10.

[36] Toepke M, Impellitteri N, JM T, WL M. Characterization of Thiol-Ene Crosslinked PEG Hydrogels. Macromolecular Materials and Engineering. 2012;10.1002/mame.201200119.

[37] Hansen TD, Koepsel JT, Le NN, Nguyen EH, Zorn S, Parlato M, et al. Biomaterial arrays with defined adhesion ligand densities and matrix stiffness identify distinct phenotypes for

tumorigenic and non-tumorigenic human mesenchymal cell types. Biomaterials Science. 2014;2:745-56.

[38] Jo BH, Van Lerberghe LM, Motsegood KM, Beebe DJ. Three-dimensional micro-channel fabrication in polydimethylsiloxane (PDMS) elastomer. Journal of Microelectromechanical Systems. 2000;9:76-81.

[39] Thibault C, Severac C, Mingotaud A, Vieu C, Mauzac M. Poly(dimethylsiloxane) contamination in microcontact printing and its influence on patterning oligonucleotides. Langmuir. 2007;23:10706-14.

[40] Hansen TD, Koepsel JT, Le NN, Nguyen EH, Zorn S, Parlato M, et al. Biomaterial arrays with defined adhesion ligand densities and matrix stiffness identify distinct phenotypes for tumorigenic and nontumorigenic human mesenchymal cell types. Biomater Sci. 2014;2:745-56.

[41] Kloxin AM, Kloxin CJ, Bowman CN, Anseth KS. Mechanical Properties of Cellularly Responsive Hydrogels and Their Experimental Determination. Advanced Materials. 2010;22:3484-94.

[42] Lu X, Dunn J, Dickinson AM, Gillespie JI, Baudouin SV. Smooth muscle alpha-actin expression in endothelial cells derived from CD34+ human cord blood cells. Stem Cells Dev. 2004;13:521-7.

[43] Yoder MC. Human endothelial progenitor cells. Cold Spring Harb Perspect Med. 2012;2:a006692.

[44] Attisano L, Wrana JL. Smads as transcriptional co-modulators. Curr Opin Cell Biol. 2000;12:235-43.

[45] Murakami M, Kawachi H, Ogawa K, Nishino Y, Funaba M. Receptor expression modulates the specificity of transforming growth factor-beta signaling pathways. Genes Cells. 2009;14:469-82.

[46] Leight JL, Wozniak MA, Chen S, Lynch ML, Chen CS. Matrix rigidity regulates a switch between TGF-β1-induced apoptosis and epithelial-mesenchymal transition. Mol Biol Cell. 2012;23:781-91.

[47] Galustian C, Dye J, Leach L, Clark P, Firth JA. Actin cytoskeletal isoforms in human endothelial cells in vitro: alteration with cell passage. In Vitro Cell Dev Biol Anim. 1995;31:796-802.

[48] Cevallos M, Riha GM, Wang X, Yang H, Yan S, Li M, et al. Cyclic strain induces expression of specific smooth muscle cell markers in human endothelial cells. Differentiation. 2006;74:552-61.

[49] Zhang H, Chang H, Wang LM, Ren KF, Martins MC, Barbosa MA, et al. Effect of Polyelectrolyte Film Stiffness on Endothelial Cells During Endothelial-to-Mesenchymal Transition. Biomacromolecules. 2015;16:3584-93.

[50] Nie L, Lyros O, Medda R, Jovanovic N, Schmidt JL, Otterson MF, et al. Endothelial-mesenchymal transition in normal human esophageal endothelial cells cocultured with esophageal adenocarcinoma cells: role of IL-1β and TGF-β2. Am J Physiol Cell Physiol. 2014;307:C859-77.

[51] Zeng ZZ, Yao H, Staszewski ED, Rockwood KF, Markwart SM, Fay KS, et al. alpha(5)beta(1) Integrin Ligand PHSRN Induces Invasion and alpha(5) mRNA in Endothelial Cells to Stimulate Angiogenesis. Transl Oncol. 2009;2:8-20.

[52] Koepsel J, Loveland S, Schwartz M, Zorn S, Belair D, Le N, et al. A chemically-defined screening platform reveals behavioral similarities between primary human mesenchymal stem cells and endothelial cells. Integrative Biology. 2012;4:1508-21.

[53] Hudalla G, Koepsel J, Murphy W. Surfaces That Sequester Serum-Borne Heparin Amplify Growth Factor Activity. Advanced Materials. 2011;23:5415-+.

[54] Dalton BA, McFarland CD, Underwood PA, Steele JG. Role of the heparin binding domain of fibronectin in attachment and spreading of human bone-derived cells. J Cell Sci. 1995;108 (Pt 5):2083-92.

Chapter 6:

Outlook and Conclusions

Eric H Nguyen, William L. Murphy. Customizable biomaterials to model complex effects of anti-angiogenic drug treatments in vitro. *In preparation.*

6.1 Conclusions

The studies in this work demonstrated the implementation of poly(ethylene glycol) (PEG) hydrogels in enhanced-throughput arrays to investigate endothelial cell (EC) biology and pathology. In chapter 3, cell adhesivity, hydrogel stiffness and VEGF sequestration by PEG hydrogels were defined to consistently enable vascular network formation by human ECs, including human umbilical vein endothelial cells (HUVECs) and ECs derived from induced pluripotent stem cells, seeded onto hydrogel surfaces. Afterward, the hydrogels were used in chemical screening arrays to identify vascular disruptive compounds from a library of unknown chemicals with a greater sensitivity than that of standard Matrigel-based screening systems. In chapter 4, hydrogel arrays containing encapsulated HUVECs modeled how vascular network formation is impacted by orthogonally varied cell adhesivity and stiffness. These studies, additionally, highlighted differential responses to VEGF inhibition with varying hydrogel compositions. Finally, in chapter 5 hydrogel arrays modeled how two-dimensional and three-dimensional culture contexts and hydrogel stiffness affect potentially pathogenic EC responses to TGF-β signaling, with cells demonstrating radically different responses to TGF-β signaling whether they were cultured on fibronectin-coated polystyrene, on hydrogel surfaces, or within hydrogel spots.

In each study, defined cell signaling cues such as integrin-binding peptides, VEGF-binding peptides and crosslinking molecules in the hydrogels were orthogonally controlled using thiol-ene "click" chemistry [1]. Additionally, hydrogel properties were systematically tuned across ranges of values, resulting in a comprehensive library of hydrogel formulations that could only be efficiently tested using enhanced-throughput experimental techniques. Materials and chemistries used in these studies see broad applicability in optimizing materials for therapeutic vascular tissue engineering and identifying candidate ECM-driven mechanistic pathways as therapeutic targets in vascular disorders. Particularly, the orthogonal material customization techniques used here enable the construction of sophisticated models of normal and diseased tissues for investigating long-term effects of drug treatments, a capability not explored *in vitro* using current technology.

6.2 Outlook and future directions

A critical limitation of *in-vitro* models of human vasculature, particularly those used to identify anti-angiogenic drugs for cancer treatment, is that they only model the effects of initial vascular disruption and are unable to model side effects and long-term effects of anti-angiogenic treatment. A significant contribution of this thesis is that it provides a toolset, namely systematically customizable hydrogels, to generate increasingly advanced models of vasculature to recreate the side effects of anti-angiogenic drug treatment. Here we speculate on how customizable biomaterials, along with endothelial cells of pathological origins, can be applied toward the creation of advanced *in-vitro* models of angiogenic rebound, vascular normalization, and endothelial-mesenchymal transition (EndMT). These three scenarios, described in chapter 2,

represent impactful side effects of current anti-angiogenic treatment methods that are currently poorly understood.

6.2.1 Endothelial cells from pathological origins

To model side effects of anti-angiogenic drug treatment vascular tissue models must be able to generate diseased vasculature. A potential approach to achieving this is the use of endothelial cells from known pathological origins. These cell types, which may be derived from induced pluripotent stem cells or directly harvested from diseased tissue, have a unique ability to display diseased phenotypes in vascular models prior to exposure to the model environment. For example, pathological network formation was recently modeled when endothelial cells were derived from induced pluripotent stem cells (IPSCs) of diabetic patients [2], and the capabilities of IPSC-derived endothelial cells can generate endothelial cells from cancer patients. Primary endothelial cells have also been derived from cancer tumors and exhibit properties such as enhanced migration, resistance to apoptosis and the ability to form denser networks of tubules and sprouting capillaries compared to normal endothelial cells, as demonstrated by hepatocellular carcinoma tumor–derived endothelial cells [3]. Finally, endothelial cells with prolonged exposure to pathological environments have demonstrated an ability to exacerbate tissue pathology. For example, human umbilical vein endothelial cells (HUVECs) treated with cancer-derived factors and inflammatory factors were shown to activate pro-metastatic signaling pathways in lung carcinoma cells [4]. These properties warrant a need to implement cell types of pathological origin when modeling the effects of anti-angiogenesis treatment.

6.2.2 Angiogenic rebound

Angiogenic rebound is characterized as the reassembly of vascular networks that were initially disrupted by anti-angiogenic drug treatment. Modeling this phenomenon requires the ability to sustain cell adhesion, viability and migration after anti-angiogenic drug treatment. In customizable biomaterials described in this thesis, additional adhesion ligands such as YIGSR and IKVAV can be systematically added to RGD-functionalized PEG hydrogels to optimize cell viability and adhesion and thereby improve cell survivability after initial network disruption. Materials may also be tailored for culture of IPSC-ECs and cancer-derived endothelial cells to address a hypothesis that pathological origins may enable improved endothelial cell drug resistance and improved angiogenic rebound.

One cause of the angiogenic rebound is the elevated quantity of angiogenic growth factors secreted by fibroblasts and cancer cells into the extracellular environment after anti-angiogenic treatment. These effects can be recapitulated by using photopolymerizable hydrogels and patterning techniques reviewed in chapter 2 to culture segregated populations of endothelial cells and growth factor-secreting cells. The addition of growth factor-binding ligands to a customizable material can maintain an elevated presence of growth factors for long periods of time. Additionally, the use of hydrogels with hypoxia-induced crosslinking would result in the maintenance of hypoxia and consequent upregulation of endogenous growth factor secretion in the model tumor environment. Successful implementation of these features potentially lead to

models where angiogenic rebound is observable in time frames resembling those observed *in vivo*, and mechanisms may be targeted to prevent network reformation in tumors.

6.2.3 Vascular normalization

The objective of modeling vascular normalization is to demonstrate the transformation of dysfunctional vasculature into stable, patent vasculature by short-term anti-angiogenic drug treatment. Vascular network features such as network area and stability must be clearly observable as potential markers of normalization events, and increased biomimicry of vascular models will enable the determination of meaningful drug concentration ranges that predictably trigger normalization. Initial pathological network formation may be achieved through the use of cancer-derived endothelial cells in order to generate disorganized and disrupted vasculature prior to exposure to drugs and chemicals.

Future models of normalization will require the co-cultures of endothelial cells and growth factor secreting cells that can react to anti-angiogenic drug treatment in order to account for endogenous signals that skew effective doses of anti-angiogenic drugs. To this end, optimized concentrations of growth factor-binding ligands should also be present to account for enhanced growth factor stability in *in-vivo* tissues. Additionally, studies of vascular normalization may need to be done in materials that drive anti-angiogenic drugs to improve vascular network coherence. For example, in chapter 4 3D models of tubule network formation have revealed a hydrogel with low modulus and high RGD concentration [5] that caused the VEGF inhibitor SU5416 to stabilize vascular networks rather than disrupt formation. Finally, customizable materials need to be adapted for systems that permit fluid perfusion through model vascular

networks in order to observe the impact of drug treatments on vessel leakiness and stability. Successful generation of normalization models will reveal appropriate dose rates, time tables and biomarkers to recognize and control normalization *in vivo*.

6.2.4 Metastatic switch and mesenchymal transformation

A critical side effect associated with anti-angiogenic drug treatment, specifically the inhibition of VEGF signaling, is the onset of pathological phenotypes in endothelial cells. One example of this phenotypic switch is EndMT, where endothelial cells, with TGF-β signaling, switch phenotypes to mesenchymal cells [6-11] that contribute to cancer growth and metastasis [12-14]. Evidence has emerged to demonstrate that inhibition of VEGF signaling by anti-angiogenic drug treatment enables a rise in migratory phenotypes in endothelial cells and cancer cells in mouse models [15], as VEGF is known to attenuate TGF-β activity [16].

The identification of enhanced cancer metastasis as a side effect of angiogenic inhibition highlights an urgent need to characterize the effects of VEGF inhibition in tumor-like environments that change endothelial responses to TGF-β. These environmental variables can possibly include TGF-β concentration [17], integrin interactions with the ECM [18, 19] and β-catenin [20], cell-cell contacts [21], and co-cultures with supporting cell types [22]. The effects of specific interactions between endothelial cells and the ECM in modulating the specific outcome of EndMT are only beginning to be answered [23]. One particular study has begun pioneering discoveries of how substrate properties impact endothelial cell phenotypic switching. Here, cell-adhesive poly(L-Lysine) / Hyalouronic Acid films increased the propensity of HUVECs to undergo TGF-β1-mediated endothelial-mesenchymal transition on substrates with

increasing stiffness [24]. Results such as these begin to further implicate pathological extracellular environments as encouraging the transformation, and investigations can be furthered using biomaterial customization methods described in this thesis. In chapter 5 it was hypothesized that hydrogels functionalized using only RGD lack functionality of full-length proteins to mediate EndMT. The versatility of the hydrogels studied in this thesis enables the addition and optimization of numerous other biomolecules to endothelial culture substrates. A particularly compelling example of a candidate biomolecule is heparin binding molecules [25, 26] to facilitate binding, concentration and stabilization of soluble TGF-β locally to endothelial cell populations. Other ligands, including PHSRN peptide, acts synergistically with RGD in full-length fibronectin to potentially mediate the transition as well [27]. A greater understanding of ECM-modulation of EndMT include discovery of appropriate dosing ranges for achieving vascular disruption while avoiding EndMT, as well as revelation of therapeutic targets to prevent the transition.

6.3 References

[1] Fairbanks BD, Schwartz MP, Halevi AE, Nuttelman CR, Bowman CN, Anseth KS. A Versatile Synthetic Extracellular Matrix Mimic via Thiol-Norbornene Photopolymerization. Advanced Materials. 2009;21:5005-10.

[2] Chan XY, Black R, Dickerman K, Federico J, Levesque M, Mumm J, et al. Three-Dimensional Vascular Network Assembly From Diabetic Patient-Derived Induced Pluripotent Stem Cells. Arterioscler Thromb Vasc Biol. 2015.

[3] Xiong YQ, Sun HC, Zhang W, Zhu XD, Zhuang PY, Zhang JB, et al. Human hepatocellular carcinoma tumor-derived endothelial cells manifest increased angiogenesis capability and drug resistance compared with normal endothelial cells. Clin Cancer Res. 2009;15:4838-46.

[4] Franses JW, Drosu NC, Gibson WJ, Chitalia VC, Edelman ER. Dysfunctional endothelial cells directly stimulate cancer inflammation and metastasis. Int J Cancer. 2013;133:1334-44.

[5] Nguyen EH, Zanotelli MR, Schwartz MP, Murphy WL. Differential effects of cell adhesion, modulus and VEGFR-2 inhibition on capillary network formation in synthetic hydrogel arrays. Biomaterials. 2014;35:2149-61.

[6] Medici D, Shore E, Lounev V, Kaplan F, Kalluri R, Olsen B. Conversion of vascular endothelial cells into multipotent stem-like cells. Nature Medicine. 2010;16:1400-U80.

[7] Diez M, Musri M, Ferrer E, Barbera J, Peinado V. Endothelial progenitor cells undergo an endothelial-to-mesenchymal transition-like process mediated by TGF beta RI. Cardiovascular Research. 2010;88:502-11.

[8] Kitao A, Sato Y, Sawada-Kitamura S, Harada K, Sasaki M, Morikawa H, et al. Endothelial to Mesenchymal Transition via Transforming Growth Factor-beta 1/Smad Activation Is Associated with Portal Venous Stenosis in Idiopathic Portal Hypertension. American Journal of Pathology. 2009;175:616-26.

[9] Cooley BC, Nevado J, Mellad J, Yang D, St Hilaire C, Negro A, et al. TGF-β signaling mediates endothelial-to-mesenchymal transition (EndMT) during vein graft remodeling. Sci Transl Med. 2014;6:227ra34.

[10] Medici D, Potenta S, Kalluri R. Transforming growth factor-beta 2 promotes Snail-mediated endothelial-mesenchymal transition through convergence of Smad-dependent and Smad-independent signalling. Biochemical Journal. 2011;437:515-20
.
[11] Coll-Bonfill N, Musri MM, Ivo V, Barberà JA, Tura-Ceide O. Transdifferentiation of endothelial cells to smooth muscle cells play an important role in vascular remodelling. Am J Stem Cells. 2015;4:13-21.

[12] Zeisberg E, Potenta S, Xie L, Zeisberg M, Kalluri R. Discovery of endothelial to mesenchymal transition as a source for carcinoma-associated fibroblasts. Cancer Research. 2007;67:10123-8.

[13] Potenta S, Zeisberg E, Kalluri R. The role of endothelial-to-mesenchymal transition in cancer progression. British Journal of Cancer. 2008;99:1375-9.

[14] Lin F, Wang N, Zhang TC. The role of endothelial-mesenchymal transition in development and pathological process. IUBMB Life. 2012;64:717-23.

[15] Lu KV, Chang JP, Parachoniak CA, Pandika MM, Aghi MK, Meyronet D, et al. VEGF inhibits tumor cell invasion and mesenchymal transition through a MET/VEGFR2 complex. Cancer Cell. 2012;22:21-35.

[16] Yamauchi K, Nishimura Y, Shigematsu S, Takeuchi Y, Nakamura J, Aizawa T, et al. Vascular endothelial cell growth factor attenuates actions of transforming growth factor-beta in human endothelial cells. J Biol Chem. 2004;279:55104-8.

[17] Goumans MJ, Lebrin F, Valdimarsdottir G. Controlling the angiogenic switch: a balance between two distinct TGF-b receptor signaling pathways. Trends Cardiovasc Med. 2003;13:301-7.

[18] Munger J, Harpel J, Giancotti F, Rifkin D. Interactions between growth factors and integrins: Latent forms of transforming growth factor-beta are ligands for the integrin alpha v beta 1. Molecular Biology of the Cell. 1998;9:2627-38.

[19] Alghisi G, Ponsonnet L, Ruegg C. The Integrin Antagonist Cilengitide Activates alpha V beta 3, Disrupts VE-Cadherin Localization at Cell Junctions and Enhances Permeability in Endothelial Cells. Plos One. 2009;4.

[20] Liebner S, Cattelino A, Gallini R, Rudini N, Iurlaro M, Piccolo S, et al. beta-Catenin is required for endothelial-mesenchymal transformation during heart cushion development in the mouse. Journal of Cell Biology. 2004;166:359-67.

[21] Aisagbonhi O, Rai M, Ryzhov S, Atria N, Feoktistov I, Hatzopoulos A. Experimental myocardial infarction triggers canonical Wnt signaling and endothelial-to-mesenchymal transition. Disease Models & Mechanisms. 2011;4:469-83.

[22] Zhang Z, Wang J, Xu Y, Jiang Z, Wu R, Wang L, et al. Menstrual blood derived mesenchymal cells ameliorate cardiac fibrosis via inhibition of endothelial to mesenchymal transition in myocardial infarction. International Journal of Cardiology. 2013;168:1711-4.

[23] Mahler GJ, Frendl CM, Cao Q, Butcher JT. Effects of shear stress pattern and magnitude on mesenchymal transformation and invasion of aortic valve endothelial cells. Biotechnol Bioeng. 2014;111:2326-37.

[24] Zhang H, Chang H, Wang LM, Ren KF, Martins MC, Barbosa MA, et al. Effect of Polyelectrolyte Film Stiffness on Endothelial Cells During Endothelial-to-Mesenchymal Transition. Biomacromolecules. 2015;16:3584-93.

[25] Hudalla GA, Murphy WL. Biomaterials that regulate growth factor activity via bioinspired interactions. Adv Funct Mater. 2011;21:1754-68.

[26] Hudalla G, Koepsel J, Murphy W. Surfaces That Sequester Serum-Borne Heparin Amplify Growth Factor Activity. Advanced Materials. 2011;23:5415-8.

[27] Zeng ZZ, Yao H, Staszewski ED, Rockwood KF, Markwart SM, Fay KS, et al. alpha(5)beta(1) Integrin Ligand PHSRN Induces Invasion and alpha(5) mRNA in Endothelial Cells to Stimulate Angiogenesis. Transl Oncol. 2009;2:8-20.